ANALYTICAL INVESTIGATIONS FOR IN – SITU TESTING OF NON – DUCTILE RC BUILDINGS

by

Mehmet Ülker

B.S., Civil Engineering, Boğaziçi University, 2007

Submitted to the Institute for Graduate Studies in
Science and Engineering in partial fulfillment of
the requirements for the degree of
Master of Science

Graduate Program in Civil Engineering
Boğaziçi University
2009

ANALYTICAL INVESTIGATIONS FOR IN – SITU TESTING OF NON – DUCTILE RC BUILDINGS

APPROVED BY:

Assist. Prof. Hilmi Luş (Thesis Supervisor)	.....
Assist. Prof. Kutay Orakçal (Thesis Co-Supervisor)	.....
Prof. Mustafa O. Erdik	.....
Prof. Erdal Şafak	.....
Assoc. Prof. Cem Yalçın	.....

DATE OF APPROVAL: 12/06/2009

ACKNOWLEDGEMENTS

I would like to express my sincere gratitude to my thesis supervisors Assistant Professor Dr. Hilmi Luş and Assistant Professor Dr. Kutay Orakçal for their invaluable guidance and help during the preparation of this thesis. I would like to mention their patience, giving me inspiration and hope when I was stuck at dead-ends.

I would also like to thank Associate Professor Dr. Cem Yalçın, Professor Dr. Erdal Şafak and Professor Dr. Mustafa O. Erdik for their kind and supportive attitude to me and showing high interests and valuable advices to my thesis.

I am also grateful to TUBITAK for the scholarship for my expenditures.

I have very much benefited from the discussions with my dear “Civil Engineer” friends; Umut Karacadağlı, Hamdi Kul, Alperen Turak, Murat Güngör Tekin, Denizhan Uluğtekin, and Musa Rahmanlar. I thank them all for their support and friendship throughout the preparation of this thesis.

I am grateful to my parents for the endless support, encouragement and love they have given me throughout my life. I would like to express my gratefulness to my love Meltem Eser, without whom probably I would have never done this work.

ABSTRACT

In order to perform an in-situ pushover test on a real, existing building, a test setup developed via a comprehensive study is required. The scope of this study is to propose a test setup for in-situ testing of a typical reinforced concrete building constructed in Turkey in the 1970's.

First of all, previous research on field and laboratory testing of different strengthening methods and nonlinear analytical modeling techniques in the literature are investigated. The accuracy of available nonlinear modeling techniques are evaluated by analyzing a typical Taiwanese school building, namely the Hsin-Tseng Junior High School building, and comparing analysis results with experimental results by Tu et al.[1]. It is observed that material properties, cracked section stiffnesses, building geometry, existence of windowsills, and nonlinear modeling techniques selected affect the results of the analyses significantly.

Sehit Adem Yavuz Primary School in Istanbul is chosen as a case-study building and an in-situ testing scheme is proposed for the building. By using geometrical properties and material properties of the case building, a preliminary test setup is proposed. The proposed setup comprises testing of four 2-storey-single bay test frames, including (i) a bare frame, (ii) an infilled frame, (iii) an infilled frame strengthened with Carbon-Fiber-Reinforced-Polymers, and (iv) a frame with reinforced concrete infill wall. In the light of the analytical modeling techniques investigated, the proposed tests are analyzed via nonlinear static pushover analyses conducted using commercial computer software program SAP2000 v11.0.0 for blind prediction of the test results. The behavior of the test frames are examined in terms of lateral load-lateral displacement responses and hinge formation sequences. The final test setup for the in-situ tests is developed in accordance with the analyses results. For the proposed tests, the proposed construction work needs to be conducted before testing. Hydraulic loading equipment, load cells, assemblage systems for test frames and reaction block, out of plane resistant frame systems, reference columns for measurements, displacement sensors, and data acquisition systems necessary for testing are also identified.

ÖZET

Gerçek bir bina üzerinde statik itme deneylerini yapmak için kapsamlı bir araştırma sonucunda oluşturulmuş bir test düzeneğine ihtiyaç vardır. Bu çalışmanın amacı, 1970'li yıllarda Türkiye'de yapılmış tipik bir betonarme yapıda saha deneyleri yapmak için test düzeneği önermektir.

İlk olarak literatürdeki farklı güçlendirme yöntemleri üzerine saha ve laboratuar deneyleri ve doğrusal olmayan analitik modelleme teknikleri incelenmiştir. İncelenen doğrusal olmayan modelleme tekniklerinin doğruluğu, tipik bir Tayvan okul binası olan Hsin-Tseng okul binasına yapılan analitik çalışma sonuçlarının Tu [1] tarafından yapılmış olan deneysel çalışma sonuçlarıyla karşılaştırılması sonucu değerlendirilmiştir. Malzeme özelliklerinin, çatlamış kesit rijitliğinin, bina geometrisinin, binanın parapet içerme durumunun ve seçilen doğrusal olmayan modelleme tekniklerinin analiz sonuçlarını önemli bir ölçüde etkilediği gözlemlenmiştir.

İstanbul'daki Şehit Adem Yavuz İlköğretim Okulu örnek bina olarak seçilmiş ve saha deney düzeneği bu okul için önerilmiştir. Binanın geometrik özellikleri ve malzeme özellikleri kullanılarak, öncü bir deney düzeneği önerilmiştir. Önerilen deney düzeneği (i) boş deney çerçevesi, (ii) bölme duvarlı deney çerçevesi, (iii) CFRP ile güçlendirilmiş bölme duvarlı deney çerçevesi ve betonarme perde duvar ile güçlendirilmiş deney çerçevesinden oluşan, dört adet iki-katlı-tek-açıklıklı deney çerçevesini içerir. İncelenen analitik modelleme teknikleri ışığında, belirlenen deney düzeneklerinin doğrusal olmayan statik itme analizi SAP2000 v11.0.0 bilgisayar programı kullanılarak deney sonuçlarını tahmin etmek için yapılmıştır. Yatay yük-yatay deplasman davranışları ve plastik mafsal oluşum sıralaması kullanılarak test çerçevelerinin davranışları incelenmiştir. Analiz sonuçlarına uygun olarak, deney düzeneklerinin son hali oluşturulmuştur. Önerilen düzeneklerde, yapılması gereken inşaat işleri deneylerden önce yapılmalıdır. Deneyleri yapmak için gereken hidrolik yükleme sistemleri, yük hücreleri, deney çerçeveleri ve reaksiyon bloğu için yükleme sistemleri, düzlem dışı dönme hareketini engelleyici çerçeve sistemleri, ölçümler için kullanılacak referans kolonları, deplasman ölçerler (LVDTler) ve data toplama sistemleri de belirlenmiştir.

TABLE OF CONTENTS

ACKNOWLEDGEMENTS iii
ABSTRACT iv
ÖZET v
LIST OF FIGURES x
LIST OF TABLES xviii
LIST OF SYMBOLS/ABBREVIATIONS xx
1. INTRODUCTION 1
1.1. General Concepts 1
1.2. Scope and Summary of Contents 2
2. LITERATURE SURVEY 4
2.1. In-situ Tests 4
2.2 Seismic Rehabilitation Techniques 6
3. ANALYTICAL MODELLING AND PUSHOVER ANALYSIS 14
3.1. Material Models 14
3.1.1. Concrete Models 14
3.1.2. Reinforcing Steel Models 19
3.2. Nonlinear Behavior Models for Structural Elements 21
3.2.1. Modeling the Frame Members 21
3.2.1.1. Moment (M) Hinges. 21
3.2.1.2. Axial Force (P)-Moment (M) Hinges. 22
3.2.1.3. Axial Force (P) Hinges 22
3.2.1.4. Shear (V) Hinges. 23
3.2.2. Modeling of the Infill Walls 31
3.2.2.1. Axial Force (P) Hinges for Brick Walls. 33
3.2.3. Modeling of Shear Walls 40
3.2.4. Modeling of Infill Walls Strengthened with CFRP 41
3.3. Nonlinear Static Analysis (Pushover Analysis) 45
4. ANALYTICAL MODELING OF THE HSIN-TSENG JUNIOR HIGH SCHOOL BUILDING 47
4.1. General Properties of the Building 47

4.2. In-Situ Test Results 50
4.3. Analytical Modeling 51
4.4. Analysis Results 55
5. DETERMINATION OF AN IN-SITU TESTING CONFIGURATION FOR A TYPICAL RC SCHOOL BUILDING 62
5.1. The Demand for In-Situ Tests 62
5.2. Public Buildings for In-Situ Tests 63
5.3. General Properties of Şehit Adem Yavuz Primary School Building 64
5.4. Material Properties of Şehit Adem Yavuz Primary School 68
5.5. Proposed Test Setup 68
5.6. Properties of Test Frames (Block-A) 75
5.7. Properties of the Reaction Block (Block-B) 76
5.8. Work Flowchart and Time Schedule 78
6. NONLINEAR ANALYSIS OF STATIC TEST FRAMES AND BLIND PREDICTION OF IN-SITU TEST RESULTS 81
6.1. Modeling of the Structure and Analysis Procedure 81
6.2. Sample Calculations for Nonlinear Hinges 83
6.2.1. Moment (M) Hinges 83
6.2.2. Normal Force-Moment (P-M) Hinges 85
6.2.3. Axial Hinges (P) 87
6.2.4. Shear (V) Hinges 89
6.2.5. Axial (P) Hinges for Brick Walls 91
6.2.6. Axial (P) Hinges for Tension Ties 93
6.2.7. Shear (V) Hinges for RC Walls 94
6.3. Analyses Results 96
6.3.1. Analysis Results of Test Frames 96
6.3.1.1. Capacity Determination of Bare Frame. 97
6.3.1.2. Hinge Formation Sequence of Bare Frame. 97
6.3.1.3. Capacity Determination of Infilled Frame. 98
6.3.1.4. Hinge Formation Sequence of Infilled Frame (Chen's [34] Model). 100
6.3.1.5. Capacity Determination of Infilled Frame Strengthened with CFRP 101

6.3.1.6. Hinge Formation Sequence of Infilled Frame Strengthened with CFRP 101
6.3.1.7. Capacity Determination of RC Wall Strengthened Frame. 102
6.3.1.8. Hinge Formation Sequence of RC Wall Strengthened Frame. 105
6.3.1.9. Comparison of Analyses Results. 105
6.3.1.10. Comparison of Analyses Results to Literature 106
6.3.1.11. The Effects of Column Splice Lengths to Analysis Results. 107
6.3.2. Analysis Results for Block-B 108
6.3.2.1. Capacity Determination for Block-B. 112
6.3.2.2. Comparison of the Results for Different Loading Cases. 115
6.3.3. Analysis Results of Steel Resisting Frames 117
6.3.3.1. First Proposal. 117
6.3.3.2. Second Proposal. 118
7. DETERMINATION OF TEST EQUIPMENTS AND SPECIFICATIONS OF EQUIPMENTS FOR IN-SITU TESTS 122
7.1. Hydraulic Loading Equipment 122
7.2. Load Cells 123
7.3. Loading Equipments 124
7.4. Assemblage System of Test Frames 124
7.5. Assemblage System of Frames of Block-B 125
7.6. Assemblage System of Shear Wall at Block-B 126
7.7. Triangular Steel Resisting Truss System 127
7.8. Steel Braces 128
7.9. Reference Columns of Test Frames 128
7.10. Reference Columns of Block-B 128
7.11. Linear Variable Displacement Transformers (LVDT) 129
7.12. Data Acquisition System 129
7.13. Summary of Required Equipments for In-Situ Static Tests 129

8. SUMMARY, CONCLUSIONS AND RECOMMENDATIONS FOR FUTURE WORK 131
8.1. Summary 131
8.2. Conclusions 131
8.3. Recommendations for Future Work 134
APPENDIX A: DRAWINGS OF SEHIT ADEM YAVUZ PRIMARY SCHOOL 136
APPENDIX B: GENERAL VIEWS OF THE PROPOSED TEST CONFIGURATION 141
APPENDIX C: DETAILED DRAWINGS OF ASSEMBLAGE SYSTEMS OF TEST FRAMES AND BLOCK-B 143
REFERENCES 147

LIST OF FIGURES

Figure 3.1. Hognestad stress-strain model of concrete 14

Figure 3.2. Stress-strain relationship of concrete according to Mander's Model 16

Figure 3.3. Modified Kent and Park Model for concrete 16

Figure 3.4. Stress-strain relationship for reinforcement steel 20

Figure 3.5. Typical moment-curvature relationship for a nonlinear moment hinge 22

Figure 3.6. Force-displacement relationship for a typical nonlinear axial hinge 23

Figure 3.7. Force-displacement relationship for a typical nonlinear shear hinge 25

Figure 3.8. Flexural deformation in a column 27

Figure 3.9. Bar (bond) slip in a column 28

Figure 3.10. Shear deformation in a column 29

Figure 3.11. Shear force-displacement relationship for a typical nonlinear shear hinge. 31

Figure 3.12. Representation of the equivalent truss model 33

Figure 3.13. Types of brick laying and failure path for brick wall 36

Figure 3.14. Force-displacement relationship for axial hinge of an equivalent truss 39

Figure 3.15. Schematic diagram of equivalent wide column model of RC wall 40

Figure 3.16. Structural modeling for infill struts and CFRP ties 42

Figure 3.17. Stress-strain models for infill struts and CFRP ties..... 42

Figure 4.1. Plan view and cross-sectional dimensions of the column elements of Hsin-Tseng Junior High School building (in cm's)..... 48

Figure 4.2. Side view of the test setup (in cm's) 49

Figure 4.3. Flexure failure (left hand side) and flexure-shear failure (right hand side) of the test building 50

Figure 4.4. Pushover curve of the Hsin-Tseng Junior High School building 51

Figure 4.5. Generalized forms of effective stiffness values..... 52

Figure 4.6. Typical moment-curvature analysis for a C1 type column..... 53

Figure 4.7. Representation of the rigid windowsills used in the analysis 54

Figure 4.8. Representation of the rigid windowsills used by Wu and Xue 54

Figure 4.9. Three dimensional computer model of the Hsin-Tseng Junior High School 54

Figure 4.10. Analytical versus experimental pushover curves of the building-1 56

Figure 4.11. Deformation behavior of the building 57

Figure 4.12. Analytical versus experimental pushover curves of the building-2 58

Figure 4.13. Analytical versus experimental pushover curves of the building-3 59

Figure 4.14. Analytical versus experimental pushover curves of the building-4 59

Figure 4.15. Analytical versus experimental pushover curves of the building-5 60

Figure 5.1. Floor plan of a typical Turkish school building 63

Figure 5.2. General view of Şehit Adem Yavuz Primary School building..... 64

Figure 5.3. Plan view of Şehit Adem Yavuz Primary School..... 66

Figure 5.4 Side view of Şehit Adem Yavuz Primary School..... 67

Figure 5.5. Computer model of the whole building before construction works 69

Figure 5.6. Computer model of the building after construction works..... 70

Figure 5.7. General view of the test setup from preliminary computer model 71

Figure 5.8. Setup to prevent local failures of the test frame (assemblage system)..... 71

Figure 5.9. Typical loading system..... 72

Figure 5.10. General view of out-of-plane resisting frame..... 73

Figure 5.11. General view of out-of-plane resisting frame and test frame 73

Figure 5.12. General view of one of the triangular trusses 74

Figure 5.13. General view of the out-of-plane resisting triangular trusses and test frame..... 74

Figure 5.14. General view of the static test frame 75

Figure 5.15. Plan view of Block-B 77

Figure 5.16. Flowchart for required construction works 79

Figure 5.17. Time schedule for in-situ tests 80

Figure 6.1. Computer models of two-dimensional test frames 82

Figure 6.2. Computer model of three-dimensional reaction block 82

Figure 6.3. Lateral loading pattern in static test frames 83

Figure 6.4. Moment-curvature relationship of beam B101 84

Figure 6.5. Backbone model of plastic moment hinge of beam B101 85

Figure 6.6. P-M interaction curve of column C201 86

Figure 6.7. Linearized interaction curve of column C201 87

Figure 6.8. Axial force-displacement relationship of column C102 88

Figure 6.9. Normalized force-plastic rotation relationship of column C201 90

Figure 6.10. Force-displacement relationship of column C201 91

Figure 6.11. Nonlinear axial hinge of first storey infill walls 92

Figure 6.12. Nonlinear axial hinge of second storey infill walls 93

Figure 6.13. Stress-strain relationship of the tension tie 94

Figure 6.14. Top and side views of RC wall 95

Figure 6.15. Shear force-drift ratio relationship of shear hinge of first storey RC shear wall 96

Figure 6.16. Displacement-lateral force relationship of bare frame 97

Figure 6.17. Hinge formation sequence for the bare frame 98

Figure 6.18. Displacement-lateral force relationship of infilled frame model by Chen.. 99

Figure 6.19. Displacement-lateral force relationship of infilled frame by Binici and Ozcebe model 99

Figure 6.20. Hinge formation sequence of infilled frame..... 100

Figure 6.21. Displacement-lateral force relationship of infilled frame strengthened with CFRP 101

Figure 6.22. Hinge formation sequence of infilled frame strengthened with CFRP 102

Figure 6.23. Typical shear wall analysis in SAP2000.v11.0.0[26]..... 103

Figure 6.24. Displacement-lateral force relationship of RC wall strengthened frame by first model..... 103

Figure 6.25. Displacement-lateral force relationship of RC wall strengthened model by second model 104

Figure 6.26. Hinge formation of RC wall strengthened frame 105

Figure 6.27. Comparison of displacement-lateral force curves of different strengthening methods..... 106

Figure 6.28. Location of brace elements at axis 6 109

Figure 6.29. Cross sectional view of brace elements (in mm's) 110

Figure 6.30. Stress-strain relationship of steel 110

Figure 6.31. Plan view of the building with locations of test frames 111

Figure 6.32. Frame labeling of Block-B 112

Figure 6.33. Lateral force-displacement relationship of Block-B when loading along frame 1 113

Figure 6.34. Lateral force-displacement relationship of Block-B when loading along frame 2 113

Figure 6.35. Lateral force-displacement relationship of Block-B when loading along frame 3 114

Figure 6.36. Lateral force-displacement relationship of Block-B when loading along frame 4 115

Figure 6.37. Comparison of four loading conditions 116

Figure 6.38. Computer model of three dimensional, rectangular steel frame system.... 117

Figure 6.39. General views of cross sections of frame/brace elements 118

Figure 6.40. Computer model of triangular truss system 119

Figure 6.41. Cross sections of double angles for truss members 119

Figure 6.42. General views of final test setup and triangular truss system 121

Figure 7.1. Schematic view of hydraulic loading equipment 123

Figure 7.2. Typical view for slim load cell 124

Figure 7.3. General view of loading equipments 124

Figure 7.4. General views of Assemblage Systems of test frames 125

Figure 7.5. General view of installed assemblage system for frames of Block-B 126

Figure 7.6. General view of assemblage system for shear wall at Block-B 126

Figure 7.7. Dimensions of steel resisting truss system (mm) 127

Figure 7.8. General views of LVDTs 129

Figure A.1. Plan view of basement floor of Sehit Adem Yavuz Primary School 137

Figure A.2. Plan view of ground floor of Sehit Adem Yavuz Primary School 138

Figure A.3. Plan view of first storey of Sehit Adem Yavuz Primary School 139

Figure A.4. Plan view of second storey of Sehit Adem Yavuz Primary School 140

Figure B.1. Three dimensional general view of the test setup-1 141

Figure B.2. Three dimensional general view of the test setup-2 142

Figure B.3. General view of the gusset plates and M40 bolts 142

Figure B.4. General view of the loading system 142

Figure C.1. General view and dimensioning of assemblage system of test frames..... 144

Figure C.2. General view and dimensioning of assemblage system of frames of Block-B..... 145

Figure C.3. General view and dimensioning of assemblage system of shear wall of Block-B..... 146

LIST OF TABLES

Table 2.1. Summary of various strengthening methods by different researchers 12

Table 3.1. Mechanical properties of reinforcing steel 19

Table 3.2. Strain and strength values for S220 and S420 according to TEC 2007 20

Table 3.3. Data points for the nonlinear axial hinge of Figure 3.6..... 23

Table 3.4. Data points for the nonlinear shear hinge of Figure 3.7 26

Table 3.5. Parameters for the nonlinear shear hinge in Figure 3.11 31

Table 3.6. Parameters of the nonlinear axial hinge of equivalent trusses..... 39

Table 5.1. Member sections and reinforcement details 76

Table 5.2. Member sections and reinforcement details 77

Table 6.1. Normalized moment-curvature values of beam B101 84

Table 6.2. Linearization points of the interaction diagram (C201) 86

Table 6.3. Normalized force-displacement curve of column C102..... 88

Table 6.4. Summary of shear capacity calculation-contribution of concrete 89

Table 6.5. Summary of shear capacity calculation-contribution of steel and total shear capacity 89

Table 6.6. Normalized force-plastic rotation values of frame members 90

Table 6.7. Nonlinear axial hinge parameters of first storey infill wall 92

Table 6.8 Nonlinear axial hinge parameters of second storey infill wall 92

Table 6.9. Summary table for the effects of different strengthening methods 106

Table 6.10. Comparison of analytical study results to literature 107

Table 6.11. Factor of safety values for tests 116

Table 6.12. Sectional properties of frame / brace elements..... 118

Table 6.13. Sectional properties of double angle sections..... 120

Table 7.1. Summary of required equipments for in-situ static tests 130

LIST OF SYMBOLS/ABBREVIATIONS

A_d	Cross-sectional area of the equivalent truss
A_g	Gross cross sectional area
A_{sw}	Total cross-sectional area of the transverse reinforcement
A_{str}	Area of the composite strut
A_{tie}	Area of the composite tension tie
A_V	Shear area
b_k	The smaller dimension of the confined core measured from outside to outside of ties
b_w	Width of the section
d, d_e	Effective depth of the section
d_B	Diameter of the longitudinal reinforcement
E	Modulus of elasticity
E_c	Modulus of elasticity of concrete
E_s	Modulus of elasticity of steel
E_d	Modulus of elasticity of the equivalent truss member
E_f	Modulus of elasticity of FRP
E_{in}, E_{inf}	Modulus of elasticity of the infill material
E_m	Modulus of elasticity of mortar
E_u	Secant stiffness
E_p	The crack elasticity modulus
E_{50}	Elasticity modulus of the brick wall
f_{bc}	Uniaxial compression strength of the brick
f_{bt}	Splitting strength of the brick
f_c	Maximum compressive strength in concrete

f_{cc}	Compression strength of the confined concrete
f_{ck}	Characteristic compressive strength of concrete
f_{co}	Compression strength of the unconfined concrete
f_{crt}	Cracking stress
f_{ct}	Flexural tensile strength of concrete
f_{mbt}	Splitting strength of the interface of the brick and mortar
f_{mc}	Uniaxial compression strength of mortar (infill plaster composite)
f_{mv}	Shear strength of the mortar bed joint
f_{pt}	Tensile strength of the plaster
f_{su}	Ultimate strength of reinforcement
f_{sy}	Yielding strength of reinforcement
f_{ut}	Tensile strength
f_{us}	Ultimate strength
f_{yt}	Yield strength of transverse reinforcement
f_{ywd}	Design yield strength of transverse reinforcement,
f_{ywk}	Yield strength of transverse reinforcement
g_h	Horizontal seam width of the brick
g_v	Vertical seam width of the brick
G	Shear modulus
h	Height of a member
h_{inf}	Height of the infill wall
H_b	Height of the brick wall
I	Moment of inertia
I_c	Column moment of inertia
K	Curvature
l, L	Length of a member
l_s	Total length of the transverse reinforcing bars

L_d	Length of the equivalent truss
M	Moment
M_{pc}	Moment capacity of the column
M_{pj}	Minimum moment capacities of the column or the beam
M_u	Ultimate moment capacity
M_Y	Moment at yielding of the longitudinal reinforcement
P,N, Nd	Axial force
s	Spacing of the transverse reinforcement bars
t_f	Thicknesses of FRP
t_{in}, t_{inf}	Thickness of the infill wall
t_p	Thicknesses of plaster
t_{tie}	Thickness of the composite tension tie
T_b	Thickness of the brick wall
u	Bond stress between the longitudinal reinforcement and the concrete
u_u	Ultimate displacement of the brick wall
V	Shear Force
V	Nominal shear stress
V_c	Shear carried by concrete
V_{cc}	Corner crushing
V_{cr}	Cracking strength of concrete
V_n	Ultimate strength of the brick wall
V_p	Plastic shear capacity
V_r	Residual strength of the brick wall
V_{ss}	Sliding shear
V_{us}	Ultimate strength of the diagonal compressive strut
V_{ut}	Tensile capacity
V_u	Ultimate shear capacity
V_w	Shear carried by the shear reinforcement

w	Width of a member
w_f	Width of the FRP
w_s	Width of strut
W_b	Width of the brick wall
W_d	Depth of the equivalent truss
α	Dimensionless parameter to account for the frame infill contact length
α, β	Strength modification factor
δ_a	Axial failure displacement
δ_s	Flexure-shear failure displacement
Δ_{FL}	Displacement due to flexure,
Δ_{SL}	Displacement due to bar (bond) slip
Δ_{SH}	Displacement due to shear
Δ_{Ycalc}	Lateral displacement under which the longitudinal reinforcement in the column first yields
ε_c	Strain of unconfined concrete
ε_{cc}	Strain of confined concrete under the maximum compression stress
ε_{co}	Strain of unconfined concrete under the maximum compression stress
ε_{coc}	Corresponding strain for the compression strength f_{cc}
ε_{cu}	Ultimate strain value of the confined concrete
$\varepsilon_{f,eff}$	Effective strain
ε_{sh}	Strain of at the beginning of strain hardening
ε_{su}	Ultimate strain of reinforcement
ε_{sy}	Yielding strain of reinforcement
ε_{50h}	Difference of the strains in the descending regions of the confined and unconfined curves corresponding to $0.5f_c$
ε_{50u}	Strain corresponding to $0.5f_c$

ϕ	Angle of the diagonal line to the horizontal line of the brick wall
Φ_Y	Curvature at yielding of the longitudinal reinforcement
η_l	Modification coefficient for modulus of elasticity
θ	Critical crack/failure angle-assumed as 65°
θ	Strut inclination angle
ρ''	Transverse steel ratio
ρ_s	Volumetric transverse steel ratio
σ_c	Compression stress of concrete
σ_N	Vertical stress of the brick wall
τ_f	Frictional strength of the interface of the brick and mortar
ν	Poisson's ratio
ψ	Adjusting factor for the cracking strength

AISC	American Institute of Steel Construction
ATC	American Technology Council
CFRP	Carbon Fiber Reinforced Polymer
FRP	Fiber Reinforced Polymer
FEMA	Federal Emergency Management Agency
LVDT	Linear Variable Displacement Transformer
RC	Reinforced Concrete
SAP	Structural Analysis Program
TEC 2007	Turkish Earthquake Code 2007
TS 500	Requirements for Design and Construction of Reinforced Concrete Structures
XTRACT	Cross Section Analysis Program for Structural Engineers

1. INTRODUCTION

1.1.General Concepts

Turkey is one of the countries which experienced many destructive earthquakes in recent years such as, 2003 Bingöl Earthquake, 1999 Kocaeli-Gölcük and Bolu-Düzce Earthquakes, 1998 Adana-Ceyhan Earthquake, 1995 Dinar Earthquake, 1992 Erzincan-Tunceli Earthquake, 1983 Erzurum-Kars Earthquake, etc. The collapse of buildings, bridges and other structures, failure of non-structural components, and fire hazard resulting from broken gas or power lines cause most of the deaths and injuries during a seismic event. It is possible to solve this problem by constructing new structures according to earthquake codes and rehabilitating the existing ones by suitable methods.

It is believed that a significant portion of the building stock in Turkey was constructed between years 1970-1980. They include some common seismic deficiencies which cause significant hazard during a seismic event. These deficiencies can be summarized as insufficiencies in structural design, poor workmanship, poor quality of construction materials, formation of soft-weak stories, non-ductile reinforcement details, strong beam-weak column construction and torsion caused from poor arrangement of infill walls and the load bearing system. The above defined deficiencies cause ductility, strength and stiffness problems in the existing structural system. The entire building stock has to be seismically rehabilitated in order to reduce hazards that may occur in future earthquakes. Due to this fact, suitable rehabilitation techniques have to be implemented.

There are many experimental and analytical studies by researchers worldwide to examine the effects of various seismic rehabilitation techniques. Many of these studies were done in laboratory conditions to simulate the effects of strong ground motion to two-dimensional and sometimes three-dimensional frame specimens, in order to identify the collapse mechanisms and determine the effects of seismic rehabilitation techniques on the response. Most of these tests were done on scaled specimens that were constructed with deficiencies, but they cannot completely simulate real life specimens. There are few in-situ studies on real life buildings all over the world. The lack of field testing is mainly due to

economical considerations as well as the shortage of suitable buildings to be used as test specimens. Turkey can take on the role of a pilot region to run full scale static and dynamic in-situ tests due to having a testable building stock.

This thesis is prepared to provide the foundation for running full scale in-situ pushover tests for determining the seismic behavior of typical RC buildings in Turkey. It can be used as a reference study to propose test configurations for similar RC buildings. By conducting such tests, the optimum seismic rehabilitation techniques can be evaluated for such buildings.

1.2. Scope and Summary of Contents

In order to conduct an in-situ test, a test setup has to be proposed and computer based analyses have to be accomplished prior to field work for determining the required testing equipments and their capacities. The scope of this study is to define a sample in-situ testing scheme for a typical Turkish RC building. By using the information supplied in this thesis, it would be possible to prepare an appropriate in-situ testing scheme for such an RC building.

Chapter 2 of this thesis includes a comprehensive study on previous research on field and laboratory testing of different strengthening methods in literature. In Chapter 3, nonlinear modeling techniques from researchers worldwide are investigated. In Chapter 4, the efficiency of nonlinear modeling techniques presented in Chapter 3 are investigated by comparing the results of nonlinear analyses for a typical Taiwanese school building, namely the Hsin-Tseng Junior High School building, with experimental results presented in literature. In Chapter 5, a test setup is proposed for a typical Turkish school building, namely the Sehit Adem Yavuz Primary School building. The extent of the proposed tests include (i) a bare frame test, (ii) a brick infilled frame test, (iii) a CFRP strengthened brick infilled frame test, and (iv) an RC wall strengthened frame test. Also, geometrical properties and material properties of the building are detailed and an approximate time scheduling for in-situ tests is prepared in this chapter. In Chapter 6, the analyses results of test frames are summarized in terms of lateral load-displacement curves and hinge formation sequences. Also, brief information regarding the design of an out-of-plane

resisting frame is given in this chapter. In Chapter 7, the required equipment to perform in-situ pushover tests are determined in accordance with the analyses results and properties of the test frames. In the last chapter, conclusions and future recommendations are presented. The Appendices attached at the end of the thesis contains detailed drawings for the test building and the test configuration proposed.

2. LITERATURE SURVEY

2.1. In-situ Tests

The September 21, 1999 Chi-Chi earthquake caused nearly half of the school buildings in the central area of Taiwan to collapse or suffer serious damage. A total of 656 primary and secondary school buildings were damaged in that earthquake [2]. This disaster forced the Taiwanese authorities to investigate the seismic behavior of the existing school buildings and some analytical seismic evaluations as well as in-situ tests were done to evaluate the seismic performance levels of the school buildings.

A representative test on a full scale reinforced concrete school building was conducted in Taiwan on Hsin-Tseng Junior High School building at Hualien County [1]. During these investigations, both lateral and vertical loading tests were conducted on the two storey school building. In the lateral loading test, the building was separated into two parts along the longitudinal direction by cutting the structural and nonstructural elements. One part of the building was laterally strengthened by using nine steel braces located diagonally to be used as the reaction block while the other part of the building was tested. Six hydraulic jacks were placed at various columns of the reaction block to load the test structure. Displacement gauges were placed at both ends of the test frame and the loaded end of the reaction block. A 300 mm (four per cent drift) total lateral displacement was applied to the building and the base shear obtained was 1,942 kN. At 150 mm displacement (two per cent drift), a peak base shear value of 2,915 kN was obtained. Flexural and shear failure modes were identified at the end of the tests. The analytical pushover analysis of the same building predicted the same failure modes for the columns although the analytical pushover curve underestimated the lateral load capacity of the building. This was attributed by the researchers to omission of the out-of-plane contribution of the partition brick walls in the analytical model.

As a result of the tests, the lack of integral planning, lack of seismic resistance along corridors, presence of short columns and embedded pipelines, and lack of reinforcement

were identified as the key factors responsible for the collapse or high damage susceptibility of these kinds of buildings [2].

In August 2005, NCREE (National Center for Research on Earthquake Engineering) performed three in-situ pushover tests in Kouhu Elementary School at Yunlin County in Taiwan, including one bare frame, one retrofitted with RC walls and a third one retrofitted with brick walls. Before the test, a competition was announced to encourage individuals to evaluate the seismic capacity of these frames numerically. The nonlinear static analysis by Wu and Xue [3] yielded the most similar frame failure behavior and capacity curve to the actual one.

The in-situ tests and analytical studies yielded conservative results in terms of initial stiffness, ultimate strength and ductility. According to the in-situ tests, the bare frame had an ultimate load capacity of approximately 2,100 kN, the frames with the RC wing wall and the brick wing wall had an ultimate load capacity of approximately 2,800-2,900 kN. At the ultimate state, the drift ratio was half the bare frame value. The main difference between the RC wing wall and brick wing wall was that, for the frame with the brick wing wall, the lateral load capacity degraded quickly with the increase in the drift ratio.

The predictions of the analytical study were reasonably close to the results obtained during the in-situ tests, although the ultimate strength and ductility were underestimated. This was attributed to not considering the infill partition walls and floor slabs in the analysis which causes more stiffness and lateral strength.

Wu and Xue [3] also discussed the point that the lateral load pattern in the analytical studies was known from the in-situ tests. Since different lateral load patterns influence the seismic evaluation results seriously, the loading pattern use in the analytical and experimental studies might not represent the true behavior in an earthquake.

A series of in-situ experimental programs using an existing RC building, namely Reui-Pu elementary school building, was conducted in August, 2006 by Weng et al [4]. Three types of lateral loading patterns were imposed on three two-storey-two-classroom frame specimens: (i) monotonic static pushover, (ii) cyclic static pushover, and (iii)

earthquake time history input. RC shear walls were used as reaction blocks for two test buildings. For the test building under monotonic loading, steel braces were used to strengthen one part of the frame to be used as reaction wall. In addition, an innovative seismic strengthening technique, comprised of adding composite columns to partition brick walls, was also employed during these tests. The aims of these tests were to identify the dynamic behavior of typical RC school buildings built according to the design rules of common practice in Taiwan and to verify the feasibility of the innovative retrofitting technique on traditional RC school buildings.

Before the pushover tests, three types of excitations, i.e. free vibration, forced vibration and microtremor measurement, were used to identify modal frequencies and damping ratios to identify the dynamic behavior of the three frame specimens. The test results showed that specimens 1 and 2 which were subjected to cyclic lateral loading collocating with the pseudo dynamic seismic tests came out with proximate results in terms of stiffness and shear strength. The results of cyclic tests confirmed the damaging behavior of school buildings observed in the prior earthquakes in Taiwan. Typical failure characteristics of school buildings such as the short-column effect and the strong-beam-weak-column behavior were observed. The monotonic pushover procedure was seen to overestimate the shear strength and the stiffness after when the structural strength begins to decay.

In their conclusions, the authors recommended further studies regarding out-of-plane behavior of brick walls, torsional effects, and retrofit measures for resisting horizontal and vertical loads.

2.2 Seismic Rehabilitation Techniques

There have been many studies on retrofitting techniques in Turkey as well as all over the world. A study by Erdem et al. [5] investigated the performance of reinforced concrete infill walls and masonry infill walls with diagonal sheets of carbon fiber reinforced polymers (CFRP). The test specimens consisted of two 1/3 scaled, two-store-three-bay frames which were detailed to contain common seismic deficiencies generally found in RC buildings in Turkey (such as low concrete strength, splices made above floor levels with

inadequate lap length, insufficient lateral reinforcement at member ends, 90° hooks at the end of ties, very poor concrete quality and formation of soft-weak stories). One of the test frames was infilled with RC in the middle bay and the other frame was infilled with masonry having diagonal CFRP sheets on it. Another frame, which didn't contain any walls, was used as the reference bare frame. The study showed that both the RC infill and masonry infill strengthened with CFRP increased the lateral load capacity up to 4.6-5.4 times the bare frame capacity. The initial stiffness of the test frames increased up to 11-13 times the bare frame value. The drift ratio under maximum lateral load decreased to 0.4-0.5 times the bare frame value. The main difference between the two strengthening methods was that the lateral load suddenly dropped down after the peak load capacity level in the CFRP strengthened masonry in-filled frame case.

The study done by Canbay et al. [6] examined the contribution of RC infill walls to seismic behavior of structural systems. Again 1/3 scaled two-storey-three-bay frames with common seismic deficiencies were used in the tests. The tests employed reversed cyclic loading up to a roof drift level of 1.6 per cent. Both lateral and vertical loads were applied at the second floor level of the specimen. The results of this study showed that the RC infill increased the lateral load capacity of the bare frame, at the ultimate state, up to 3.8 times the bare frame value, and the initial stiffness of the bare frame increased up to 15 times in the RC in-filled case. The study also showed that, during the initial cycles, 99 per cent of the lateral load was carried by the infill wall and this ratio decreased to 90 per cent after yielding of the wall. At the end of the tests, partial strengthening was recommended by the authors to use infills with full capacity.

Nishiyama and Yazgan [7] studied a simple strengthening method used on a pre-stressed brace system using concrete filled tube (CFT) and fiber reinforced concrete (FRC). The study was conducted for seismic capacity evaluation of existing RC structures according to the Japanese standards and retrofitting with single line elements. The tests were performed on two half-scale RC portal frames strengthened with different brace materials. The RC portal frames were identical to the sub-assemblage of a four storey reinforced concrete building, which was designed following the pre-1980 Japanese Building Standard. At the end of the tests, the lateral load carrying capacity of the RC portal frame without the brace was 190 kN. By installing the braces, CFT and FRC

strengthened specimens had 320 kN and 547 kN lateral load capacities, respectively. It was observed that the proposed CFT brace system increased the lateral load capacity up to 1.7 times the bare frame capacity and FRC brace system increased the lateral load capacity up to 2.9 times the bare frame capacity.

Saatcioglu et al. [8] worked on seismic performance of masonry infill walls retrofitted with CFRP sheets. Two half-scale single-storey-single-bay RC frame concrete block infill assemblies were tested under simulated seismic loading. The specimens were built to reflect the majority of existing buildings constructed prior to 1970's with frames designed mainly for gravity loads. One specimen was retrofitted with CFRP sheets for improved seismic resistance. In these tests, two aspects of the retrofit strategy employed were investigated; the amount and arrangement of CFRP sheets, and the possibility of delamination of sheets and measures against them. The results of the experiments showed that the walls were able to stiffen the frames significantly, especially during the initial stages of loading. The lateral drift was controlled by the stiffening effect of the wall. A peak load of 273 kN was attained at approximately 0.25 per cent lateral drift ratio in the non-retrofitted case. The retrofitted specimen showed a substantial increase in stiffness and strength. It was observed that CFRP sheets controlled cracking and helped improve the rigidity of the wall. A peak load of 784 kN was attained at approximately 0.3 per cent lateral drift ratio in the retrofitted case. This indicated an improvement of lateral strength by a factor of 3. It was noted that surface bonded CFRP sheets do not contribute to ductility. Upon failure of the CFRP, the wall strength reduced to a level that is equivalent to that of un-retrofitted wall.

Ozden and Akguzel [9] worked on 1/3 scaled two-storey-single-bay frames and tested (i) bare frame, (ii) infilled but not strengthened, and (iii) strengthened by means of CFRP overlays applied as cross diagonal strut schemes. The test results showed that the strengthened specimen reached an ultimate load capacity of 1.94 times the un-strengthened but infilled specimen when the CFRP diagonal strut connections fully developed. The strengthened specimen reached its displacement capacity at a value 4.3 times bigger than the un-strengthened but infilled specimen. The un-strengthened infill increased the lateral load capacity of the bare frame to 5.5 times.

Tankut et al. [10] investigated the strengthening of RC frames with relatively high strength precast concrete panels which were epoxy glued to the infill walls and dowel connected to the frames. 1/3 scaled single-storey-single-bay and two-storey-single-bay frames with hallow brick masonry infill walls were used in the experiments. It has been generally accepted that hallow brick masonry infill contributes to the lateral load capacity during the initial stage but the frame behaves like a bare frame after rapid crushing of infill. Therefore the idea behind the proposed strategy was to increase the lateral load capacity not only in the initial stage, but also during higher displacement levels. According to this test, the lateral load capacity of the strengthened specimen increased up to 2.5 times relative to the masonry infill frame and 15 times relative to the bare frame. Lateral stiffness, ductility and energy dissipation properties also increased to 2-3 times for the strengthened frame relative to the masonry infill frame.

Turk [11] worked on seismic rehabilitation of RC frames by RC infills. Five 1/3 scaled two-storey-single-bay RC frames were used in the tests. Two of the frames were constructed with common seismic deficiencies in RC buildings in Turkey. One of the frames was used as a bare frame, the other four were first damaged and then strengthened with RC infills, and were tested up to failure under reversed cyclic loading. According to this study, addition of RC infill walls increased the lateral strength 8-13 times the bare frame value. The initial stiffness was 19-24 times greater than the bare frame. The addition of RC infills increased the energy dissipation capacity significantly.

Pinto and Taucer [12] conducted assessment and retrofit studies on full scale models of existing RC frames. The experiments were performed on two full scale four-storey-three-bay frames. One of the columns on every storey was strengthened by external reinforcement bars embedded in the concrete. External confining steel plates were added to the critical zones of the strengthened column. The researchers observed that the drift ratio and the deformation capacity of the retrofitted frame at least doubled compared to the bare frame. Another frame was tested for assessing the contributions of masonry infill walls. The results of the masonry infill case showed that the base shear capacity increased approximately 3-4 times and the corresponding drift ratio decreased. The masonry infill case also gave some idea about the soft storey problem because under lateral loading, at the first step, the cracking of the first storey infill walls suddenly occurred. After this cracking,

the lateral load capacity suddenly dropped but the lowest level of the lateral load capacity of the masonry infill case was approximately two times the bare frame case.

Broken and Bertoro [13] worked on 18 different specimens strengthened with different methods. The experimental study was conducted on 1/3 scaled three-storey-single-bay frames under monotonic and cyclic loading programs. By using two jacks axially located on columns and another jack laterally located on the third storey level, the conditions in an 11 storey building were represented. According to this study, when all the frames contained infill walls, unreinforced masonry increased the lateral load capacity up to 2.82 times, reinforced hallow masonry increased the lateral load capacity up to 5.20 times, solid brick reinforced with welded wire fabric (WWF) increased the lateral load capacity up to 5.05 times, and reinforced lightweight concrete increased the lateral load capacity up to 8 times compared to the lateral load capacity of the bare frame.

Aboutaha et al. [14] studied the use of rectangular steel jackets for seismic strengthening of non-ductile, rectangular RC columns with inadequate lap splices. Short lap splices and inadequate transverse reinforcement were used in the detailing of the columns. 6 large scale columns were tested under cyclic loading. The major variables investigated in this test program were the width of the column and the amount and distribution of the anchor bolts. The results showed that, column jacketing increased the lateral load capacity of the strengthened frame up to 2 times relative to the bare frame.

The analytical study by Girgin and Darilmaz [15] investigated the seismic response of infilled frames using pushover analysis. Three five-storey-three-bay RC planar frames were used in this study. One of the frames was a bare frame, the second frame had infill walls in every span and the third frame was infilled in every span except the first storey. The frames were designed according to TEC 2007 [16]. Four different lateral loading patterns were used in the analysis to investigate the effects of loading conditions. The results showed that infill walls increase lateral resistance and initial stiffness of the frames, and this increase depends on the infill arrangement (lateral resistance increased up to 2.5-3 times in the “all spans infilled” case relative to the bare frame for different loading patterns). An irregularity of infill configuration in elevation yielded a non-uniform stiffness distribution and significantly affected the storey drifts which are generally accepted as

damage indicators. This irregularity also changed the behavior to a non-ductile one and caused different collapse mechanisms such as soft storey. The sequence of damage formation changed when infill walls were added to the structural system. Infills also have a significant effect on the reduction of the global lateral displacement.

An analytical study at a typical interior frame in a regular plan building requiring upgrade was undertaken by Binici and Ozcebe [17]. The analysis specimen was a five-storey-four-bay frame including infill walls in the first and third vertical spans for every storey, simulating typical construction characteristics in Turkey. Four cases were analyzed by subjecting the frames to an inverted triangular displacement profile along the building height. First analysis was conducted by neglecting the presence of infill walls. Second analysis was performed by considering the presence of infill walls as strut elements. Third analysis was conducted by performing an upgrade of the building with CFRPs. The final analysis was conducted for the shear wall added case, in which walls were modeled using beam column elements along the centerline of the wall. According to the results of the analyses, the presence of infill walls increased the lateral load carrying capacity by about 30 per cent, whereas the displacement capacity of the building decreased due to rapid degradation of the infill walls and neighboring frame elements once the base shear capacity was reached. CFRP retrofitting technique resulted in strength increases of about 90 per cent compared to the bare frame whereas capacity increase was about 50 per cent compared to the infilled frame. RC wall retrofit resulted in similar strength levels as the CFRP retrofit alternative. The main difference between the CFRP and RC retrofit cases was that ductility of the RC wall was found to result in a ductile behavior whereas CFRP retrofit yielded limited ductility mainly due to progressive failure of the strengthened infill walls.

Summary of the experimental studies about the influence of various strengthening methods on lateral load and drift capacity of RC frame specimens are presented in Table 2.1. In this table, values obtained experimentally for the lateral load capacity and the drift at lateral load capacity of strengthened frame specimens are compared with values obtained for bare frame and brick-infilled frame specimens whenever available.

Table 2.1. Summary of various strengthening methods by different researchers

	Increase in lateral load capacity relative to the bare frame	Increase in lateral load capacity relative to the masonry infilled frame	Increase in drift ratio at maximum. load relative to bare frame	Increase in initial stiffness relative to bare frame	Frame properties	Reference
Unreinforced Brick Infilled Frames	5.5 times	-	0.2 times	-	2 storey 1 bay	[9]
	3-4 times	-	-	-	4 storey 3 bay	[12]
	2.5-3 times	-	-	-	5 storey 3 bay (analytical)	[15]
	1.3 times	-	-	-	5 storey 4 bay (analytical)	[17]
	2.82 times	-	-	-	3 storey 1 bay (sub-assemblage of 11 storey)	[13]
Reinforced Brick Infilled Frames	5.2 times	-	-	-	3 storey 1 bay (sub-assemblage of 11 storey)	[13]
Reinforced Concrete Infilled Frames	3.8 times	-	-	15 times	2 storey 3 bay strengthened at middle bay	[6]
	5-5.4 times	-	0.5 times	11-13 times	2 storey 3 bay strengthened at middle bay	[5]
	8-13 times			19-24 times	2 storey 1 bay	[11]
	1.9 times	1.5 times			5 storey 4 bay (analytical)	[17]
	8 times	-	-		3 storey 1 bay (sub-assemblage of 11 storey)	[13]
CFRP-strentghened brick infilled frames	4.6-5.4 times	-	0.4 times	11-13 times	2 storey 3 bay strengthened at middle bay	[5]
	1.9 times	1.5 times	-	-	5 storey 4 bay (analytical)	[17]
	-	3 times	-	-	1 storey 1 bay	[8]
	10.67 times	1.94 times	4.3 times	-	2 storey 1 bay	[9]

	Increase in lateral load capacity relative to the bare frame	Increase in lateral load capacity relative to the masonry infilled frame	Increase in drift ratio at maximum. load relative to bare frame	Increase in initial stiffness relative to bare frame	Frame properties	Reference
Brick-infilled frames strengthened with high strength precast panels	15 times	2.5 times	-	2-3 times	1 storey 1 bay and 2 storey 1 bay	[10]
Column Jacketing	2 times	-	-	-	4 storey 3 bay	[12]
	2 times	-	-	-	single column jacketed with steel	[14]
Prestrssed brace system (Concrete Filled Tube)	1.7 times	-	-	-	1 storey 1 bay (sub-assemblage of 4 storey)	[7]
Prestressed brace system (Fiber Reinforced Concrete)	2.9 times	-	-	-	1 storey 1 bay (sub-assemblage of 4 storey)	[7]

3. ANALYTICAL MODELLING AND PUSHOVER ANALYSIS

In order to get satisfactory/realistic results in computer based structural analysis, the structural model and the material properties have to be defined properly in the computer model. In this chapter, the material models used in the analyses and the nonlinear behavior models of the structural systems are briefly explained.

3.1. Material Models

3.1.1. Concrete Models

Concrete is a nonlinear, inelastic, non-homogenous and anisotropic material. The strength-deformation relationship is the most important parameter to be defined for a structural model. There are many stress-strain models for concrete studied by many researchers. Richart, Brandtzaeg and Brown's Model [18], Sheikh and Uzumeri's Model [19], Mander, Preistley and Park's Model [20] are some of them.

For unconfined concrete, Hognestad concrete model [21] gives a basic stress-strain relationship. According to this, initial portion of the stress-strain curve is represented by a parabolic curve and the descending portion is represented by a straight line. Ultimate strain ε_{cu} is used as 0.0038 in this model. Figure 3.1 shows a schematic diagram of the Hognestad Curve and its formulation.

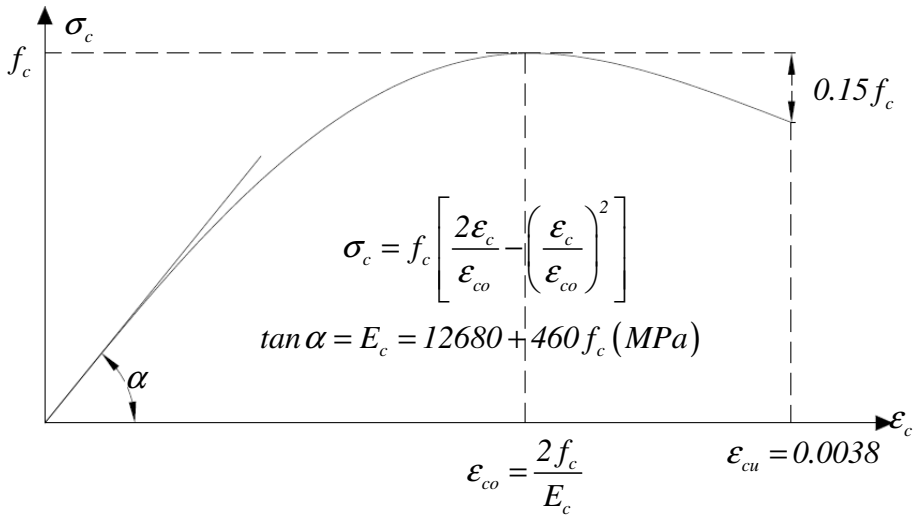

Figure 3.1. Hognestad stress-strain model of concrete

The ascending and descending portions of the Hognestad curve are formulized as:

$$\sigma_c = \begin{cases} f_c \left[\frac{2\varepsilon_c}{\varepsilon_{co}} - \left(\frac{\varepsilon_c}{\varepsilon_{co}} \right)^2 \right] \; when \; 0 \le \varepsilon_c \le \varepsilon_{co} \\ f_c \left[1 - 0.15 \frac{\varepsilon_c - \varepsilon_{co}}{0.0038 - \varepsilon_{co}} \right] \; when \; \varepsilon_{co} < \varepsilon_c \le \varepsilon_{cu} \end{cases} \tag{3.1}$$

where ε_c is the strain of unconfined concrete, ε_{co} is the strain of unconfined concrete under the maximum compression stress, σ_c is the compression stress of concrete, and f_c is the maximum compressive strength in concrete which equals to:

$$f_c = 0.85 f_{ck} \tag{3.2}$$

where f_{ck} is the characteristic compressive strength of concrete.

Mander's [20] mathematical model for stress-strain relationship works for both confined and unconfined concrete. The parameters used in this model are determined by statistical analysis of an extensive set of experimental data. For cyclic behavior, the model uses smooth connecting curves between the tension and compression envelopes. According to TEC 2007, Mander's Model can be used to model concrete. Figure 3.2 shows the graphical representation of the stress-strain model where ε_{co} refers to the strain of unconfined concrete under the maximum compression stress, ε_{cc} refers to the strain of confined concrete under the maximum compression stress, ε_{cu} refers to the ultimate strain value of the confined concrete, f_{co} refers to the compression strength of the unconfined concrete, and f_{cc} refers to the compression strength of the confined concrete.

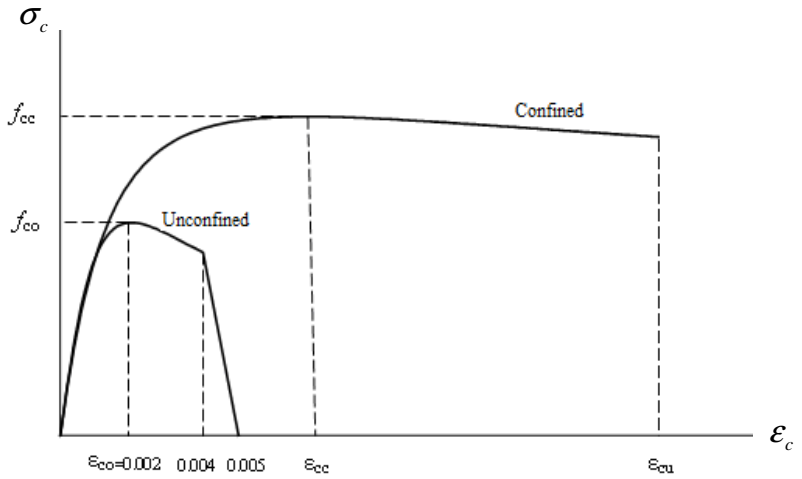

Figure 3.2. Stress-strain relationship of concrete according to Mander's Model

Another widely used model for the stress-strain relationship of concrete is the Modified Kent and Park Model [22], the details of which are presented in Figure 3.3.

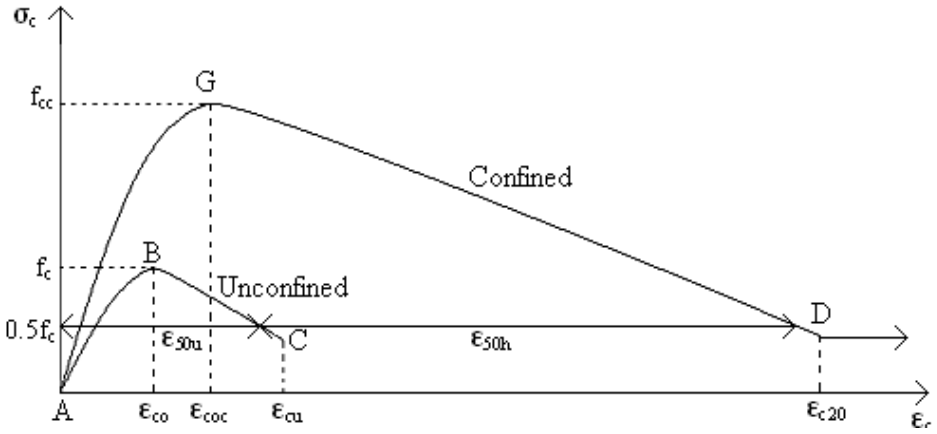

Figure 3.3. Modified Kent and Park Model for concrete

In the Modified Kent and Park Model, the strain ε_{co} corresponding to the maximum stress value of the unconfined concrete and the strain ε_{cu} corresponding to the ultimate stress value of the unconfined concrete are:

$$\varepsilon_{co} = 0.0002 \quad \varepsilon_{cu} = 0.0004 \quad Usually\, f_c = f_{ck}$$

where f_{ck} is the characteristic compressive strength of concrete.

The unconfined A-B part is formulized with a parabolic relationship similar to the Hognestad curve:

$$\sigma_c = f_c \left[\frac{2\varepsilon_c}{\varepsilon_{co}} - \left(\frac{\varepsilon_c}{\varepsilon_{co}} \right)^2 \right] \tag{3.3}$$

The unconfined B-C part is formulized with a linear relationship:

$$slope = -\left[\frac{0.5 f_c}{\varepsilon_{50u} - \varepsilon_{co}} \right] \tag{3.4}$$

where ε_{50u} is the strain corresponding to $0.5 f_c$ in the descending portion of the unconfined part B-C.

$$z_u = -\frac{slope}{f_c} = \left[\frac{0.5}{\varepsilon_{50u} - \varepsilon_{co}} \right] \tag{3.5}$$

$$\varepsilon_{50u} = \frac{3 + 0.285 f_c}{142 f_c - 1000} \geq \varepsilon_{co} \tag{3.6}$$

$$\sigma_c = f_c \left[1 - z_u \left(\varepsilon_c - \varepsilon_{co} \right) \right] \tag{3.7}$$

The confined A-G part is formulized with a parabolic relationship:

$$\sigma_c = f_{cc} \left[\frac{2\varepsilon_c}{\varepsilon_{coc}} - \left(\frac{2\varepsilon_c}{\varepsilon_{coc}} \right)^2 \right] \tag{3.8}$$

where f_{cc} refers to the compression strength of the confined concrete and ε_{coc} refers to the corresponding strain for the compression strength, and they are defined by:

$$f_{cc} = K f_c \tag{3.9}$$

$$\varepsilon_{coc} = K\varepsilon_{co} \tag{3.10}$$

in which the parameter K equals to:

$$K = 1 + \rho_s \frac{f_{ywk}}{f_c} \tag{3.11}$$

where f_{ywk} represents the yield strength of transverse reinforcement (MPa), f_c represents the compression strength of unconfined concrete, and ρ_s represents the volumetric transverse steel ratio in the cross section.

The confined G-D part is formulized with a linear relationship:

$$\sigma_c = f_{cc}\left[1 - z_c\left(\varepsilon_c - \varepsilon_{coc}\right)\right] \geq 0.2 f_{cc} \tag{3.12}$$

where the parameter z_c equals to:

$$z_c = -\frac{slope}{f_{cc}} = \left[\frac{0.5}{\varepsilon_{50u} + \varepsilon_{50h} - \varepsilon_{coc}}\right] \tag{3.13}$$

$$slope = -\left[\frac{0.5 f_{cc}}{\varepsilon_{50u} + \varepsilon_{50h} - \varepsilon_{coc}}\right] \tag{3.14}$$

where ε_{50h} is defined as the difference of the strains in the descending regions of the confined and unconfined curves corresponding to $0.5 f_c$ and it is formulized as:

$$\varepsilon_{50h} = 0.75 l_s \sqrt{\frac{b_k}{s}} \tag{3.15}$$

where l_s is the total length of the transverse reinforcing bars, b_k is the smaller dimension of the confined core measured from outside to outside of ties, and s is the spacing of the transverse reinforcement bars.

3.1.2. Reinforcing Steel Models

For reinforcement steel, the stress-strain relationship consists of three regions, elastic region, plastic plateau region and strain hardening region. The most important properties of the stress-strain diagram of reinforcing steel are the yield strength, the ultimate strength and the strain capacity. According to Turkish Building Code Requirements for Reinforced Concrete (TS500-2000) [23], the grades of reinforcement steel are specified according to the mechanical properties of steel, as Table 3.1.

Table 3.1. Mechanical properties of reinforcing steel

Mechanical Properties	Reinforcing bars					Welded Wire Mesh
	Hot Rolled			Cold Worked		
	S220a	S420a	S500a	S420b	S500bs	S500bk
Minimum Yield Strength $f_{yk}\,(MPa)$	220	420	500	420	500	500
Minimum Yield Strength $f_{su}\,(MPa)$	340	500	550	550	550	550
Minimum Strain Capacity ε_{su} $(\phi \le 32mm)$	0.18	0.12	0.12	0.10	0.08	0.05
Minimum Strain Capacity ε_{su} $(50mm \ge \phi > 32mm)$	0.18	0.10	0.10	0.10	0.08	0.05

According to TEC 2007, the stress strain relationship defined in Figure 3.4 can be used to model the reinforcement steel. In this diagram ε_{sy} refers to yielding strain of reinforcement, ε_{sh} refers to strain of at the beginning of strain hardening, ε_{su} refers to the ultimate strain of reinforcement, f_{sy} refers to yielding strength of reinforcement, and f_{su} refers to the ultimate strength of reinforcement.

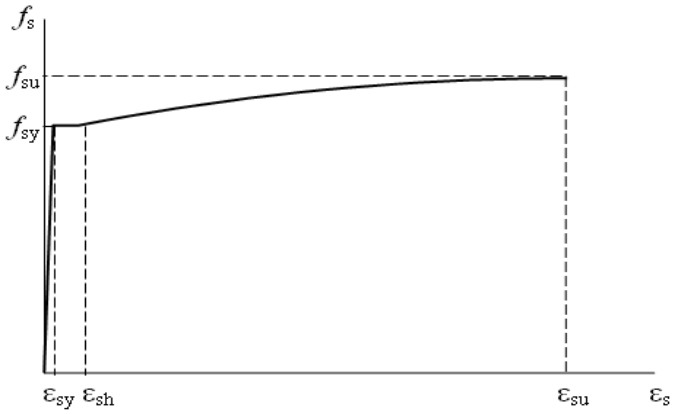

Figure 3.4. Stress-strain relationship for reinforcement steel according to TEC 2007

The equations presenting the linear and nonlinear parts of the stress strain relationship is formulized as:

$$f_s = E_s \times \varepsilon_s \quad \text{when } \varepsilon_s \le \varepsilon_{sy} \tag{3.16}$$

where E_s is the modulus of elasticity of reinforcement steel and equals to 200,000MPa.

$$f_s = f_{sy} \quad \text{when } \varepsilon_{sy} < \varepsilon_s \le \varepsilon_{sh} \tag{3.17}$$

$$f_s = f_{su} - \left(f_{su} - f_{sy}\right)\frac{\left(\varepsilon_{su} - \varepsilon_s\right)^2}{\left(\varepsilon_{su} - \varepsilon_{sh}\right)^2} \quad \text{when } \varepsilon_{sh} < \varepsilon_s < \varepsilon_{su} \tag{3.18}$$

The associated strain and strength values for S220 steel and S420 steel is given in Table 3.2.

Table 3.2. Strain and strength values for S220 and S420 according to TEC 2007

Class	$f_{sy}(MPa)$	ε_{sy}	ε_{sh}	ε_{su}	$f_{su}(MPa)$
S220	220	0.0011	0.011	0.16	275
S420	420	0.0021	0.008	0.10	550

3.2. Nonlinear Behavior Models for Structural Elements

The structural members used in this thesis consist of frame elements, infill walls, RC shear walls and infill walls strengthened with CFRP. In order to get realistic results from numerical analyses, correct structural modeling is very important. Analytical models used to investigate the behavior of the structural elements are briefly explained below.

3.2.1. Modeling the Frame Members

To represent nonlinear behavior, plastic hinges are used on frame members. These plastic hinges are placed at the regions where nonlinear behavior is expected. To represent the flexural failure mechanism in columns, inelastic axial force-moment (P-M) interaction hinges are used at both ends of the members. This behavior is simulated with inelastic M-hinges located at both ends of beam elements. To represent the shear failure mechanism, inelastic shear hinges are located at a distance of one-third of the member length to the joint. For inelastic axial behavior, plastic hinges are placed at a distance of two-third of the member length to the joint. The locations of the axial hinges are irrelevant since the axial load is constant along the length of the structural elements. The hinge length is taken equal to half the cross sectional dimension perpendicular to the axis of bending in accordance with TEC 2007.

3.2.1.1. Moment (M) Hinges. Since the inelastic flexural deformations are expected to occur at the ends of the beam and column members, moment hinges are placed there. A hinge length of h/2, where h is the section depth, is used (TEC 2007). A moment-curvature analysis, which is needed to represent the flexural behavior, has to be done in order to get the moment-curvature relationship of a section. In this thesis, a program developed by Ersoy [24] and commercial software called XTRACT-Sectional Analysis Program [25] have been employed to find the moment-curvature relations. Moment and curvature values at yield points and scale factors in accordance with the moment-curvature diagrams are entered to SAP2000.v11.0.0 [26]. Figure 3.5 shows a typical moment-relationship for a nonlinear moment hinge used in the analyses.

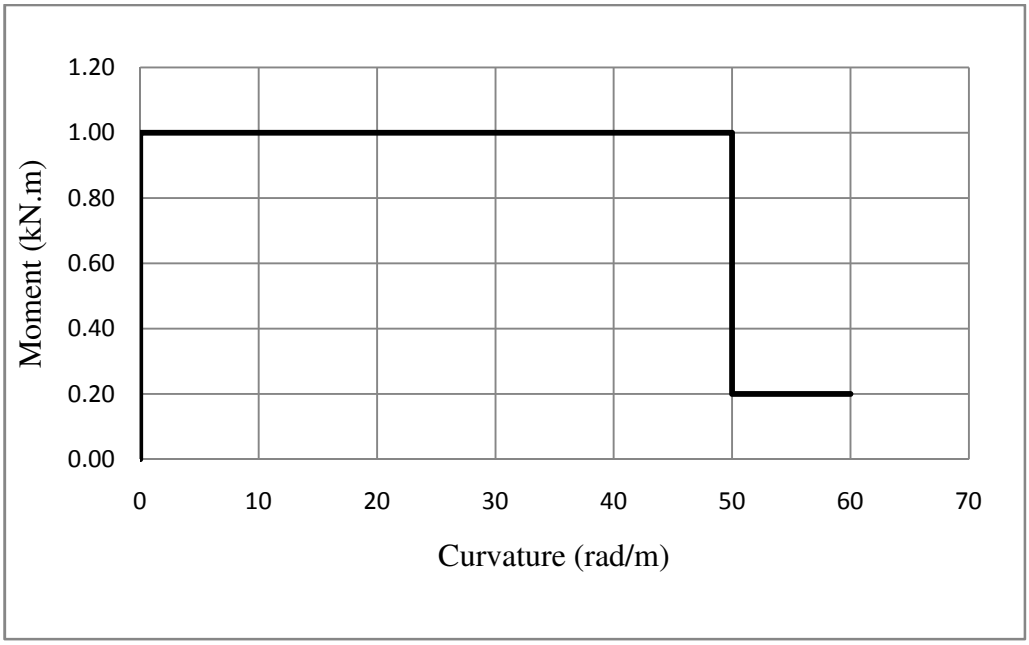

Figure 3.5. Typical moment-curvature relationship for a nonlinear moment hinge

3.2.1.2. Axial Force-Moment (P-M) Hinges. Axial force-moment interaction hinges are assigned to the end points of the column elements since nonlinear flexural deformations are expected in these regions. A hinge length of h/2 is used. The P-M interaction relationship can be acquired by Ersoy's Excel spreadsheet program or XTRACT Sectional Analysis Program. Since it is not possible to enter a continuous interaction diagram to SAP2000v.11.0.0, minimum four-point linearization is used. Pure compression point, balance point, pure bending point and pure tension point are taken into account to linearize the interaction diagram. For each of the axial force values, a moment-curvature relationship, similar to the one defined in Figure 3.5 is entered to the computer program.

3.2.1.3. Axial Force (P) Hinges. Force-displacement relationship for each section is used to determine the axial hinges. Axial hinges are used in the column members as well as the beam members to represent possible axial deformations. Although the axial forces on the beam elements are insignificant before lateral loading, they increase substantially once lateral loading is considered. For inelastic axial behavior, plastic hinges are placed at a distance of one-third of the member length to the joint. The locations of the axial hinges are irrelevant since the axial load is assumed to be constant along the height of the column. Yield force and displacement values for tension and compression have to be determined. A

sample force-displacement graph and its parameters for the corresponding nonlinear axial hinge are given in Figure 3.6 and Table 3.3, respectively.

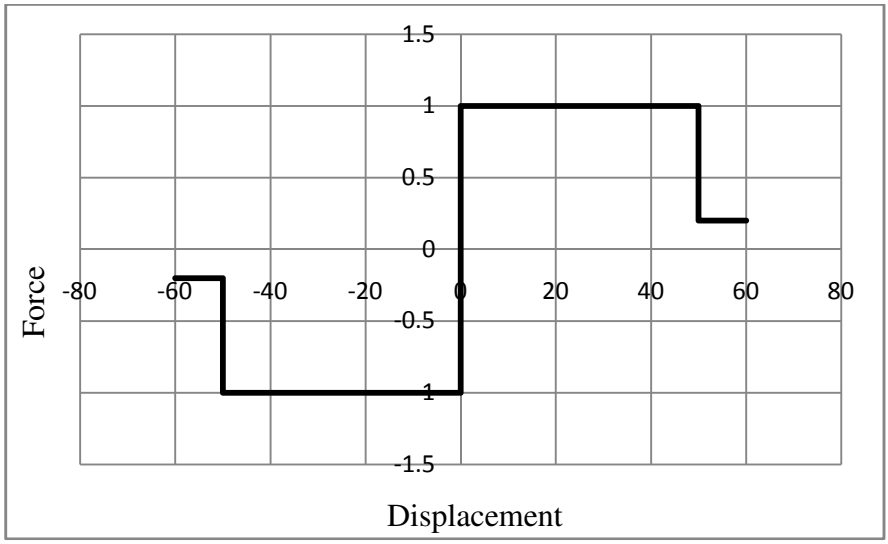

Figure 3.6. Force-displacement relationship for a typical nonlinear axial hinge

Table 3.3. Data points for the nonlinear axial hinge of Figure 3.6

Points	Disp./SF	Force/SF
-E	-60	-0.2
-D	-50	-0.2
-C	-50	-1
-B	0	-1
A	0	0
B	0	1
C	50	1
D	50	0.2
E	60	0.2

3.2.1.4. Shear (V) Hinges. The lack of transverse reinforcement and poor concrete quality can cause shear failures in RC buildings. Shear failure occurs suddenly and it's a brittle failure type. Therefore, in order to be on the safe side, lower bounds of the shear capacity for the members have to be calculated. The force-displacement relationship for each section and the corresponding shear capacity can be calculated according to TS500-2000 as:

$$V_{cr} = 0.65 f_{ct} b_w d \psi \tag{3.19}$$

where V_{cr} is the cracking strength of concrete, f_{ct} is the flexural tensile strength of concrete, ψ is the adjusting factor for the cracking strength, b_w is the width of the section, and d is the effective depth of the section.

When axial force on the member (N_d) is tension:

$$\psi = 1 + 0.3 \frac{N_d}{A_c} \qquad N_d \text{ is (-)} \tag{3.20}$$

When N_d is compression:

$$\psi = 1 + 0.07 \frac{N_d}{A_c} \qquad N_d \text{ is (+)} \tag{3.21}$$

When the normal stress on the column section is smaller than $0.5Mpa, \psi = 1$:

$$\psi = 1 \text{ for } \frac{N_d}{A_c} < 0.5MPa \tag{3.22}$$

The shear capacity of the section equals to:

$$V_{cap} = V_c + V_w \tag{3.23}$$

$$V_c = 0.8 V_{cr} \tag{3.24}$$

$$V_w = \frac{A_{sw} f_{ywk} d}{s} \tag{3.25}$$

where V_c is the contribution of concrete forces, V_w is the contribution of the steel forces, A_{sw} is the total cross-sectional area of the transverse reinforcement, *d* is the effective depth of the section, *s* is the spacing of the transverse reinforcement and f_{ywk} is the yield strength of transverse reinforcement bars.

The drift capacity at peak shear force is determined as 1.5 per cent and the drift capacity at shear failure is determined as 3 per cent according to the study of Wu and Xue [3]. A sample force-displacement graph and its parameters for a nonlinear shear hinge are given in Figure 3.7 and Table 3.4, respectively.

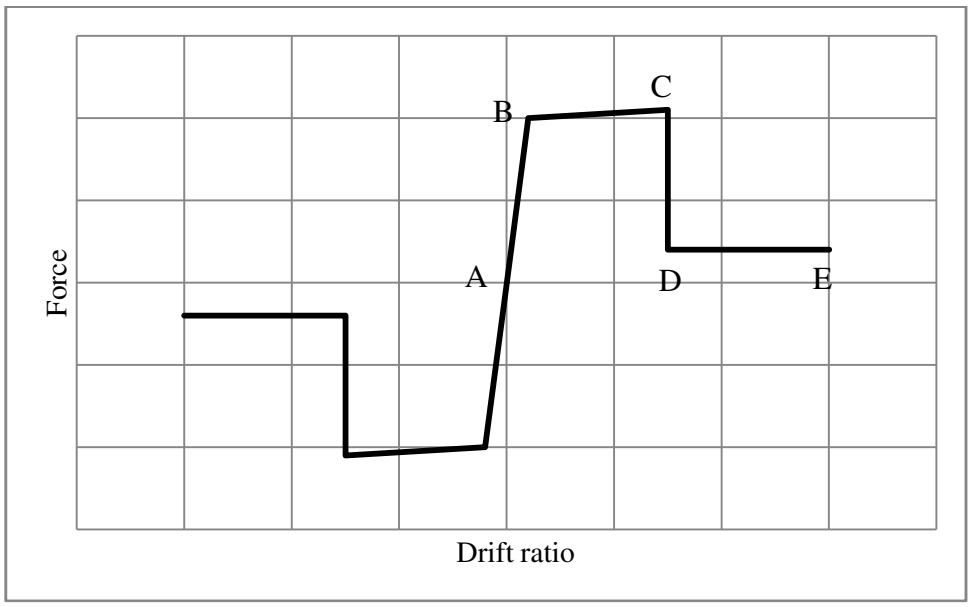

Figure 3.7. Force-displacement relationship for a typical nonlinear shear hinge

Table 3.4. Data points for the nonlinear shear hinge of Figure 3.7

Points	Drift Ratio/SF	Force/SF
-E	-0.03	-0.2
-D	-0.015	-0.2
-C	-0.015	-1.05
-B	$-\theta_y$	-1
A	0	0
B	θ_y	1
C	0.015	1.05
D	0.015	0.2
E	0.03	0.2

For shear critical columns, the idealized backbone model of Elwood and Moehle [27] was used to represent the shear load versus lateral displacement behavior. The backbone model utilizes column drift ratios at yielding, shear and axial failure as well as the yield moment derived from the column's moment-curvature response. The lateral displacement Δ_{Ycalc} under which the longitudinal reinforcement in the column first yields is calculated by summing up the displacements due to flexure (Δ_{FL}), bar (bond) slip (Δ_{SL}) and shear (Δ_{SH}):

$$\Delta_{Ycalc} = \Delta_{FL} + \Delta_{SL} + \Delta_{SH} \tag{3.26}$$

For a column that is fixed against rotation at both ends, when a moment load is induced in the column, flexural deformation resulting with lateral displacement occurs. Figure 3.8 shows this behavior.

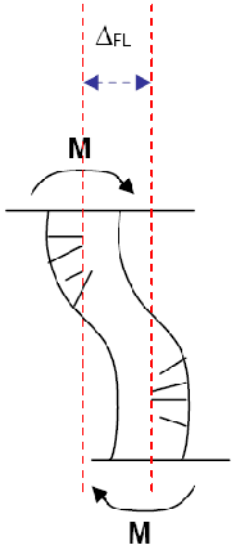

Figure 3.8. Flexural deformation in a column [27]

According to Elwood and Moehle's study, the following empirical relationship is used to calculate the lateral displacement due to flexure before the yielding of the longitudinal reinforcement occurs:

$$\Delta_{FL} = \frac{L^2 \Phi_Y}{6} \tag{3.27}$$

where L is the length of the column and Φ_Y is the column curvature at yielding of the longitudinal reinforcement.

For an RC column subjected to lateral load, the slip of the longitudinal reinforcement within the anchor block can cause elongation in the longitudinal reinforcement resulting in lateral displacement. Figure 3.9 shows this behavior.

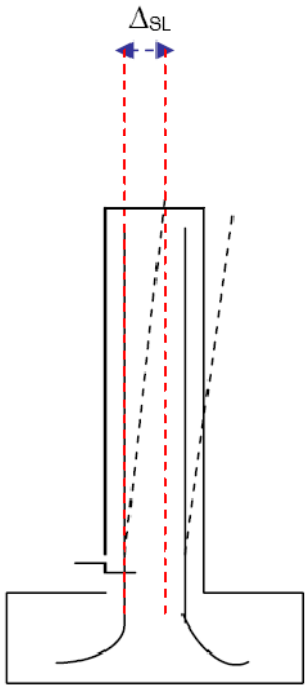

Figure 3.9. Bar (bond) slip in a column [27]

According to Elwood and Moehle's study, the following empirical relationship is used to calculate the lateral displacement due to bar (bond) slip before the yielding of the longitudinal reinforcement occurs:

$$\Delta_{SL} = \frac{L d_B f_{YL} \Phi_Y}{8u} \tag{3.28}$$

where d_B is the diameter of the longitudinal reinforcement and $u = 6\sqrt{f_c'}\,(psi)$ is the bond stress between the longitudinal reinforcement and the column footing.

For a column that is fixed against rotation at both ends, when lateral loading produces shear stresses at the column ends, displacement occurs. Figure 3.10 shows this behavior.

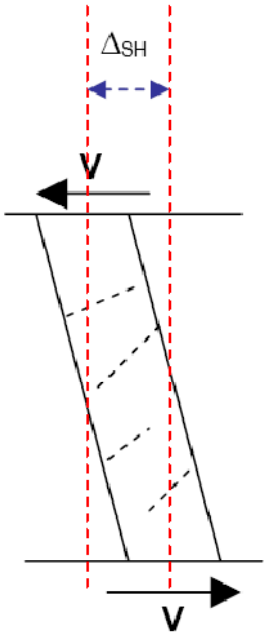

Figure 3.10. Shear deformation in a column [27]

According to Elwood and Moehle's study, the following empirical relationship is used to calculate the lateral displacement due to shear before the yielding of the longitudinal reinforcement occurs:

$$\frac{2M_Y}{GA_V} \tag{3.29}$$

where M_Y is the column moment at yielding of the longitudinal reinforcement, G is the shear modulus assuming the column is homogenous in material and A_V is the shear area of the column cross section.

For a shear critical column, deformation at shear failure is calculated according to the study by Elwood and Moehle [28]. This study was conducted on rectangular columns, confined by relatively light and widely spaced transverse reinforcement subjected to unidirectional lateral load, and shear failure was defined as the loss of 20 per cent of the maximum shear strength. According to this study, the empirical relationship given below is used for drift ratio at shear failure:

$$\frac{\delta_s}{L} = \left(\frac{3}{100}\right) + 4\rho'' - \frac{1}{500}\frac{V}{\sqrt{f_c'}} - \frac{1}{40}\frac{P}{A_g f_c'} \geq \frac{1}{100} \tag{3.30}$$

where δ_s is the flexure-shear failure displacement, L is the length of the frame member, A_g is the gross cross sectional area of the frame member, ρ'' is the transverse steel ratio, V is the nominal shear stress, and P is the axial load on the frame member.

For columns initially yielding in flexure, then developing shear failure, and finally developing axial failure, Elwood and Moehle [29] derived another empirical expression with which the drift ratio at axial load failure is estimated as:

$$d = \frac{\delta_a}{L} = \left(\frac{4}{100}\right)\frac{\left(1 + (\tan\theta)^2\right)}{\tan\theta + P\dfrac{s}{A_{st} f_{yt} d_e \tan\theta}} \tag{3.31}$$

where δ_a represents the axial failure displacement, θ represents the critical crack angle-assumed as 65°, f_{yt} represents the yield strength of transverse reinforcement, and d_e represents the depth of the column core from centerline to centerline of the ties.

The representation of a sample force-displacement relationship used for shear critical columns is shown in Figure 3.11.

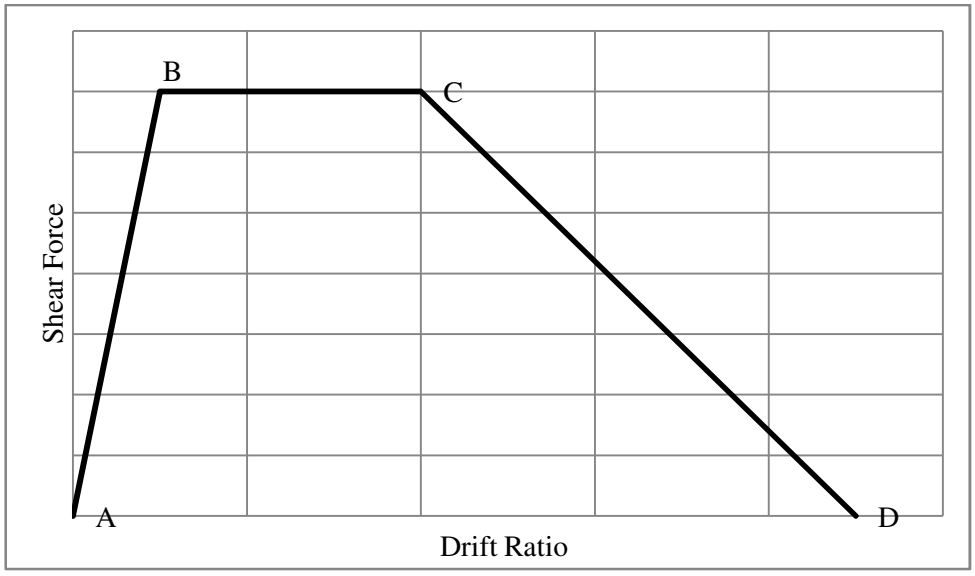

Figure 3.11. Shear force-displacement relationship for a typical nonlinear shear hinge

Table 3.5. Parameters for the nonlinear shear hinge in Figure 3.11

Points	Displacement	Shear Force /SF
A	0	0
B	Δ_Y / L	$V_u = 2M_u / L$
C	Δ_S / L	$V_u = 2M_u / L$
D	Δ_A / L	0

3.2.2. Modeling of the Infill Walls

Infills have been generally considered as non-structural elements. Although there are codes such as the Eurocode-8 [30] that include rather detailed procedures for designing infilled RC frames, presence of infills have been ignored in most of the seismic codes (except for their weight). However, even though they are considered non-structural elements, the presence of infills in RC frames can substantially change the seismic response of buildings, in certain cases producing undesirable effects (torsional effects, dangerous collapse mechanisms, soft storey effects, variations in the vibration period, etc.), or favorable effects such as increasing the seismic resistance capacity of the building [15].

There are many parametric studies done to capture the effects of infills. These studies mainly focused on evaluating experimental behavior of masonry infilled frames to obtain

some empirical formulations. The studies mainly have been based on limit strength-equivalent stiffness and/or force-deformation response.

The idea of analytical modeling of infill walls can be investigated in two categories: Micro models and macro models. Micro models include finite element models to predict the response of infilled frames, but such modeling is too time consuming when analyzing large scale structures. On the other hand, macro models allow treatment of the entire infill wall as a single unit [31]. In this study, rather than micro modeling, macro modeling is used to model the infill walls. The main disadvantage of macro modeling is that this approach does not permit study of local effects such as frame-infill interaction within the individual infilled frame subassemblies. More detailed micro-modeling approaches such as finite element models need to be used to capture the spatial and temporal variations of the local conditions within the in-filled frame [15].

An equivalent strut concept is used to model the load-deformation relationship of the infill walls with a single element pin jointed to the column members. The equivalent strut concept was first proposed by Holmes [32]. According to this study, an equivalent pin jointed diagonal strut of the same material with a width of one-third of the infills diagonal length can be used to model the infill wall. In 1971, Mainstone [33] provided empirical formulations in terms of a theoretical relation parameter λh that relates the width of the diagonal strut to the infill frame stiffness:

$$\lambda h = \sqrt[4]{\frac{\left(E_{inf} t_{inf} \sin 2\theta\right)}{4EI_c h_{inf}}} \tag{3.32}$$

where E_{inf} represents Young's modulus of the infill, E represents the frame modulus of elasticity, t_{inf} represents the thickness of the infill, I_c represents the column moment of inertia, and h_{inf} represents the height of the infill wall.

Another method to represent the infill walls is using a single equivalent column element using composite section properties. Restraint and boundary conditions of this equivalent element ought to be set properly to represent the real structure behavior [3].

3.2.2.1. Axial Force (P) Hinges for Brick Walls. Brick wall hinges used in the model are determined according to the study by Chen [34]. Because the failure behavior of the brick wall is affected by diagonal strut action and the particular construction method, the major failure path will spread across the brick joints along the diagonal direction until the wall reaches its ultimate strength. This model proposes the failure path concept to evaluate the failure behavior and to calculate the ultimate strength of the infilled brick walls, and uses the plate equation of elasticity theory and brick prism test to specify the stiffness formula of brick wall.

The equivalent truss modal used to simulate the brick wall is schematically shown in Figure 3.12.

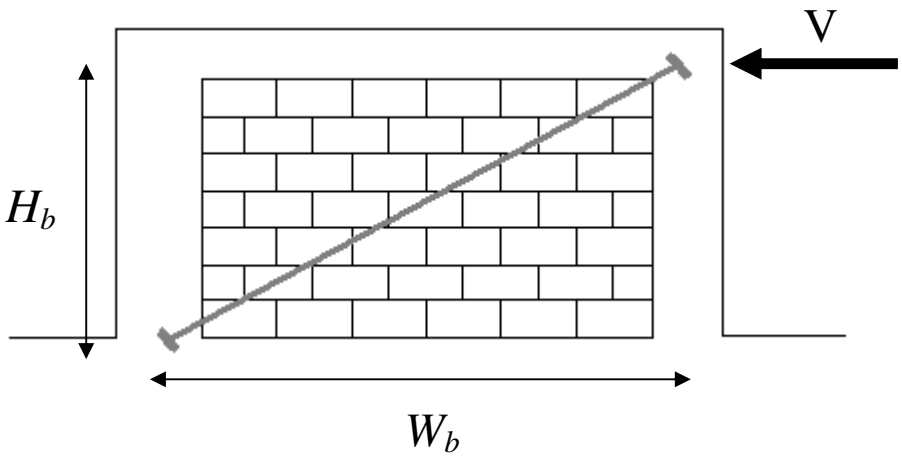

Figure 3.12. Representation of the equivalent truss model

Under a lateral load, the axial load on the truss can be calculated as:

$$P_d = \frac{V}{\cos\phi} \tag{3.33}$$

where ϕ is the angle of the diagonal line to the horizontal line of the brick wall calculated as:

$$\phi = \tan^{-1}\frac{H_b}{W_b} \tag{3.34}$$

Here, H_b is the height of the brick wall and W_b is the width of the brick wall.

The axial displacement of the truss under axial load can be calculated according to the basic mechanics of materials formula:

$$\Delta_d = \frac{P_d L_d}{E_d A_d} \tag{3.35}$$

where A_d is the cross-sectional area of the equivalent truss, L_d is the length of the equivalent truss, and E_d is the modulus of elasticity of the equivalent truss member.

The relationship between lateral load and horizontal displacement is defined as:

$$\Delta = \lambda \frac{V}{ET_b} \tag{3.36}$$

where,

$$\lambda = \left[\left(\frac{5}{4} + \frac{3}{2}\nu \right) \frac{W_b}{H_b} + \left(2 + \frac{7}{4}\nu \right) \frac{H_b}{W_b} + \left(2 + \frac{3}{2}\nu \right) \frac{H_b^3}{W_b^3} \right] \tag{3.37}$$

and ν is the Poisson's ratio which is taken to be equal to $v = 0.15$.

The geometrical condition shows that axial displacement equals:

$$\Delta_d = \Delta \cos\phi \tag{3.38}$$

By equations (3.33), (3.35) and (3.38), the equivalent truss area can be calculated as:

$$A_d = \frac{L_d T_b}{\lambda \cos^2 \phi} \tag{3.39}$$

and the depth of the equivalent truss can be calculated as;

$$W_d = \frac{A_d}{T_b} = \frac{L_d}{\lambda \cos^2 \phi} \tag{3.40}$$

The normal critical failure angle θ is influenced by the types of the bricklaying.

For Type 1 bricks;

$$\tan\theta = \frac{h + g_h}{w + g_v} \tag{3.41}$$

For Type 2 bricks;

$$\tan\theta = \frac{2\left(h + g_h\right)}{w + l + 2g_v} \tag{3.42}$$

For Type 3 bricks;

$$\tan\theta = \frac{3\left(h + g_h\right)}{2\left(w + g_v\right)} \tag{3.43}$$

For Type 4 bricks;

$$\tan\theta = \frac{2\left(h + g_h\right)}{l + g_v} \tag{3.44}$$

where, l, w and h are the length, width and thickness of the brick, respectively, and g_h and g_v are the horizontal and vertical seam width of the brick. In our analyses, we use Type 4 bricks.

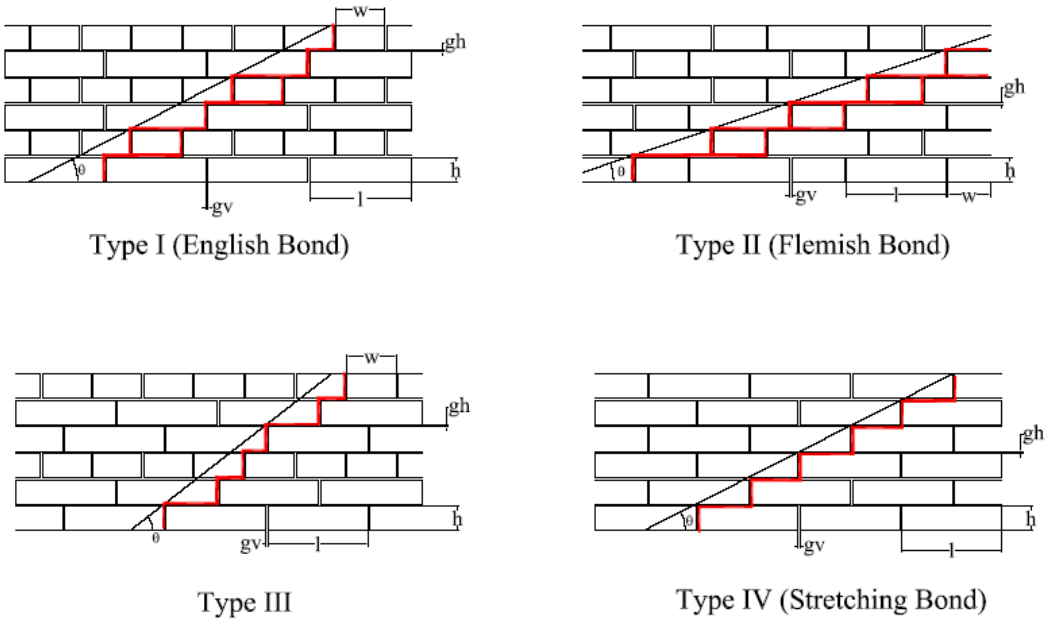

Figure 3.13. Types of brick laying and failure path for brick wall [1]

The ultimate strength V_n of the brick wall changes with the confinement of the wall For a wall confined along its four boundaries, such as the ones in our analyses, the ultimate strength can be calculated depending on θ as follows:

When $tan\theta \geq \frac{H_b}{W_b}$

$$V_n = T_b\left(W_b\tau_f + H_b\alpha f_{mbt}\right) \tag{3.45}$$

When $tan\theta < \frac{H_b}{W_b}$

$$V_n = T_b\left(W_b\tau_f + H_1\alpha f_{mbt} + \left(H_b^{'} - H_1\right)\left(\alpha f_{mbt} + \frac{\beta f_{bt}}{2}\right)\right) \tag{3.46}$$

In these expressions,

$$H_b{}' = min\left(H_b, W_b\right) \tag{3.47}$$

$$H_1 = W_b\, tan\theta \tag{3.48}$$

$$H_2 = 0.5W_b\, tan\theta \tag{3.49}$$

α and β are strength modification factors which are 0.45. τ_f is the frictional strength of the interface of the brick and mortar and it is defined as:

$$\tau_f = 0.0258 f_{mc}^{0.885} + \left(0.654 + 0.00515 f_{mc}\right)\sigma_N \tag{3.50}$$

where σ_N is the vertical stress of the brick wall and f_{mc} is the uniaxial compression strength of mortar. f_{mbt} is the splitting strength of the interface of the brick and mortar and equals:

$$f_{mbt} = 0.232\left(f_{mc}\right)^{0.338} \tag{3.51}$$

f_{bt} is the splitting strength of the brick and equals:

$$f_{bt} = 0.22 f_{bc} \tag{3.52}$$

where f_{bc} is the uniaxial compression strength of the brick.

The ultimate displacement of the brick wall u_u is;

$$u_u = \lambda \frac{V_n}{E_u T_b} \tag{3.53}$$

where T_b is the thickness of the brick wall, E_u is the secant stiffness of the brick wall when it is at the ultimate state. The crack elasticity modulus E_p is defined as:

$$E_p = 227 f_p^{'} \tag{3.54}$$

where the uniaxial compression strength $f_p^{'}$ of the bricks is:

$$f_p' = 0.27 f_{bc}^{0.7} f_{mc}^{0.3} \tag{3.55}$$

The elasticity modulus E_{50} of the brick wall equals:

$$E_{50} = 227 \eta_1 f_p' \tag{3.56}$$

where the modification coefficient η_1 is:

$$\eta_1 = 1.67 - 0.64\left(\frac{H_b}{W_b}\right) \tag{3.57}$$

Then the secant stiffness modulus E_u of the brick wall at ultimate state is:

$$E_u = \eta_2 E_{50} \tag{3.58}$$

where $\eta_2 = 0.556$ if all boundaries of the brick wall are confined.

The residual strength V_r of the brick wall depends on the presence of the windowsills.

For non-windowsill case:

$$V_r = \tau_f T_b W_b \le 0.6 V_n \tag{3.59}$$

For windowsill case:

$$V_r = 0.7 \tau_f T_b W_b \le 0.6 V_n \tag{3.60}$$

Based on the formulation above, a nonlinear axial hinge is placed at the middle of the equivalent truss for every storey of the test frames for infilled cases. The location of the

axial hinge is irrelevant since the axial load is assumed constant along the length of the equivalent truss. The parameters of the axial hinge are determined according to the lateral force-displacement relationship. The moment scale factor is $(V_n/cos\phi)$ and the rotation scale factor is $\Delta_u cos\phi$. Figure 3.14 shows a sample lateral force-displacement relationship of an equivalent truss and the parameters of the nonlinear axial hinge are given in Table 3.6.

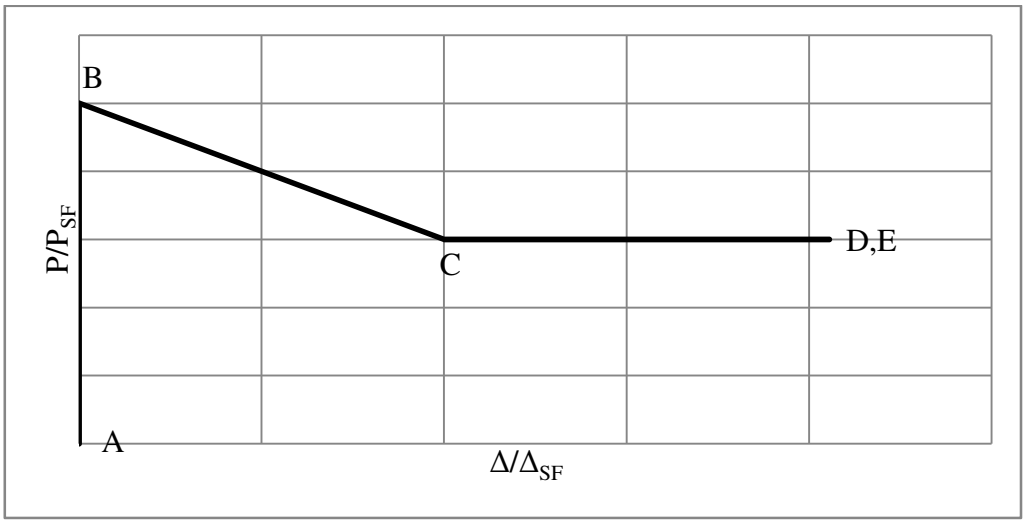

Figure 3.14. Force-displacement relationship for axial hinge of an equivalent truss

Table 3.6. Parameters of the nonlinear axial hinge of equivalent trusses

Points	Force / SF	Disp. / SF
A	0	0
B	1	0
C	V_r/V_n	1
D	V_r/V_n	$0.02H_b/(\Delta u cos\phi)$
E	V_r/V_n	$0.02H_b/(\Delta u cos\phi)$

3.2.3. Modeling of the Shear Walls

Binici and Ozcebe [17] proposed to model the shear walls using beam-column elements along the centerline of the wall. The connection between the wall and the neighboring frame elements were provided through rigid links. Modeling the shear walls with frame elements is a simple approach compared to using finite element models. It is easy to assign plastic hinges to frame elements to represent the nonlinear behavior and the procedure detailed in Section 3.2.1 can also be used to model the shear walls.

In RC wall analysis, structural behavior can be modeled by a combination of flexure, shear and slip springs. Equivalent wide column model is generally used to model RC shear walls in computer based analysis. According to the Japan Building Institute, in RC shear wall earthquake-resistance analysis, the boundary columns of a RC wall can be considered as two axial springs and the wall panel can be considered as a central equivalent wide column with flexural, axial and shear resistance[35]. It is assumed that the axial load can be shared by two boundary columns while lateral loading is taken on by RC wall panel in order to simplify the analysis. While using the commercial computer software program SAP2000.v11.0.0 in RC wall analysis, it is impossible to place plastic hinges onto shell elements. Due to this, the equivalent wide column model can be used for modeling the RC walls. As discussed previously in Section 3.2.2, without finite element models, the local deformations can't be investigated by an equivalent wide column model. Figure 3.15 represents the RC wall model consisting of an equivalent wide column in the center and two boundary columns in the edges.

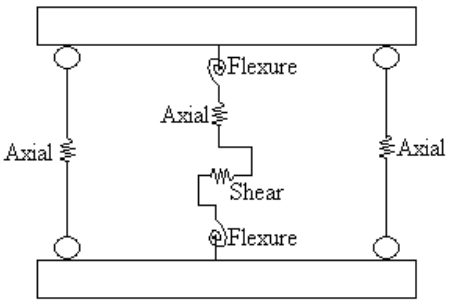

Figure 3.15. Schematic diagram of equivalent wide column model of RC wall

The axial hinge defined in Section 3.2.1.3 is used to model the boundary columns. Two flexural hinges at the column ends, a shear hinge to mid-span and an axial hinge are placed on the equivalent wide column as discussed in Section 3.2.1.2, Section 3.2.1.4 and Section 3.2.1.3 to represent the nonlinear behavior.

3.2.4. Modeling of the Infill Walls Strengthened with CFRP

Seismic retrofitting techniques investigated in the literature show that CFRP retrofit scheme is an efficient way to use hallow clay brick infill walls as lateral load resisting elements. The prior experimental studies show that CFRP increases the lateral strength and stiffness substantially. Analytical modeling of infill walls strengthened with CFRP is needed to seismically evaluate existing structures before upgrading. Modeling guidelines of CFRP strengthened infill walls for nonlinear static analysis by Binici and Ozcebe [17] is used in this study.

An infill wall strengthened with CFRP is modeled using a compression strut and a tension tie which together adequately represent the load transfer mechanism observed in prior experiments and detailed finite element analysis [17]. A trilinear stress-strain response is proposed for the truss members to simulate the behavior of the strengthened infill wall. It is assumed that CFRP, infill material and infill wall surface all contribute to the stiffness of the tension tie.

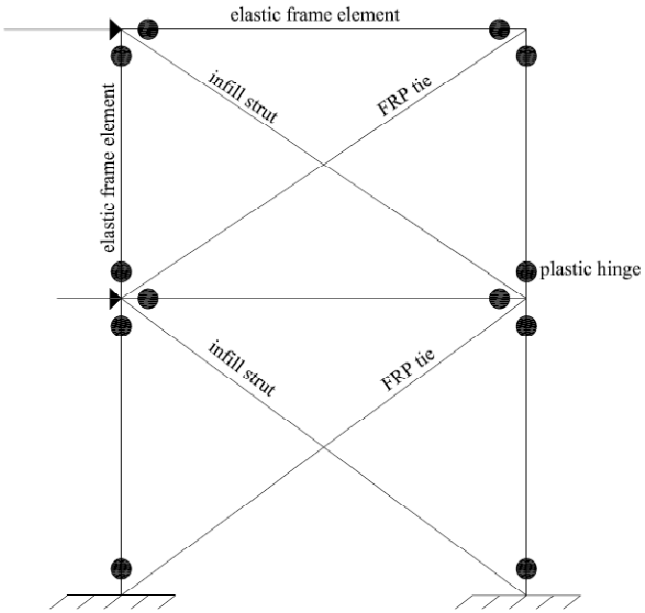

Figure 3.16. Structural modeling for infill struts and CFRP ties

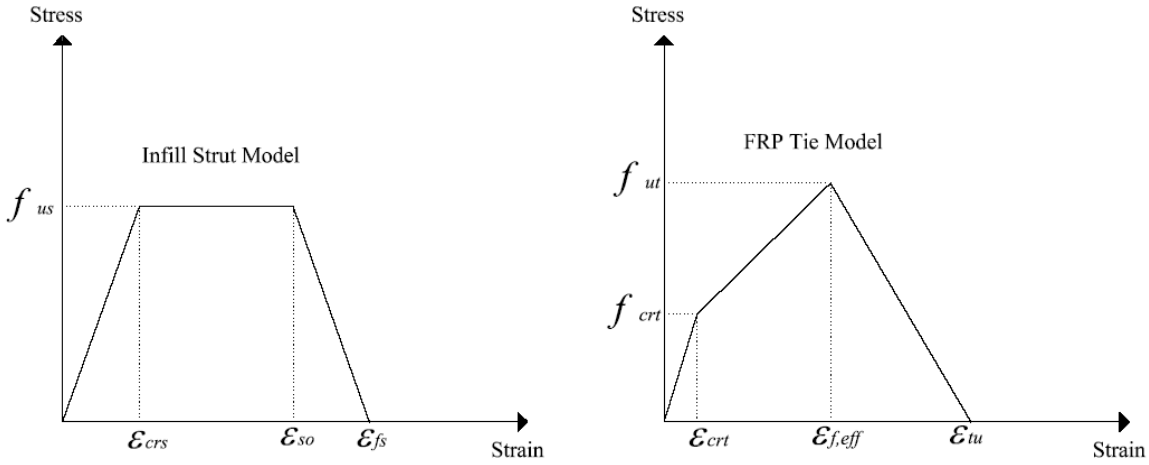

Figure 3.17. Stress-strain models for infill struts and CFRP ties

The area of the composite tension tie is:

$$A_{tie} = w_f t_{tie} \tag{3.61}$$

where w_f is the width of the CFRP provided and t_{tie} is given by:

$$t_{tie} = t_f + t_p + t_{in} \tag{3.62}$$

in which t_f, t_p and t_{in} are the thicknesses of CFRP, plaster, and infill respectively.

Cracking stress f_{crt} of the tie can be calculated via:

$$f_{crt} = \frac{V_{crt}}{A_{tie}} \tag{3.63}$$

$$V_{crt} = f_{pt} w_f \left(\left(t_{in} + t_p \right) + \frac{E_f}{E_m} t_f \right) \tag{3.64}$$

where f_{pt} is the tensile strength of the plaster, E_f and E_m are the modulus of elasticity of CFRP and mortar, respectively. The modulus of elasticity of mortar can be calculated by:

$$E_m = 5500\sqrt{f_{mc}} \tag{3.65}$$

where f_{mc} is the nominal compressive strength of mortar. Tensile capacity V_{ut} and tensile strength f_{ut} depend on the capacity of the CFRP at effective strain $\varepsilon_{f,eff}$ obtained from experimental results, at which anchor failure or deboning initiates. The tensile capacity and the tensile strength are given by:

$$V_{ut} = \varepsilon_{f,eff} w_f t_f E_f \tag{3.66}$$

$$f_{ut} = \frac{V_{ut}}{A_{tie}} \tag{3.67}$$

The strut stress-strain model is also a trilinear model with a perfectly plastic plateau and limited deformation capacity. The area A_{str} of the composite strut is computed by:

$$A_{st} = w_s t_{st} \tag{3.68}$$

where,

$$t_{st} = t_p + t_{in} \tag{3.69}$$

$$w_s = \frac{(1-\alpha)\alpha h}{\cos\theta} \tag{3.70}$$

Equation (3.70) is proposed by El-Dakhakki et al. [36] based on the work by Saneinejad and Hobbs [37] to estimate effective width of the strut. In equation (3.70), h is the height of the infill wall, θ is the strut inclination angle and α is a dimensionless parameter to account for the frame infill contact length computed by:

$$\alpha = \sqrt{\frac{2\left(M_{pj} + 0.2M_{pc}\right)}{h^2 t_{st} f_{mc}}} \tag{3.71}$$

in which M_{pj} is the minimum moment capacities of the column or the beam, M_{pc} is the moment capacity of the column, and f_{mc} is the nominal compressive strength of the infill plaster composite.

The ultimate strength V_{us} of the diagonal compressive strut is computed based on the minimum of the two capacities, namely sliding shear V_{ss} and corner crushing V_{cc}:

$$V_{us} = min\left(V_{ss}, V_{cc}\right) \tag{3.72}$$

$$V_{ss} = f_{mv} L t_{st} \tag{3.73}$$

where f_{mv} is the shear strength of the mortar bed joint and L is the width of the infill wall. An empirical equation proposed by Flanagan and Bennett [38] to predict the corner crushing strength of infill wall is:

$$V_{cc} = 250 t_{st} f_{mc} \tag{3.74}$$

where f_{mc} and the slope of the stress-strain curve E_{sm} can be obtained from uniaxial compression tests of plastered infill walls. In the absence of tests, the following equations can be used to predict the strength and stiffness of the diagonal strut.

$$f_{mc} = \frac{f_{in}t_{in} + f_{in}t_p}{t_{st}} \tag{3.75}$$

$$E_{sm} = \frac{E_{in}t_{in} + E_m t_p}{t_{st}} \tag{3.76}$$

where E_{in} is the elasticity modulus of the infill material, which generally varies between 500 to 1500 times the compressive strength of the infill material.

Finally, the ultimate strength f_{us} can be computed using:

$$f_{us} = \frac{V_{us}}{A_{st}} \tag{3.77}$$

3.3. Nonlinear Static Analysis (Pushover Analysis)

Nonlinear static analysis consists of laterally pushing the structure in one direction under static loads with a certain lateral force or displacement distribution until either a specified drift is attained or a collapse mechanism has been developed. Because linear procedures have limitations and nonlinear dynamic procedures are complicated, nonlinear static analysis is commonly used by many engineers for assessment of the performance of existing buildings. The important issue in a nonlinear static analysis is to model the structure with reasonable accuracy in representing nonlinear behavior. To make the frame elements represent the nonlinear behavior, plastic hinges are crucial. The nonlinear response of a structure is typically restricted to nonlinear hinges which are assigned on structural elements of that structure.

The analysis procedure starts with modeling of the structure according to pre-determined dimensions and geometry. At this step, material properties for the structural elements have to be assigned. Subsequently, the distribution of vertical forces from the slabs to the beam elements which have to be modeled as elastic members with cracked flexural rigidity (which was explained in Section 4.3) has to be done. A lateral load pattern has to be determined. According to TEC 2007, lateral loads should be proportional to the product of story mass and the amplitude of the first mode shape. A mass times story elevation lateral load distribution is another way to distribute the lateral loads. Defining the moment hinges, normal force hinges, shear hinges, and normal force-moment hinges according to the information given in Section 3.2 is the next step to be done. Subsequently, the hinge assignments to the frame members have to be done.

By conducting the pushover analysis, the collapse mechanism and the lateral load versus top displacement relationship can be obtained. According to this relationship, it is possible to predict the initial and pre-yield stiffness of the structure, and the yield displacement and yield force. Formation of a plastic hinge doesn't imply that the structure has reached an ultimate state. After a plastic hinge occurs, redistribution takes place and system continues to take load. When the number of plastic hinges becomes sufficient to develop a collapse mechanism, the model becomes unstable and analysis can be terminated.

4. ANALYTICAL MODELING OF THE HSIN-TSENG JUNIOR HIGH SCHOOL BUILDING

An analytical study to predict the performance level and deformation behavior of Hsin Tseng Junior High School is done to check the accuracy of the modeling techniques detailed in Chapter 3. The results of the analyses are compared to the in-situ test results of the building detailed in Section 2.1. Also, a comprehensive investigation on the key parameters affecting the force-displacement relationship is undertaken.

4.1. General Properties of the Building

Tu et al. [1] reported that Hsin-Tseng Junior High School was a traditional Taiwanese school building consisting of two storeys. The structural system of the building consisted of RC frames. The structural plan of the building and the side view of the test setup are represented in Figure 4.1 and Figure 4.2, respectively. In order to conduct the tests detailed in Section 2.1, the building was separated to two parts along the longitudinal direction by cutting the structural and non-structural elements. One part of the building was laterally strengthened to be used as a reaction block by 9 steel braces located diagonally. The test block was a 2 storey building which had nine 3.33 m spans in the longitudinal direction. The transverse direction of the building included two 4 m classroom spans and a 2.4 m corridor span. The storey heights were 3.9 m for the first floor and 3.6 m for the second floor. More than half of the columns on axis B (Figure 4.1) and all of the columns on axis D had 1.05 m high windowsills that would be expected to cause short column effects. The vertical load carrying elements consisted of 4 types of rectangular RC columns as detailed in Figure 4.1.

The material properties were determined before the tests. The average compressive strength of concrete was 23.3 MPa in the second floor and 21.8 MPa in the first floor, while yielding strength of longitudinal and transverse reinforcement steel was distributed between 314 MPa and 480 MPa.

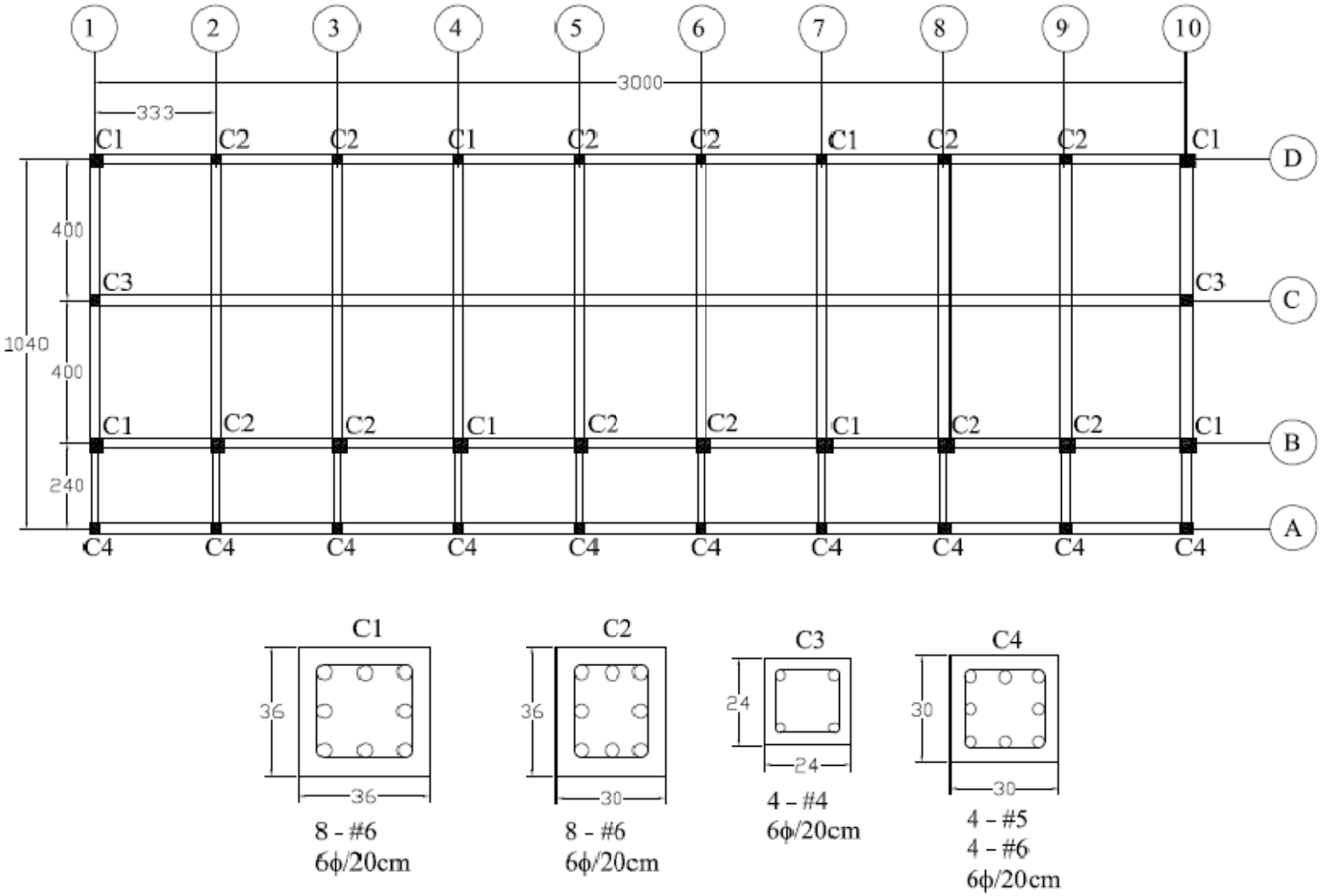

Figure 4.1. Plan view and cross-sectional dimensions of the column elements of Hsin – Tseng Junior High School

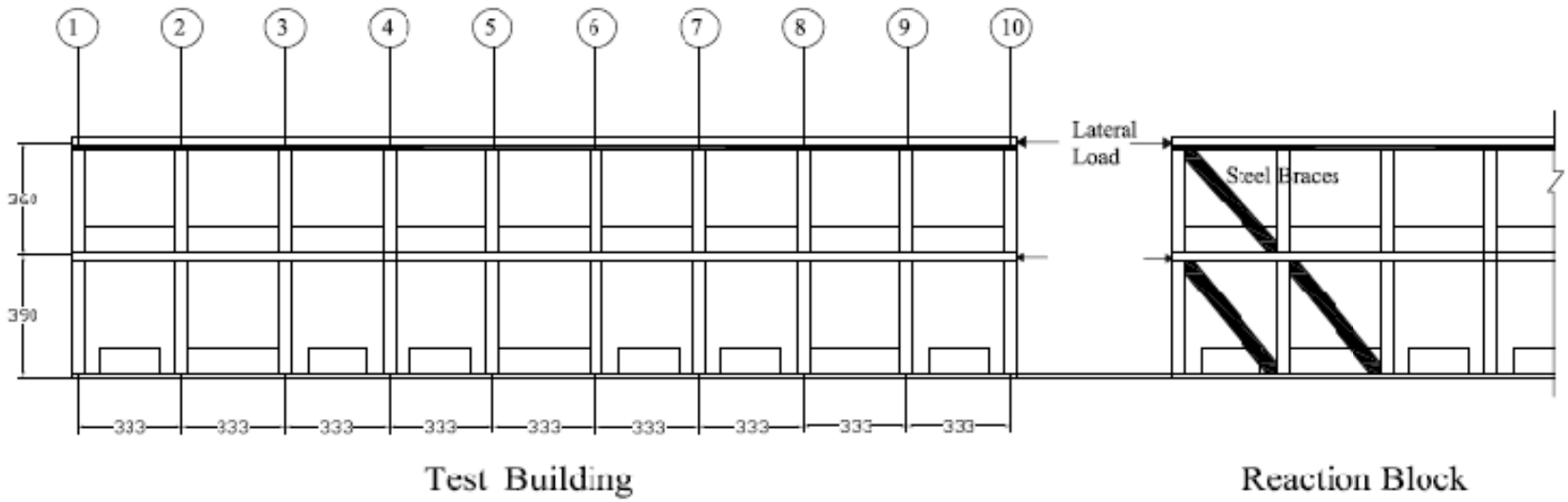

Figure 4.2. Side view of the test setup (in cm's)

4.2. In-Situ Test Results

Both lateral and vertical tests were done to evaluate the seismic behavior of the building. In the lateral tests, 300 mm (four per cent drift) total lateral displacement on the roof floor was applied to the building and the base shear was monitored as 1,942 kN. At 150 mm lateral displacement (two per cent drift), 2,915 kN base shear was monitored, and this value was the lateral load capacity. Flexural and shear failure modes were observed in the column elements during the tests. The diagonal cracks caused by shear showed that the short-column effect occurred. All of the columns failed during the tests whereas the beams and slabs remained almost undamaged [1]. Wu and Xue [3] reported that the behavior of the traditional low rise school buildings in Taiwan could be considered as shear frames. This behavior was also seen in the in-situ tests of Hsin Tseng Junior High School building. Figure 4.3 represents the flexural failure of the unsupported columns and flexure-shear failure of the columns partially encased by windowsills.



Figure 4.3. Flexure failure (left hand side) and flexure-shear failure (right hand side) of the test building [1]

Figure 4.4 represents the experimentally obtained base shear versus roof displacement curve of the test building. This figure is obtained by digitizing a picture from the study of Tu et al. [1] using commercial computer software program Didger [39].

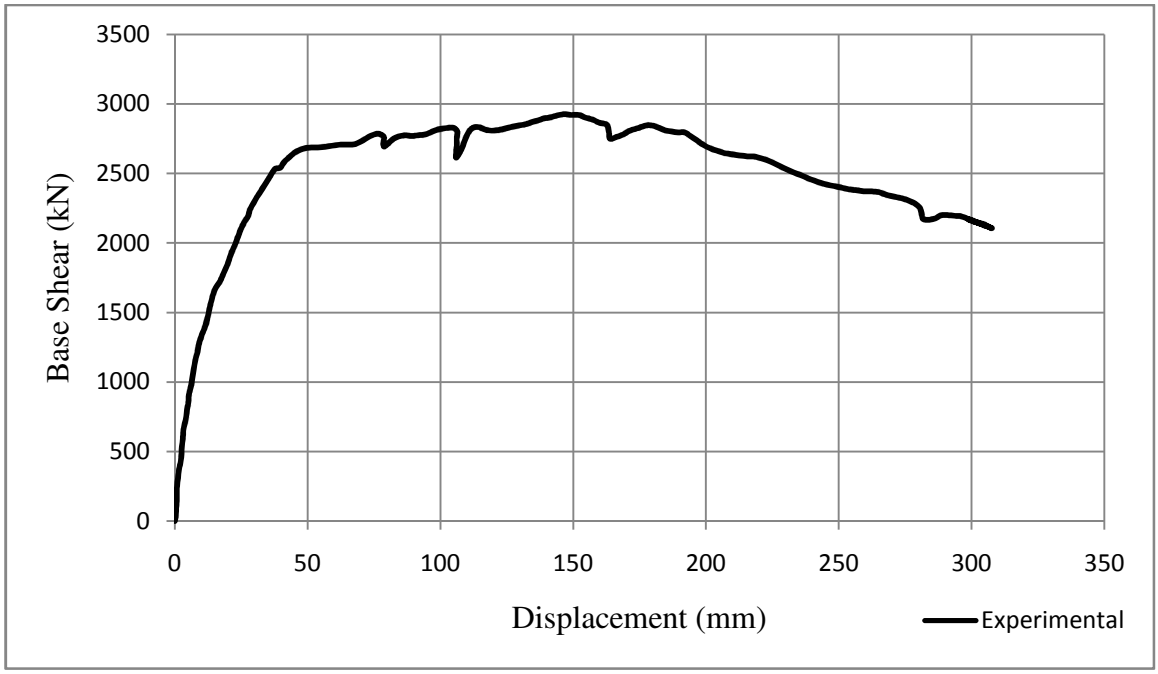

Figure 4.4. Pushover curve of the Hsin-Tseng Junior High School building

4.3. Analytical Modeling

The displacement controlled nonlinear static analysis of the school building is conducted via commercial computer software program SAP2000.v11.0.0 [26]. Frame elements are used to model the structural members. Because the traditional low rise school buildings in Taiwan behaves like shear frames, the slabs and beams are assumed as rigid elements. The columns, supported by windowsills, are assumed as shear-critical columns in accordance with the assumption that windowsills may cause short column effects. Due to this, the idealized backbone model of Elwood and Moehle [27], explained in Section 3.2.1.4, is used to model these columns. For the unsupported columns, P-M hinges on both ends of the column members and shear hinges in the middle region of the column members are used to represent the nonlinear behavior.

The moduli of elasticity E_c of the concrete for first and second stories are calculated in accordance with TS500-2000 [23] and Eurocode-2 [40], using formulas 4.1 and 4.2, respectively:

$$E_c = 3250\sqrt{f_{ck}} + 14000 \tag{4.1}$$

$$E_c = 9500(f_{ck} + 8)^{1/3} \tag{4.2}$$

A mean modulus of elasticity value of 30,000 MPa is used both for the first and second storey concrete. The effective stiffness (cracked section stiffness) is a crucial parameter affecting the performance level of the building. Figure 4.5 represents the generalized forms of the effective stiffness values according to FEMA 356 [41] and TEC 2007 [16].

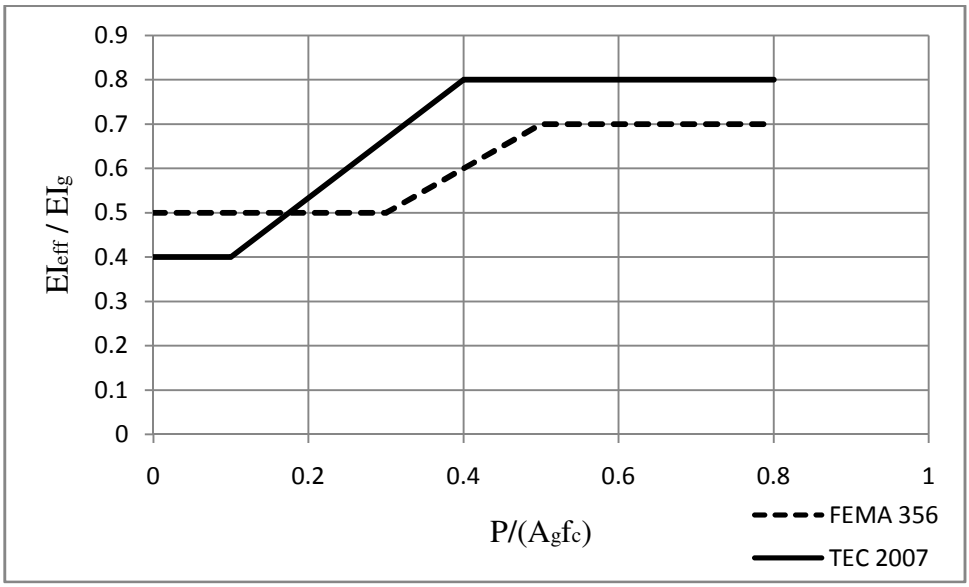

Figure 4.5. Generalized forms of effective stiffness values

Rather than using code generalized values for effective section stiffness, using moment-curvature relationship may give more accurate results. Due to this, the effective stiffness values of the column members are calibrated according to the moment-curvature relationship of the sections at the yield point. For instance, a C1 type column under a 300 kN vertical load has an effective stiffness value of $0.5EI$ according to FEMA 356 [41] and $0.42EI$ according to TEC 2007 [16]. The moment-curvature analysis in Figure 4.6 shows a $137kN.m$ yield force at $0.01rad/m$ curvature resulting with $0.46EI$ effective stiffness.

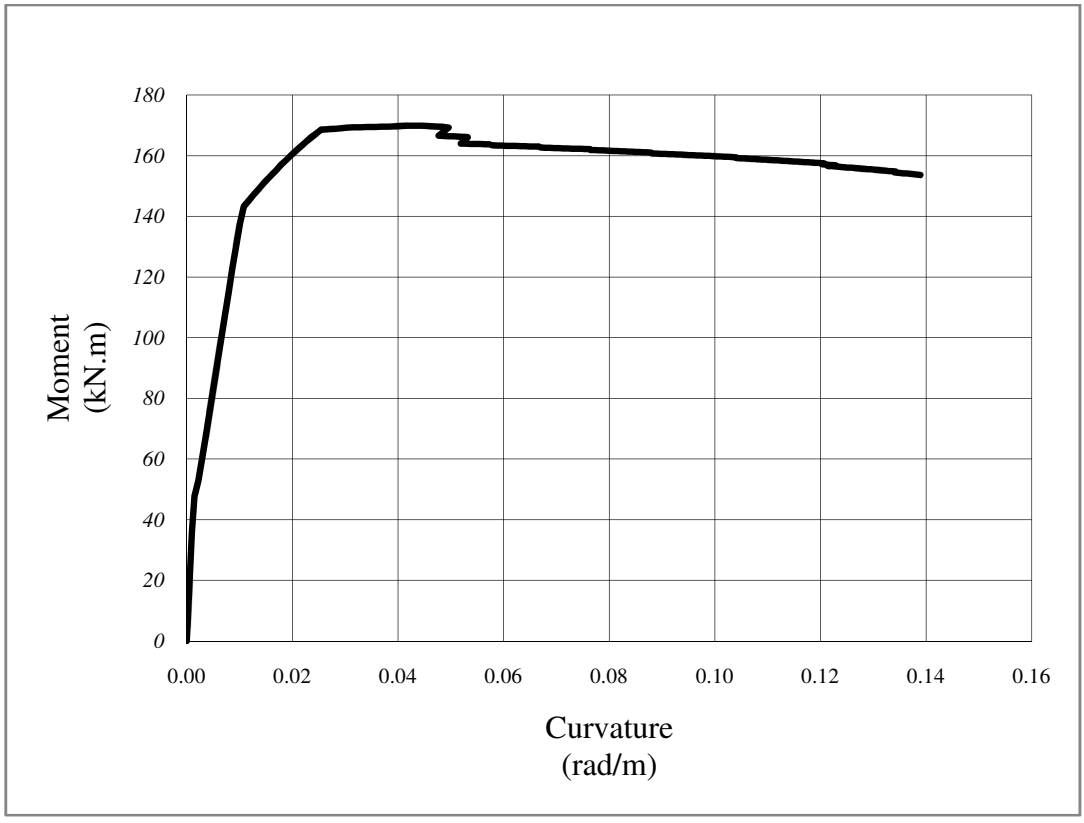

Figure 4.6. Typical moment-curvature analysis for a C1 type column

Windowsills are modeled according to the equivalent truss concept detailed in Section 3.2.2. While calculating the equivalent truss representing the windowsills, standard $19 \times 19 \times 13.5$ cm bricks are used. Uniaxial compression strength of the brick and mortar are assumed as 16 MPa and 1.4 MPa, respectively. Horizontal and vertical seam widths are assumed as 0.5 cm. The modulus of elasticity of the windowsills is assumed as 3,000-6,000 MPa in accordance to the equivalent truss concept and a former study by Hanoğlu [42]. According to prior studies in the literature, the windowsills of traditional Taiwan school buildings remain elastic under lateral forces; due to this, two rigid diagonal steel braces are used in the computer model. On the other hand, Wu and Xue [3] offered using non-prismatic column members which are wider in the windowsill regions to represent windowsills. Figure 4.7 and Figure 4.8 represents the two types of windowsills:



Figure 4.7. Representation of the rigid windowsills used in the analysis



Figure 4.8. Representation of the rigid windowsills used by Wu and Xue [3]

The same lateral loading ratio (1:3) used in the experimental study is used in the analytical study. The three-dimensional computer model of the Hsin-Tseng Junior High School building can be seen in Figure 4.9.

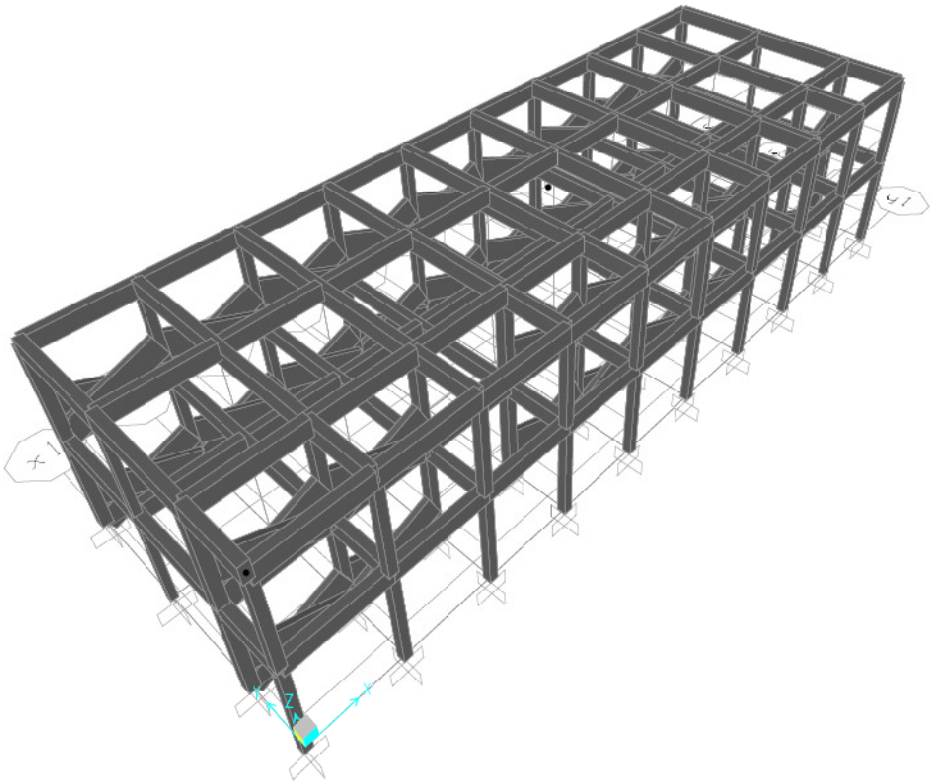

Figure 4.9. Three dimensional computer model of the Hsin-Tseng Junior High School

4.4.Analysis Results

A step by step investigation to analyze the effects of parameters on the building performance is done. In the last step of the analysis, rigid beam members, rigid windowsill members and plastic column members are used according to the data given in Section 4.1. In the analysis, 23.3 MPa and 21.8 MPa are used for concrete compressive strengths with modulus of elasticity of 30,000 Mpa, 400 MPa is used for longitudinal reinforcement bar strength and 310 MPa is used for transverse reinforcement bar strength with modulus of elasticity of 200,000 MPa. Equivalent diagonal braces with cross sectional area of 0.192 m^2 and with modulus of elasticity of 6,000 MPa are used to model the windowsills. The effective stiffness values of the column members are calculated in accordance with the relevant moment-curvature relationships.

The nonlinear behavior of the column members is represented by using shear hinges detailed in Figure 3.11 on the shear critical columns (which are the columns supported by windowsills resulting to short columns) and P-M hinges and shear hinges detailed in Figure 3.5 and Figure 3.7, respectively, on the unsupported columns. For the shear hinges on the shear critical columns, Elwood and Moehle's [27] approach to define the plastic shear capacity is used. According to this, the plastic shear capacity V_p is calculated as:

$$V_p = \frac{2M_u}{L} \tag{4.3}$$

where M_u is the moment capacity of the column cross section at balance point.

For the P-M hinges, an axial force-moment interaction analysis is done for the section. Moment-curvature relationship of the section is determined according to the variable axial loads on the section and used in the nonlinear analysis. A hinge length of half the section depth $(depth/2)$ is used.

Figure 4.10 represents the experimental pushover curve compared with the analytical one under the above defined conditions.

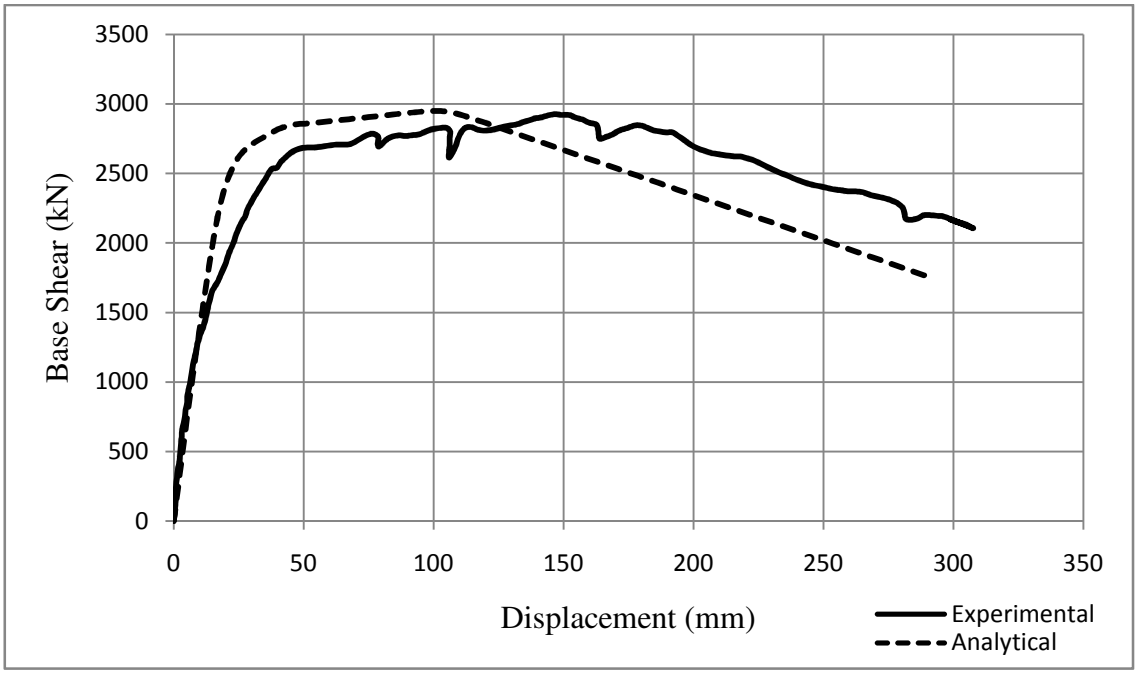

Figure 4.10. Analytical versus experimental pushover curves of the building-1

According to this analysis, yielding of the building occurred under 2,615 kN lateral load at 25 mm lateral displacement. The lateral load capacity is monitored as 2,949 kN at 100 mm lateral displacement. After this point, the lateral load degraded approximately with a linear relationship with the increasing displacement. According to these results, it is observed that the initial portion of the analytical pushover curve matches with the experimental one, which means the initial stiffness of the building is correctly estimated. The pre-yield stiffness of the analytical curve overestimates the experimental one. This discrepancy might be due to some damage the building experienced in the field tests, causing decrease in stiffness before the yielding point, which is impossible to be simulated in the computer analysis. The degradation of the analytical curve occurs earlier than it does in the experimental results, meaning that displacement capacity of the building is underestimated.

Figure 4.11 represents the deformation behavior of the building. In accordance with this, the predetermined shear critical columns initially experienced flexural yielding of the longitudinal reinforcement. Following this, lateral load level of the columns increased with increasing displacement. At the peak lateral force value, shear capacity was reached and the shear force started to degrade. At this point shear failure occurs and diagonal cracks

occur in the column. The unsupported columns (C3 and C4) didn't show shear failure during the analysis. In these columns, only flexural failure occurred. The second storey of the building didn't show any failure except three of the columns.

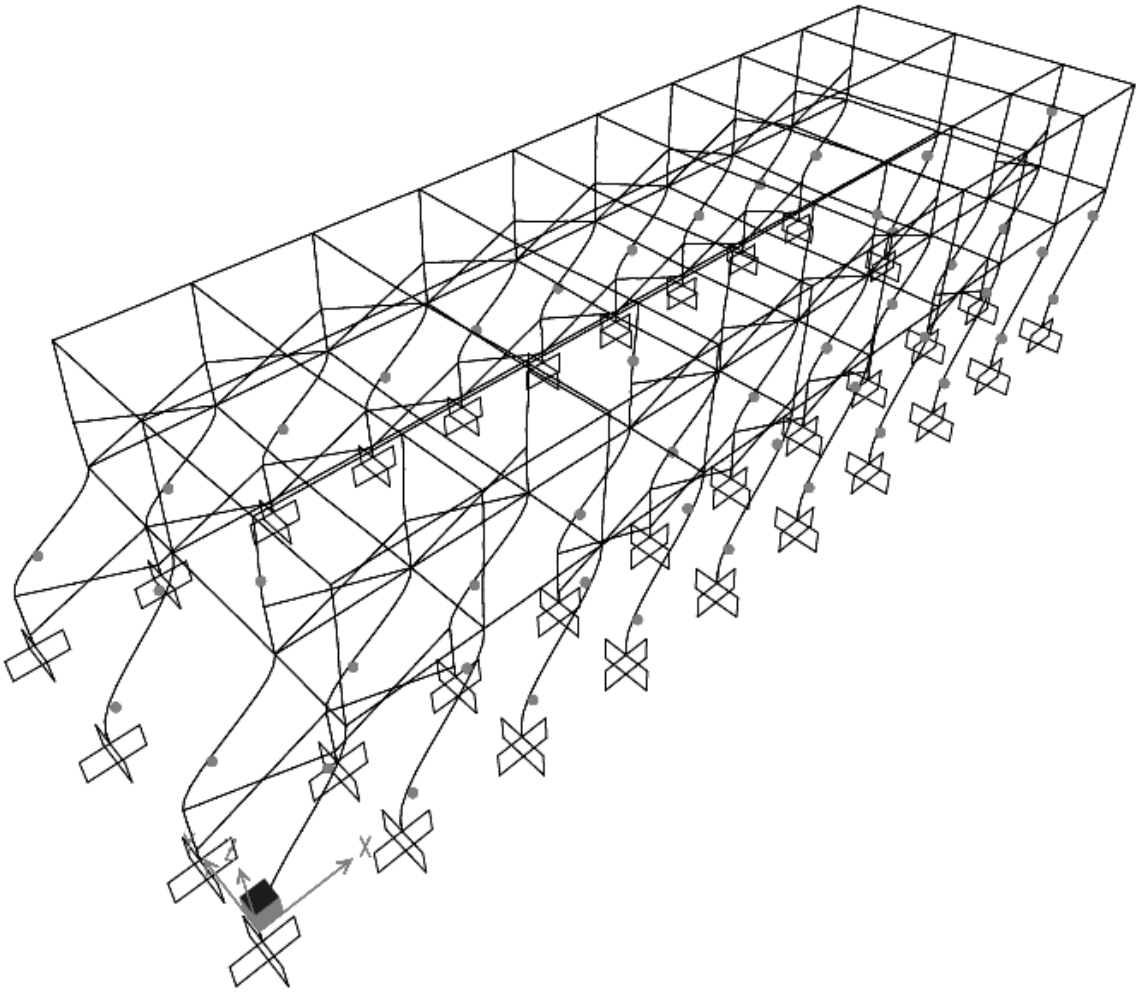

Figure 4.11. Deformation behavior of the building

If the same analysis is repeated with using the shear capacities of the column sections under gravity loads only (V_u) rather than using plastic shear capacities (V_p), the lateral load capacity of the building increases. The reason of this behavior is that shear capacities of the column sections is higher than the shear demands due to bending in Hsin-Tseng Junior High School building. Figure 4.12 represents the comparison of the analytical and experimental pushover curves for this situation.

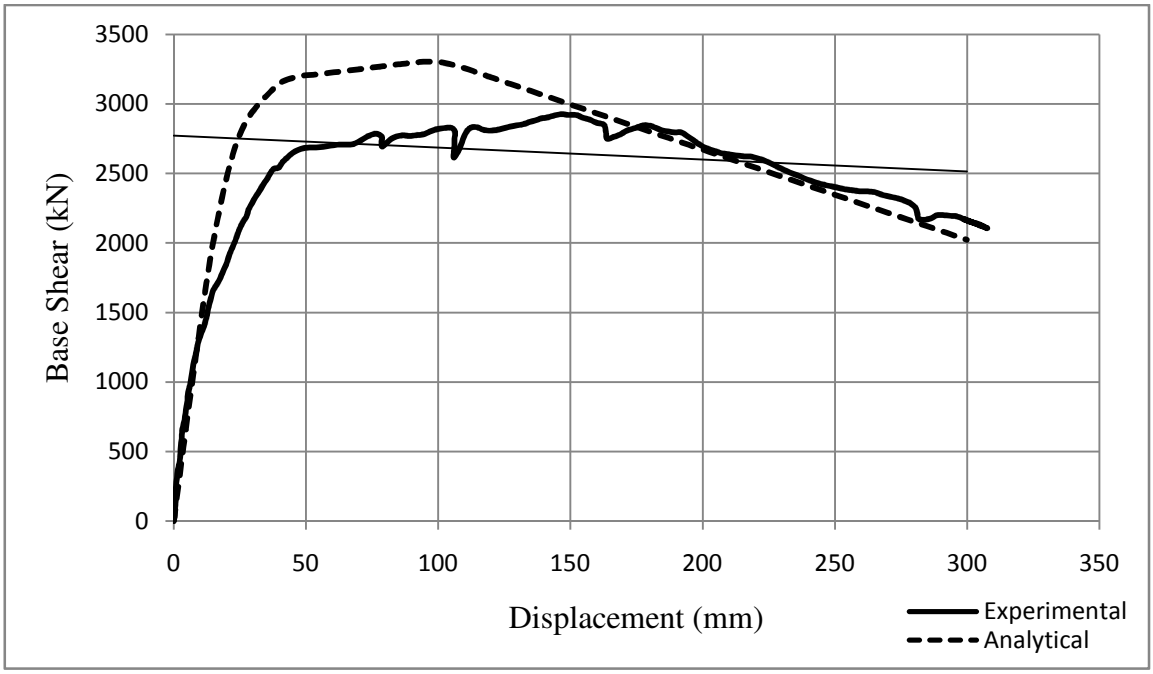

Figure 4.12. Analytical versus experimental pushover curves of the building-2

According to this analysis, yielding of the building occurred under 2,780 kN lateral load at 25 mm lateral displacement. The lateral load capacity is monitored as 3,304 kN at 97 mm lateral displacement. After this point, the lateral load degraded approximately with a linear relationship with increasing displacement. According to these results, the same deformation characteristics occur in a higher lateral load capacity if the shear capacities of the columns are used rather than the plastic shear capacities. In this failure type, the columns supported by the windowsills are forced to fail from shear by ignoring flexural deformations. Figure 4.11 shows the hinges occurred on the structure in this analysis.

If the same analysis is repeated with effective stiffness values calculated in accordance with FEMA 356 [41] for columns, the initial stiffness increases, and the difference in the secant stiffness becomes higher. The lateral load capacity is found as 3,334 kN at 84 mm lateral displacement in this case. Figure 4.13 represents the force-displacement relationship for this case.

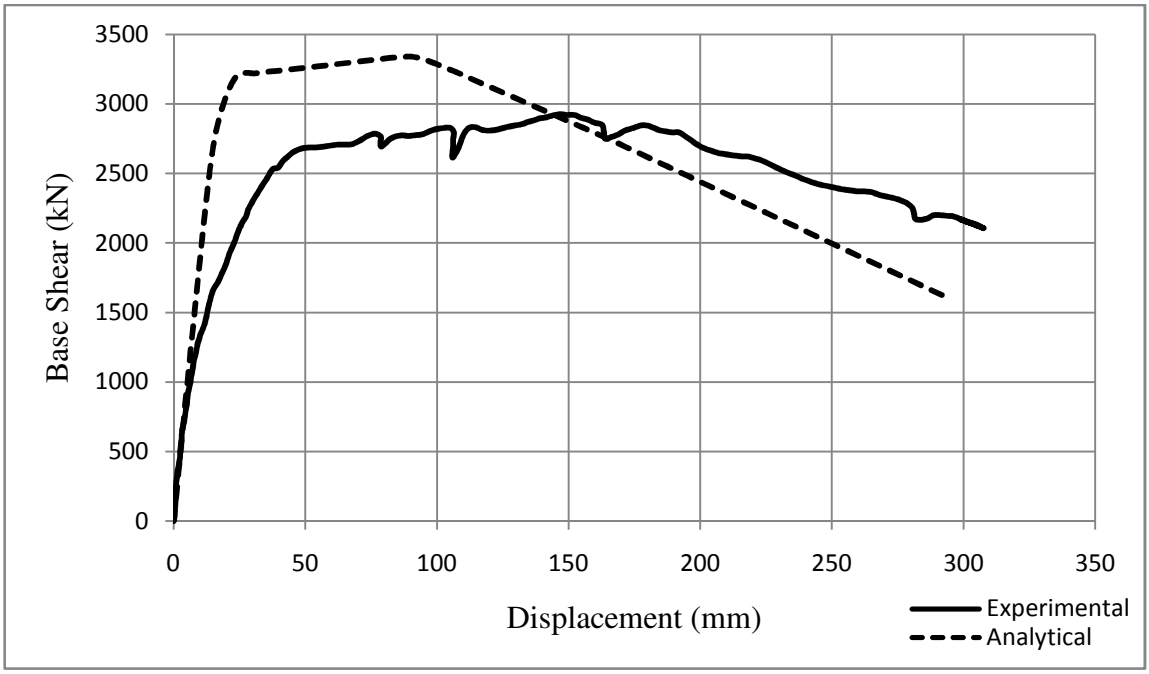

Figure 4.13. Analytical versus experimental pushover curves of the building-3

Modeling the diagonal brace members that represents the windowsills with moment and torsion releases in the ends, the initial stiffness of the building decreases, resulting lateral load capacity of 3,289 kN at a displacement of 108 mm, compared to the non-released one. Figure 4.14 represents this behavior.

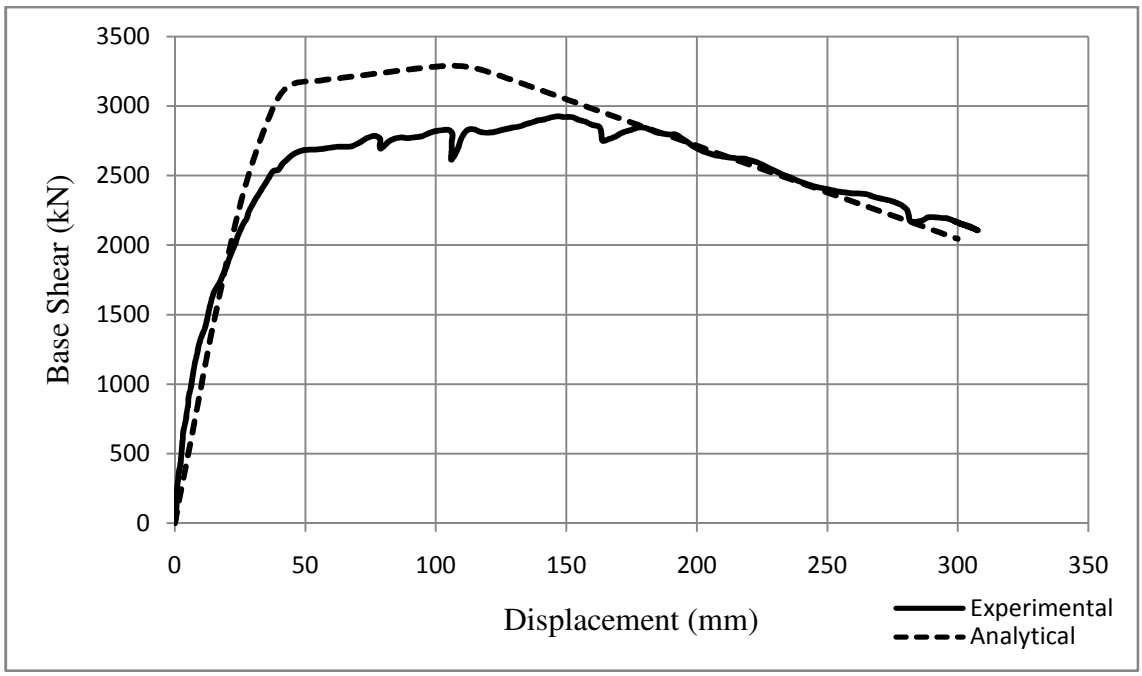

Figure 4.14. Analytical versus experimental pushover curves of the building-4

During the analysis, it is observed that the modulus of elasticity and the effective modulus of elasticity of concrete is the main parameter affecting the stiffness of the whole structure. In our analysis 30,000 MPa concrete modulus of elasticity is used in accordance with Eurocode-2 [40] and TS500-2000 [23]. The approximation of modulus of elasticity by ACI code is formulized as:

$$E_c = 4750\sqrt{f_{ck}} \text{ (in MPa)} \tag{4.4}$$

resulting with concrete modulus of elasticity of 23,000 MPa. If the E_c value used before (30,000 MPa) is changed with 23,000 MPa, the pushover curve in Figure 4.15 is obtained.

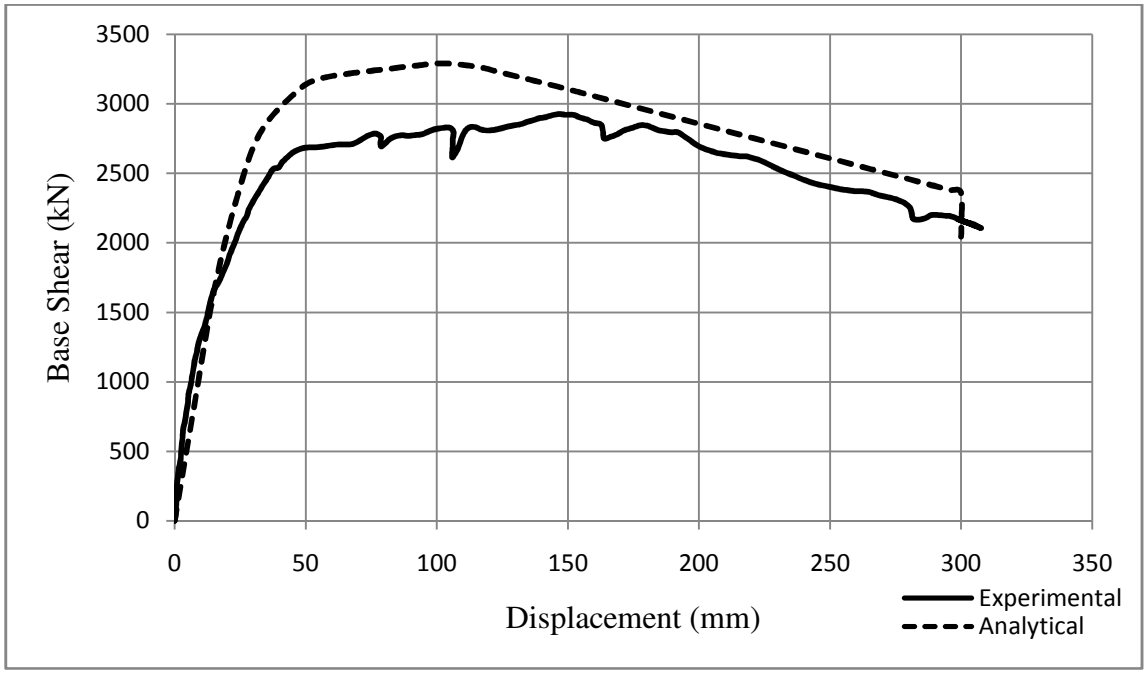

Figure 4.15. Analytical versus experimental pushover curves of the building-5

According to this curve, the initial stiffness of the building decreased. The lateral load capacity of 3,290 kN at a displacement of 102 mm is observed in this case.

It is observed that using modulus of elasticity of the equivalent braces representing the windowsills as 3,000 MPa or 6,000 MPa does not affect the pushover curve significantly. Only a small difference in the initial stiffness value occurs.

In all of the analyses, the lateral load capacity is reached in smaller displacements than the experimental one. The dominant deformation type in this building is shear. If a rational calibration can be done to the displacement capacities of the shear hinges, the displacement level for peak lateral load capacity in the in-situ tests might be observed.

If all of the analyses are considered, the collapse mechanism obtained from the analytical studies is approximately identical with that in the in-situ tests. All of the unsupported columns in the building fail due to flexure at both ends. The columns supported by the windowsills initially fail in flexure due to yielding of the longitudinal steel and then shear failure occurs. The short column effect is observed in these structural elements. It is seen that approximately no damage occurs in the structural elements of the upper floor. Nearly all of the displacement occurs on the first floor, and this was also observed in the in-situ tests.

The lack of information about the windowsill materials, not considering the out of plane behavior of the transverse infill walls and using a range of strength rather than a single number for longitudinal and transverse reinforcement steel might be some of the reasons for the differences between the experimental and analytical curves.

5. DETERMINATION OF AN IN-SITU TESTING CONFIGURATION FOR A TYPICAL RC SCHOOL BUILDING

Chapter 5 of this thesis proposes an in-situ testing scheme for a typical Turkish school building, namely the Şehit Adem Yavuz Primary School, in İstanbul. The content of the proposed static tests include (i) a bare frame test, (ii) a brick infilled frame test, (iii) a brick infilled frame strengthened with CFRP test, and (iv) an RC infill wall strengthened frame test. The equipment that is needed to conduct the in-situ tests and the analytical predictions of the test results are also detailed in this chapter.

5.1. The Demand for In-Situ Tests

There are many experimental and analytical studies conducted by researchers worldwide to examine the effects of seismic rehabilitation techniques. Many of them were done in laboratory conditions at universities to simulate the effects of earthquakes in two-dimensional and sometimes three-dimensional frames to identify the collapse mechanisms and determine the seismic improvement provided by seismic rehabilitation techniques. Most of these tests were conducted on scaled specimens that were constructed with perfect deficiencies. It is impossible to reflect the actual structural behavior with these specimens. There are few studies done in field on real buildings, all over the world. The lack of in-situ testing is mainly due to economical considerations and shortage of suitable buildings to be used as test specimens. Turkey can assume the role of a pilot region to run full scale static and dynamic in-situ tests due to the existing building stock scheduled for demolition.

It is believed that a significant portion of the building stock in Turkey was constructed in years 1970-1980. Due to the fact that majority of these buildings include common seismic deficiencies (such as insufficiencies in structural design, poor workmanship, poor quality of construction materials, formation of soft-weak stories, non-ductile reinforcement details, strong beam-weak column construction and torsion caused from poor arrangement of infill walls and load bearing system) which cause ductility, strength and stiffness problems in the structural system, a retrofitting program is needed.

By conducting a series of in-situ pushover tests, it might be possible to determine the most efficient retrofitting technique for seismic improvement.

5.2. Public Buildings for In-Situ Tests

It is impossible to rehabilitate the structural system of all the structures with the same methodology. Due to this, the rehabilitation methodologies have to be determined according to the structural system of buildings. For such a study, public buildings may be chosen as preferred buildings due to having the greatest risk under seismic excitation. Most of the public buildings (schools, hospitals, governmental buildings, etc.) in Turkey include typical structural plans according to their functions. For instance, the general characteristics of typical school buildings in Turkey are:

- 3-4 stories
- 10-13 bays in longitudinal direction
- 3-4 bays in transverse direction
- Structural system composed of RC frames
- Low concrete quality
- 20-30 cm thick hallow brick infill walls

Figure 5.1 shows the floor plan of a typical Turkish school building:

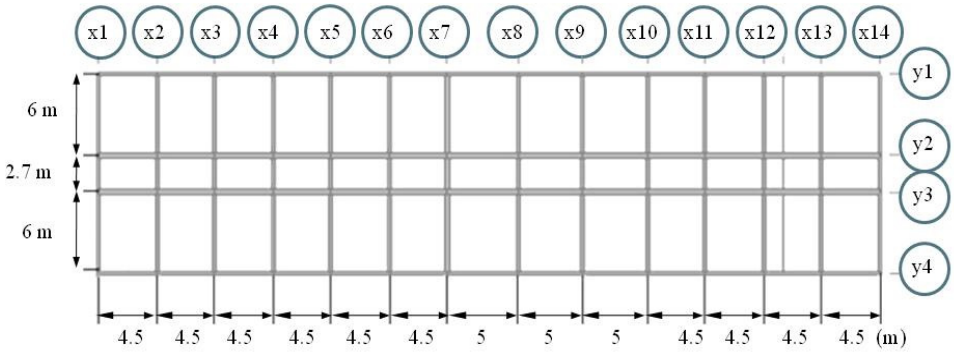

Figure 5.1. Floor plan of a typical Turkish school building

Accordingly, a primary school building, namely Şehit Adem Yavuz Primary School, was chosen as the sample school building to be analyzed for predicting the seismic performance level and determining the effects of different rehabilitation techniques to lateral load capacity and collapse mechanisms. By predicting the test results and determining the testing scheme, an in-situ test can be run and the effective retrofitting technique can be determined in order to seismically rehabilitate such buildings.

5.3. General Properties of Şehit Adem Yavuz Primary School Building

Şehit Adem Yavuz Primary School building consists of two blocks, A and B, which are separated from each other by a seismic joint. Block-A was constructed in 1976 and Block-B was constructed in 1985. Each block has one ground floor, one basement floor and two normal floors. The floors forming the structure are on the same elevation for both of the buildings. The floor height is 4.05 m on the basement floor, 3.15 m on the ground floor and 3.10 m on the other floors. The structural system of both blocks is RC. Loads are transferred to the columns via plates-beams. The cross-sections of lateral and horizontal structural elements vary throughout the structure. Figure 5.2 shows a general view of Şehit Adem Yavuz Primary School building.



Figure 5.2. General view of Şehit Adem Yavuz Primary School building

Block-A has plan dimensions of 27.70 ×14.10 m. Typical floor area is 310 m^2, whereas total building area is 1240 m^2. There is a central heating room, a dining room and a conference hall on the basement floor. On the ground floor, there are classrooms and

restrooms, whereas on the top floors, there are classrooms, a library, a teacher's room and restrooms.

Block-B has plan dimensions of 17.15 x 7.40 m. Typical floor area is 127 m^2, whereas total building area is 528 m^2. On the basement and ground floors, there are classrooms and restrooms, whereas on the top floors, there are classrooms, a computer laboratory, a science-technology laboratory and restrooms.

The general construction quality of the building has been determined as "low" in site surveys. Tests conducted by private firms have also confirmed the quality of the structural system as "low". However, no visual structural damage was observed. Figure 5.3 and Figure 5.4 show a general plan and side views of the school building. In the plan view, Block-A is partitioned as A1, A2, A3 and A4, and this notation will be used henceforth.

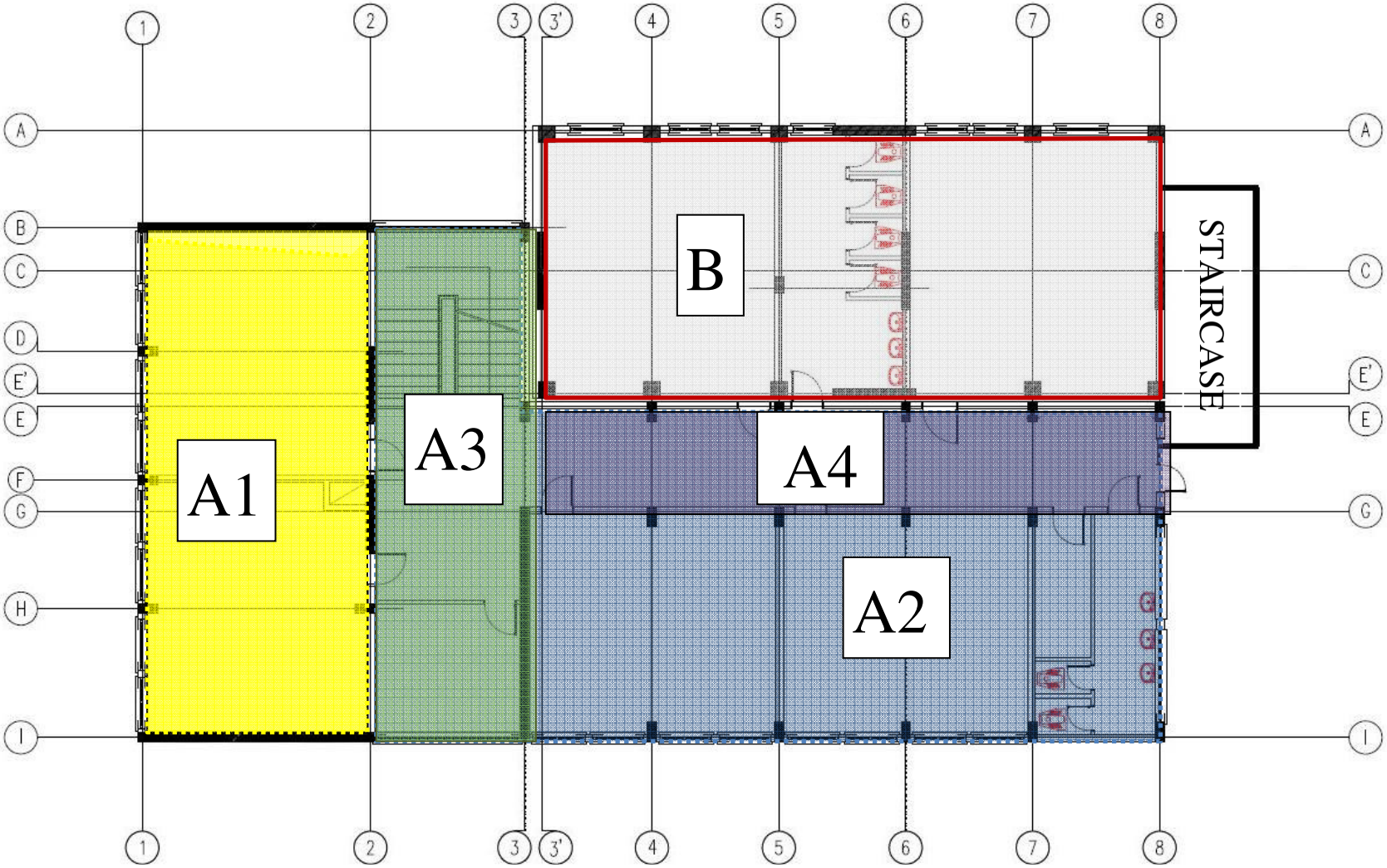

Figure 5.3. Plan view of Şehit Adem Yavuz Primary School

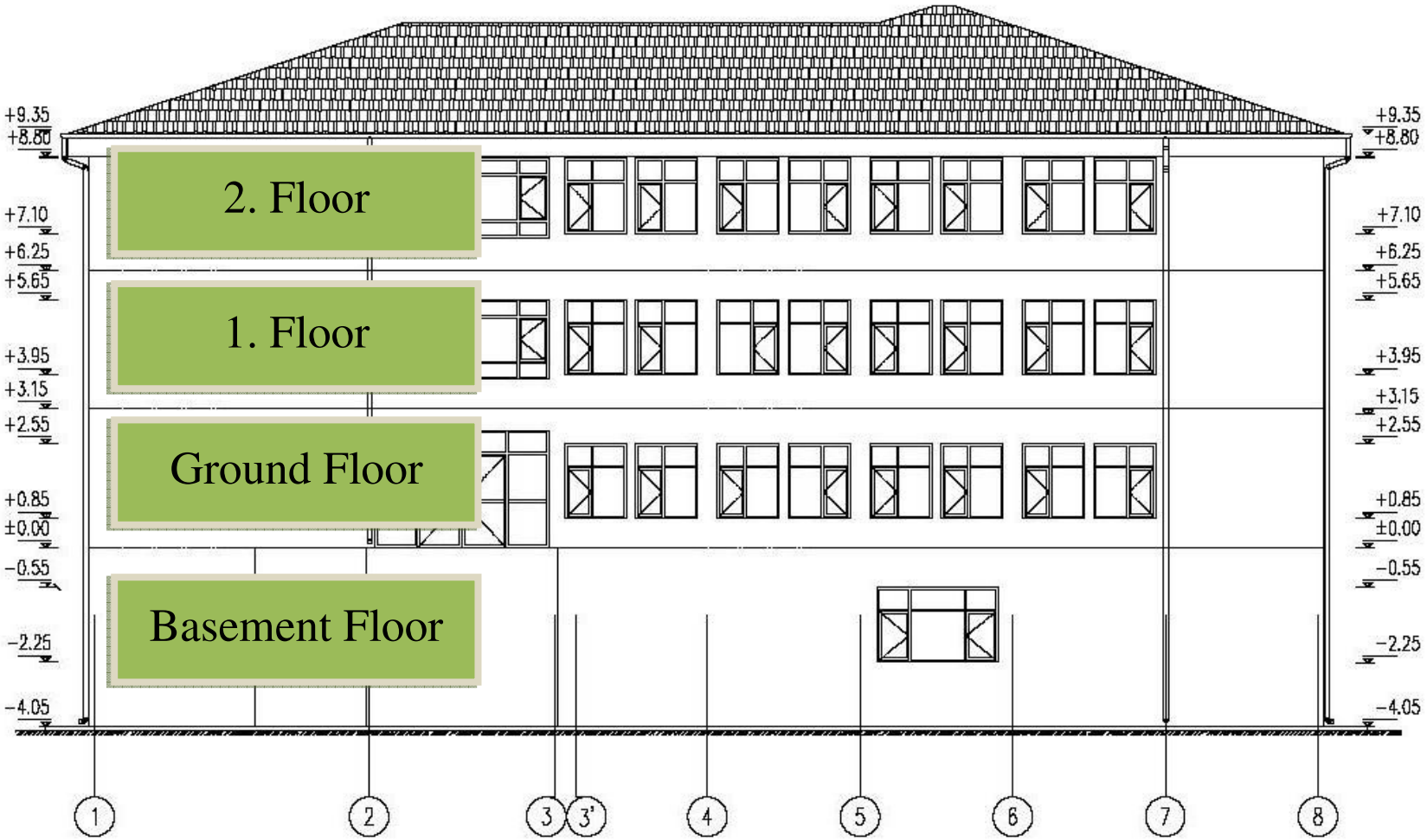

Figure 5.4 Side view of Şehit Adem Yavuz Primary School

5.4. Material Properties of Şehit Adem Yavuz Primary School

All of the studies required by "Medium Knowledge Level" among the knowledge level specifications in the TEC 2007 [16] have been performed by a private construction firm in order to determine the structural system and material properties in a reliable way.

The material properties of Şehit Adem Yavuz Primary School was obtained by core drilling methods and destructive experiments. According to the data obtained, it is observed that Block-A of the school building has a concrete compressive strength of 4 MPa and concrete tensile strength of 0.7 MPa. Block-B has a concrete compressive strength of 18 MPa and concrete tensile strength of 1.49 MPa.

By using ferro-scan electronic reinforcement detection devices, the placement of both the longitudinal and the transverse reinforcement are determined. Yield strength of the reinforcement bars and ultimate strength of the reinforcement bars are estimated as 220 MPa and 300 MPa, respectively. The destructive tests show that St-1 plain reinforcing bars were used in the building. It has been observed in all horizontal and vertical structural members of the blocks that there was effectively no confinement. The stirrup spacing has been observed to be around 250 mm. The diameters of both horizontal and longitudinal reinforcement bars were also determined. It is estimated that $\phi 14 - \phi 16$ reinforcement bars were used both in columns and beams, and $\phi 8$ reinforcement bars were used as stirrups. The clear cover was 30 mm measured from the outer side of the stirrup.

5.5. Proposed Test Setup

According to the given geometrical properties and material properties of the building, a test setup is proposed. It is proposed that Block-A should be used for static tests and dynamic tests. A1 region of Figure 5.3 should be used in the dynamic tests and A2 region of Figure 5.3 should be used in the static tests. Block-B is planned to be used as a specimen in the dynamic tests and as a reaction block in the static tests. Using Block-B as a reaction block rather than constructing a new one would be economically feasible. In order to investigate the effect of infill walls to frame performance behavior and test two types of seismic rehabilitation techniques, namely (i) infilled frame strengthened with CFRP and

(ii) RC infilled frame, four similar frames are needed (three test frames + a bare frame). It is impossible to obtain four similar, three-dimensional frames in this building. Due to this reason, it is determined that static tests should be performed on two-dimensional frames. The physical availability of the building led to the conclusion that the static test specimens should be two storey-single bay frames. In order to perform these tests, the following construction works are needed to be completed:

- Demolishment of the roof of Block-A,
- Total demolishment of the staircase block,
- Total removal of A3 and A4 regions (Figure 5.3),
- Removal of the top two floors of A2 region,
- Cutting of the ceiling slabs on basement floor and ground floor from 50 cm to the right and to the left hand side of the 4-5-6-7 axis in A2 region,
- Cleaning of all rubble.

Figure 5.5 and Figure 5.6 show three-dimensional computer models of the building before and after the construction works, respectively.

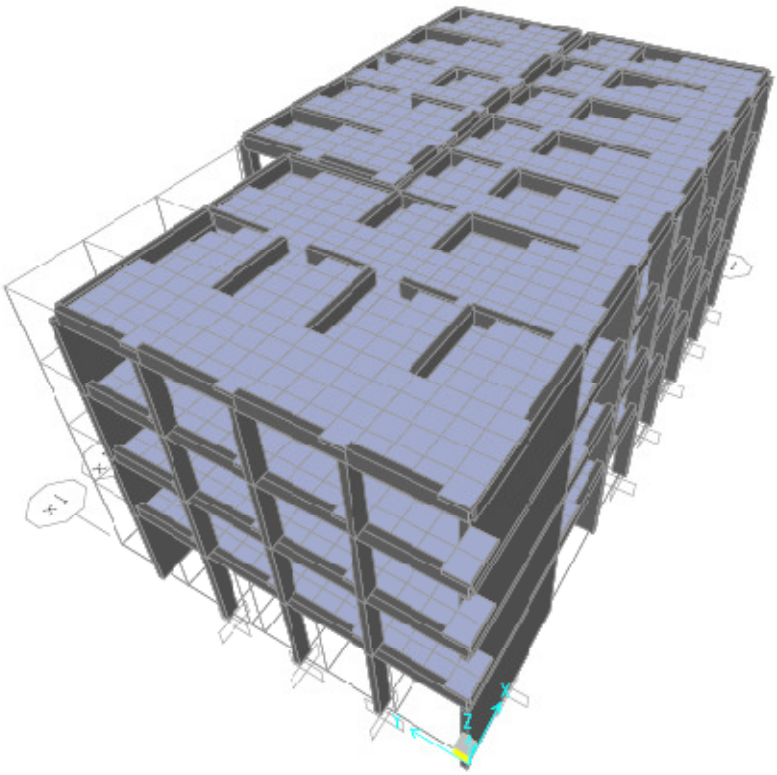

Figure 5.5. Computer model of the whole building before construction works

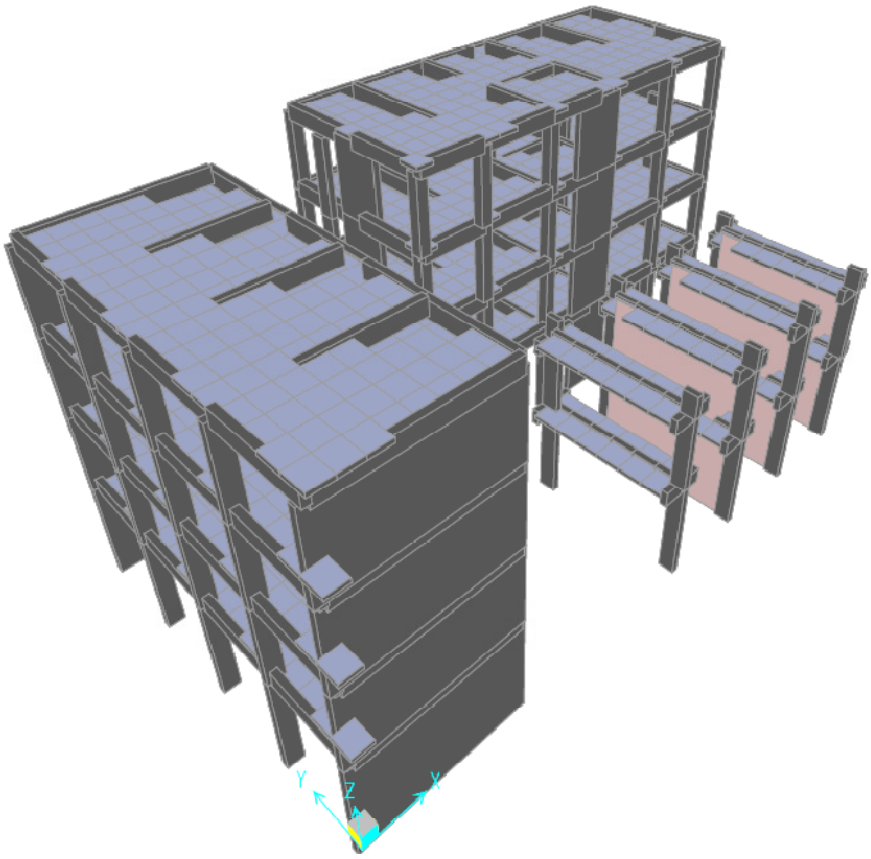

Figure 5.6. Computer model of the building after construction works

The required materials and works to be done to perform the above defined in-situ static tests are determined accordingly. In these tests, lateral loads would be applied to the test frame on storey levels, which means that two hydraulic actuators would be needed for a two storey test frame. The capacities of actuators should be determined according to results of the analyses of the strengthened test frames. The maximum lateral load and the maximum displacement can be used to determine load and stroke capacities of hydraulic actuators. Hydraulic actuators must have positive and negative stroke capacities to be able to perform cyclic static tests. Also, electric air pump, load cells, pipes, valves, bolts, etc., suitable with the chosen hydraulic actuators, would be required.

The connection details of loading equipment are another issue to be considered to perform in-situ pushover tests. The test frame would be supported such that local failures would not be observed. While pulling the test frame, tension occurs in the region of the test frame where the actuator is connected, and tensile stresses may cause local failures which have to be prevented. Similarly, lateral loads that would be applied to the test frame would

also act on the reaction block, and local failures in the reaction block would have to be prevented. Figure 5.7 shows the test setup designed preliminarily for the bare frame.

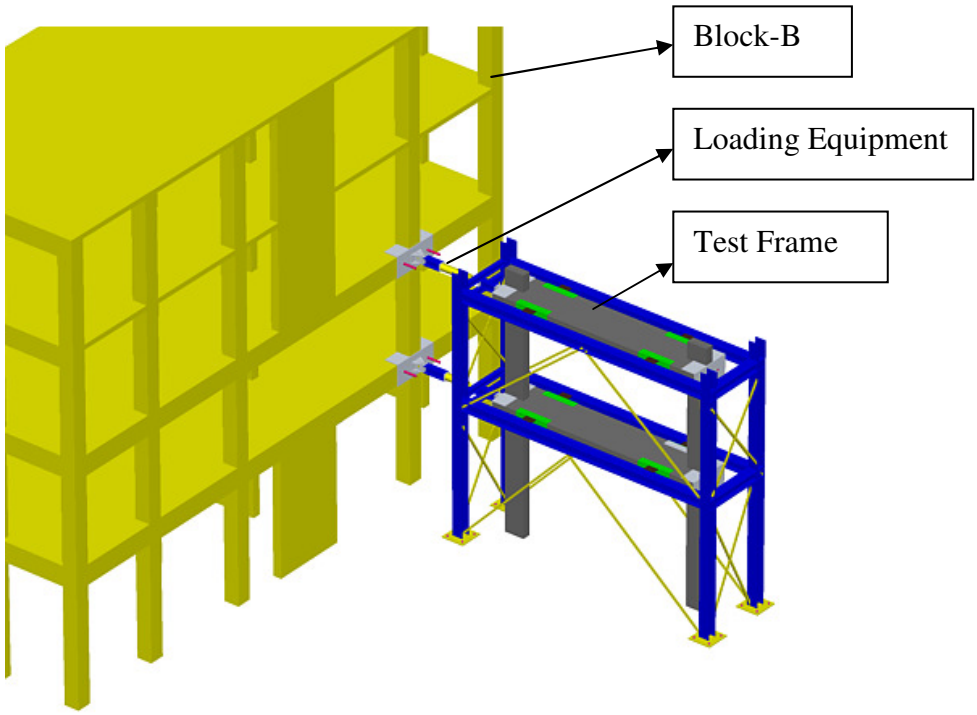

Figure 5.7. General view of the test setup from preliminary computer model

The setup shown in Figure 5.8 is proposed to be used to prevent local failures in test frames. The steel plates would be connected to the test frame on both edges and steel cables would be used to connect both ends. In general, local tensile failures would be expected to occur while pulling the test frame. By using the setup shown in Figure 5.8, while pulling on the test frame, it would actually be pushed from the other end due to the load transfer mechanism of the cables.

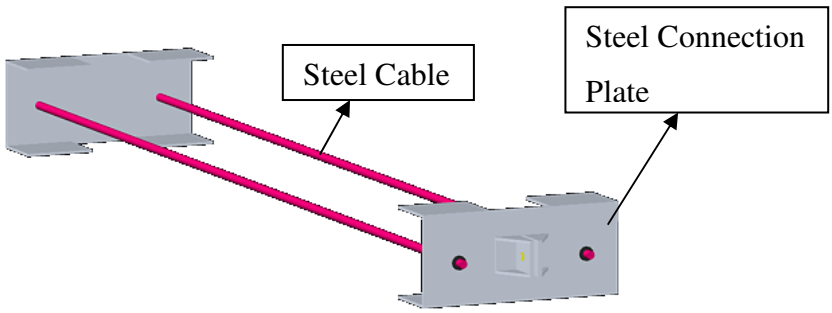

Figure 5.8. Setup to prevent local failures of the test frame (assemblage system)

Hydraulic actuators have limited length, which depends on their stroke capacities. The span between the reaction block and test frame is three meters. In order to prepare a stable loading system, extension steel sections would be needed. At the end points, ball and socket joints would be needed to prevent failure of the end joint. Figure 5.9 show the typical loading system that could be used in the in-situ tests.

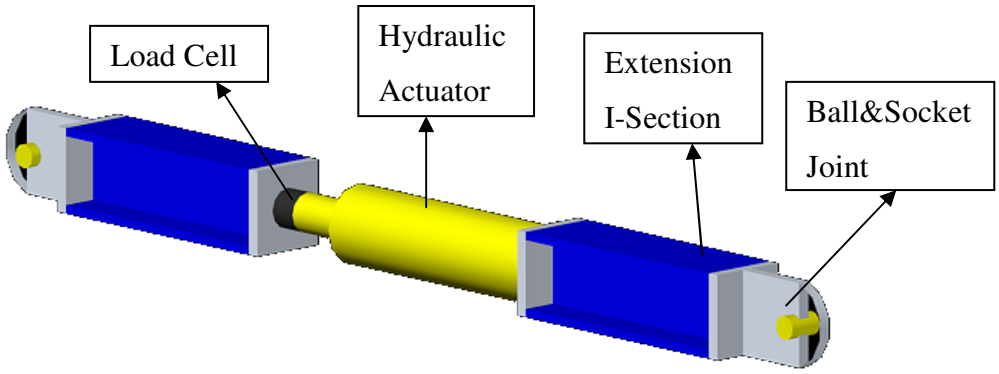

Figure 5.9. Typical loading system

Out-of-plane twisting of test frames results with premature failures, which means the tests can't reach their scope. In order to perform static pushover tests, test frames have to be limited to deform only in testing direction. Using a three dimenional rectangular frame is one of the proposed systems that can be used for resisting out-of-plane twisting. Spacings of the elements of this frame are determined according to dimensions of test frame. Because a high stiffness is needed, cross steel ties on both sides of resisting frame are used. At storey levels, overhanging I-sections placed in transverse direction are needed to prevent out-of-plane actions. While loading the test frame, it is possible for the frame to be damaged due to frictional forces that occur between the overhanging I-profiles and the slab of test frame. Due to this, steel plates connected to the slabs of the test frames would be needed. C-shaped steel plates are chosen to be used to prevent these damages. Before tests, C-shaped steel plates and overhanging I-sections have to be greased to supply smooth, friction reduced surfaces. Using such a resisting frame also provides safety while testing. By designing this frame considering the maximum vertical load that can be exerted by the test frame, the possible damage that can occur to the testing equipment can be prevented if a sudden collapse occurs. Figure 5.10 shows the general view of the three dimensional out-of-plane resisting frame proposed.

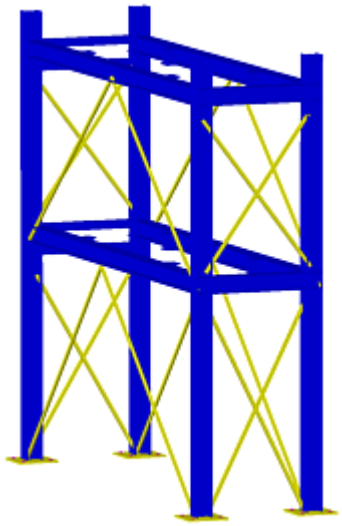

Figure 5.10. General view of out-of-plane resisting frame

Figure 5.11 shows general views of tests frame, out-of-plane resisting frame, overhanging steel I-profiles, and steel C-plates.

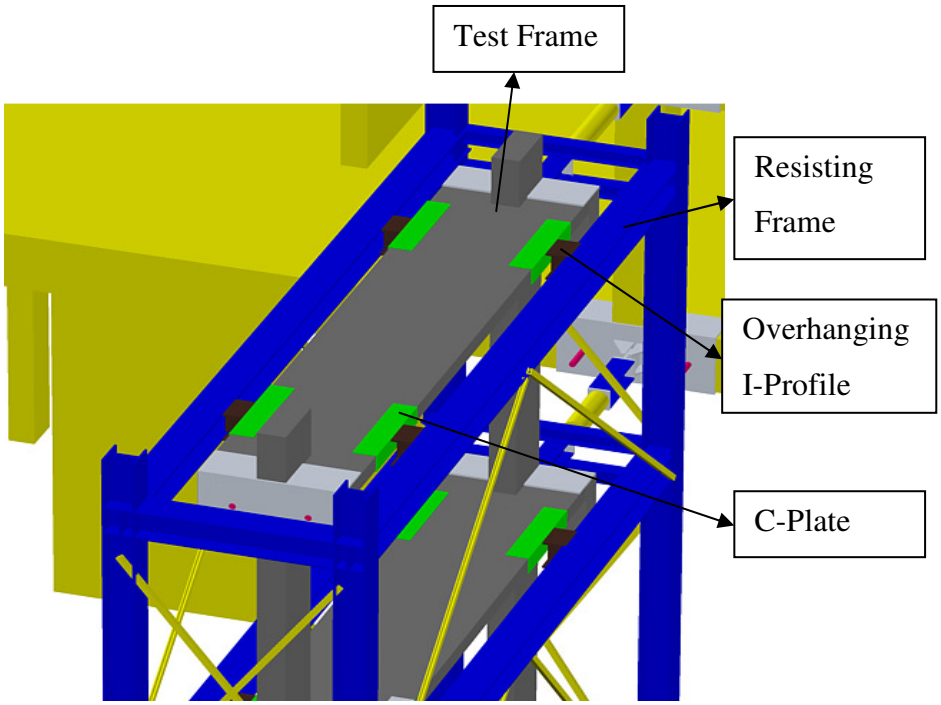

Figure 5.11. General view of out-of-plane resisting frame and test frame

Second proposed system to prevent out-of-plane twisting of test frame is a triangular truss system. Figure 5.12 shows the general view of one of the triangular trusses.

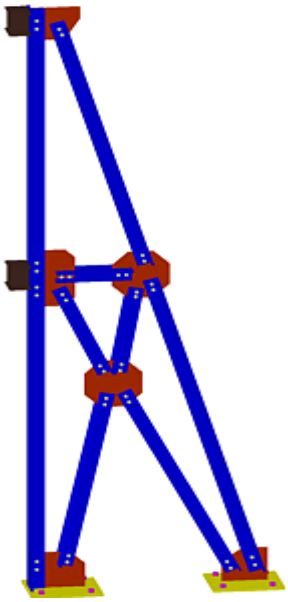

Figure 5.12. General view of one of the triangular trusses

As in the first resisting frame system proposed, extension I-sections and C-plates located on slabs of test frames are needed. Figure 5.13 shows the general view of the resisting triangular truss system and test frame.

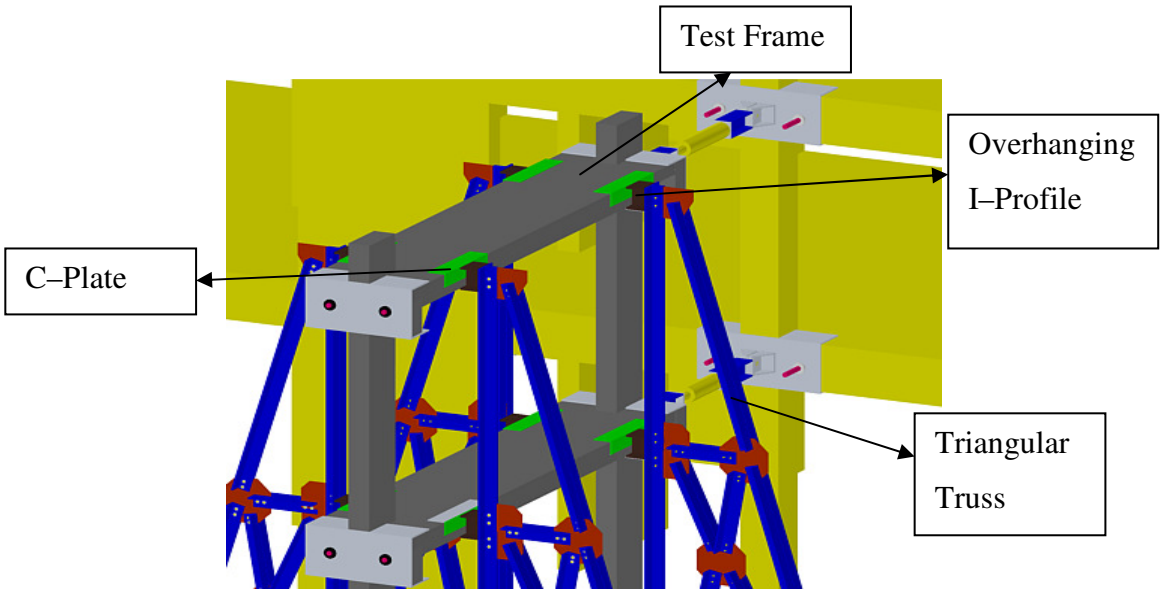

Figure 5.13. General view of the out-of-plane resisting triangular trusses and test frame

By estimating the loads that can be exerted on steel resisting systems, cross sectional dimensions of steel profiles for both systems are determined in Section 6.3.3. According to the analysis results, the usable system is determined and detailing of the structure is done.

5.6. Properties of Test Frames (Block-A)

The remaining four, two-storey-single-bay planar frames in region A2 have similar properties in terms of geometry and material properties of the structural elements. Figure 5.14 presents the test frames that are proposed for static tests.

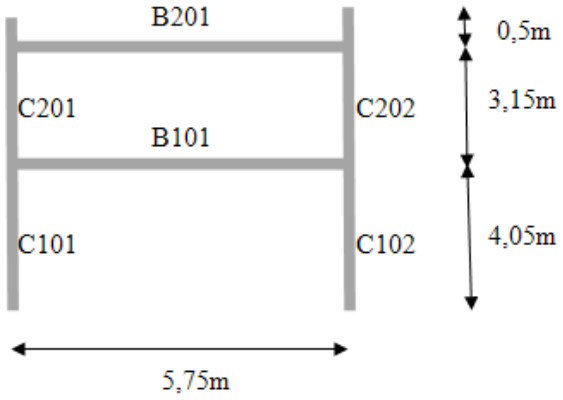

Figure 5.14. General view of the static test frame

Table 5.1 presents the dimensions and reinforcement details of the column and beam sections shown in Figure 5.14.

Table 5.1. Member sections and reinforcement details

Member	b (mm)	h (mm)	Longitudinal Reinforcement	Transverse Reinforcement	General View
C101	250	600	8 – ϕ16	ϕ8 / 250	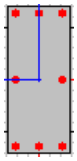
C102	250	700	8 – ϕ16	ϕ8 / 250	
C201	250	550	8 – ϕ16	ϕ8 / 250	
C202	250	550	8 – ϕ16	ϕ8 / 250	
B101	250	600	3 – ϕ16	ϕ8 / 250	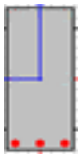
B201	250	600	3 – ϕ16	ϕ8 / 250	

The slab thickness is 150 mm. The mass of each story is determined as 12 tons. Cracked stiffness values are assigned to columns and beams. Cracked stiffness coefficients are taken as 0.40 for beams, and varied between 0.40 and 0.80 for columns, based on the level of axial load on each, according to TEC 2007 [16]. For detailed analysis, moment-curvature relationships are used to define the cracked stiffness coefficients.

5.7. Properties of the Reaction Block (Block-B)

Figure 5.15 presents the plan view of Block-B. There exist 450 x 450 mm^2 and 450 x 250 mm^2 column sections, 250 x 600 mm^2, 350 x 600 mm^2 and 250 x 400 mm^2 beam sections and 250 x 2250 mm^2 and 2100 x 250 mm^2 shear wall sections in Block-B.

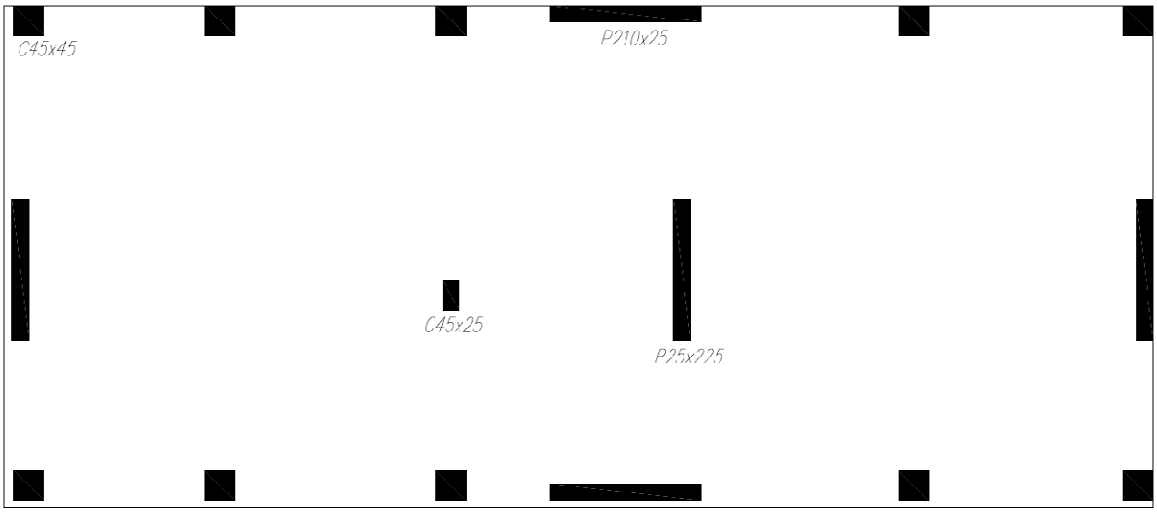

Figure 5.15. Plan view of Block-B

Every storey has identical structural elements in Block-B. Due to this, the member sections and reinforcement details are given in Table 5.2 according to member dimensions.

Table 5.2. Member sections and reinforcement details

	b(mm)	h(mm)	Longitudinal Reinforcement	Transverse Reinforcement
Column (C)	450	450	$8-\phi16$	$\phi8/250$
Column (C)	250	450	$6-\phi16$	$\phi8/250$
Beam (B)	250	600	$3-\phi16$	$\phi8/250$
Beam (B)	350	600	$3-\phi16$	$\phi8/250$
Beam (B)	250	400	$3-\phi16$	$\phi8/250$
Shear Wall(P)	250	2250	$32-\phi12$	$\phi8/250$
Shear Wall (P)	250	2100	$28-\phi12$	$\phi8/250$

Also in Block-B the slab thickness is 150 mm. Cracked stiffness values are assigned to columns and beams. Cracked stiffness coefficients are taken as 0.40 for beams, and varied between 0.40 and 0.80 for columns, based on the level of axial load on each, according to TEC 2007 [16]. For detailed analysis, moment-curvature relationships are used to define the cracked stiffness coefficients.

5.8. Work Flowchart and Time Schedule

In accordance with the proposed test setup for Sehit Adem Yavuz Primary School building, a flowchart for the required construction works, which is shown in Figure 5.16, was prepared. Also, an approximate time schedule was prepared by using computer software program Microsoft Project 2003. According to this schedule, a time period of 16 weeks is enough for in-situ pushover tests. Figure 5.17 shows the prepared Gannt Chart which shows the weekly progression of the schedule.

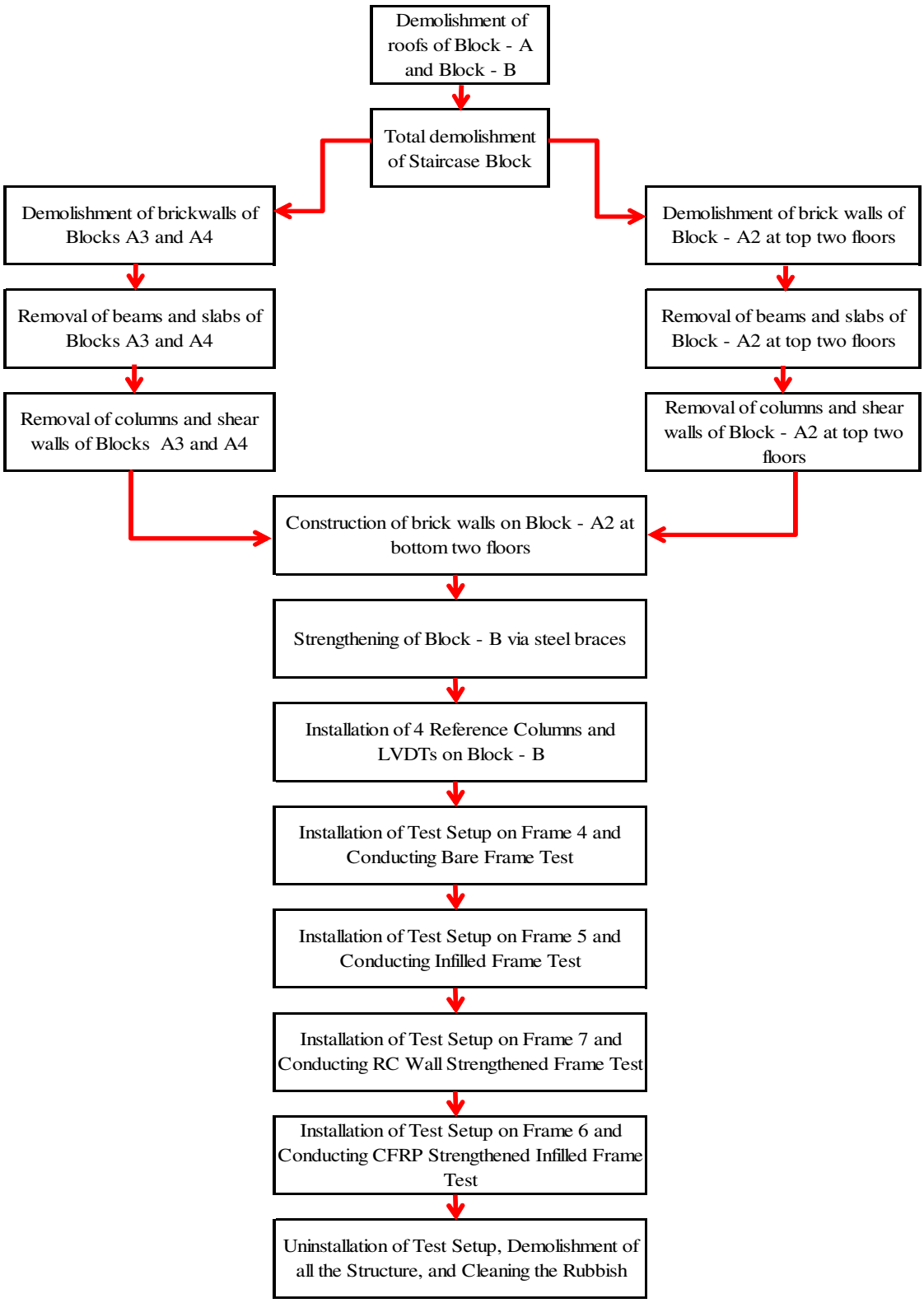

Figure 5.16. Flowchart for required construction works

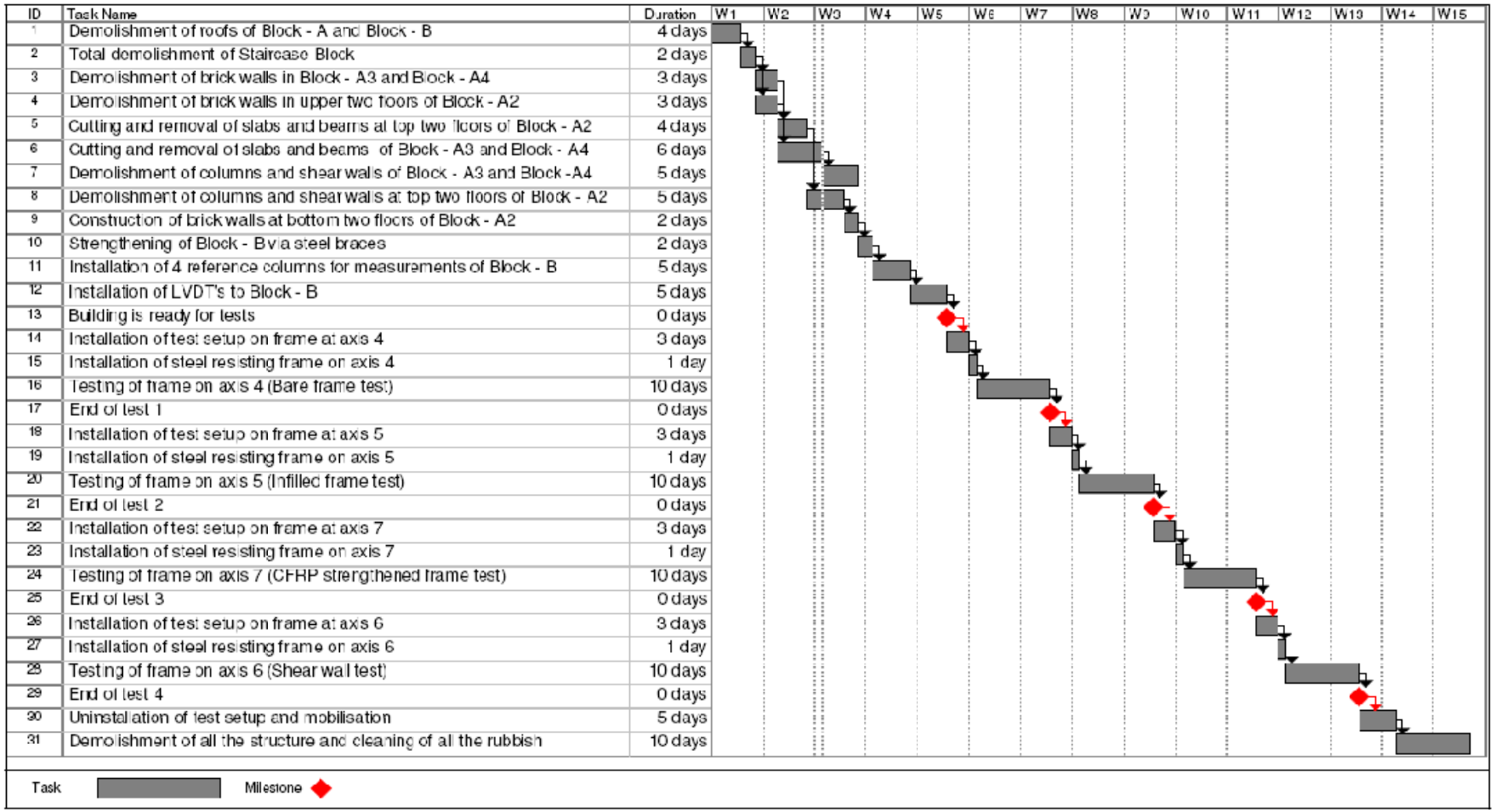

Figure 5.17. Time schedule for in-situ tests

6. NONLINEAR ANALYSIS OF STATIC TEST FRAMES AND BLIND PREDICTION OF IN-SITU TEST RESULTS

The displacement controlled nonlinear static analyses of static test frames and reaction block of Şehit Adem Yavuz Primary School building were done using the commercial computer software program SAP2000.v11.0.0 [26].

6.1. Modeling of the Structure and Analysis Procedure

Two-dimensional structural models for static test frames and three-dimensional structural model for reaction block were developed by SAP2000.v11.0.0 [26] according to the building information given in Section 5.3. Elastic frame elements were used to model the structural members. The nonlinear behavior of the frame members were represented by moment hinges, axial force-moment hinges, shear hinges, and axial hinges as detailed in Section 3.2. Infill walls were modeled according to the equivalent truss concept detailed in Section 3.2.2. While calculating the equivalent trusses representing the infill walls, standard 190×190×135 mm bricks were used. In accordance with a prior study by Atmaca [44], uniaxial compression strength of the brick and mortar were assumed as 16 MPa and 5 MPa, respectively. Horizontal and vertical seam widths were assumed as 5 mm. Wide columns, located at the center of the spans, were used to model the shear walls. A compression strut and a tension tie were used to model the CFRP strengthened infilled wall as described in Section 3.2.4. Figure 6.1 shows computer models of (i) bare frame, (ii) infilled frame, (iii) infilled frame strengthened with CFRP, and (iv) RC wall strengthened frame and Figure 6.2 shows three-dimensional computer model of reaction block.

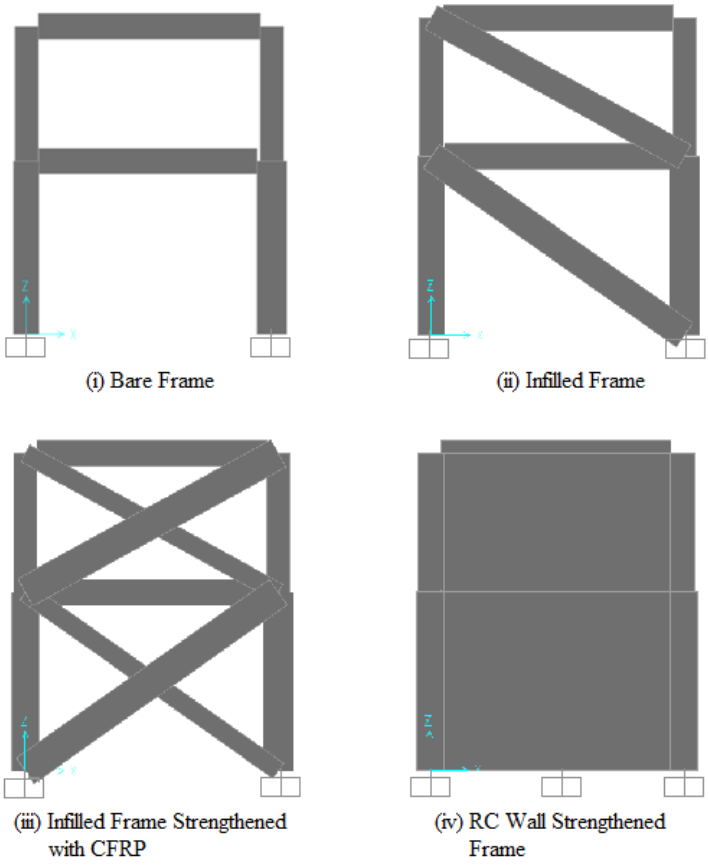

Figure 6.1. Computer models of two-dimensional test frames

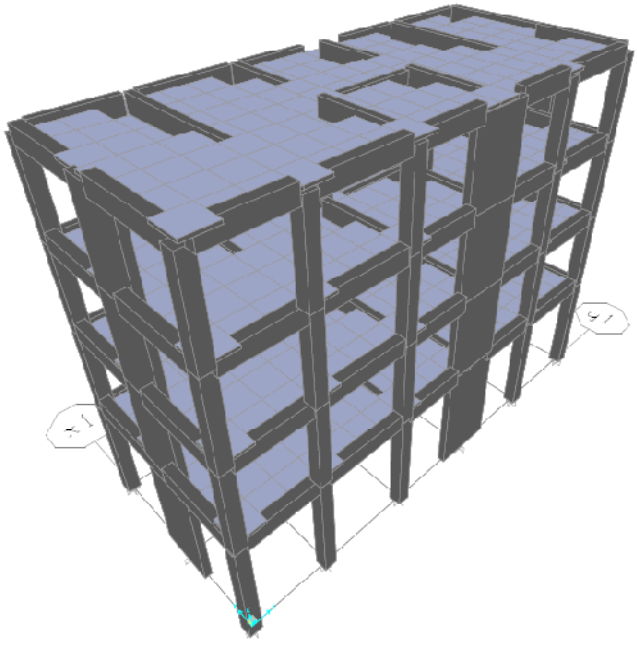

Figure 6.2. Computer model of three-dimensional reaction block

The analyses were displacement controlled up to a maximum lateral displacement of 250 mm. Frame members included plastic moment hinges, axial hinges, and shear hinges on beams, and normal force-moment interaction hinges, shear hinges, and axial hinges on columns. Lateral loads were applied on both floors of static test frames in proportion to mass times story elevation. The same lateral loading pattern used in static test frames were applied on first two floors of the reaction block in the opposite direction. Figure 6.3 shows the lateral loading pattern in static test frames.

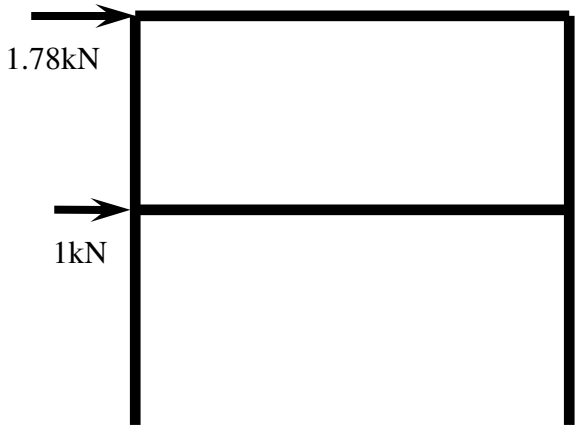

Figure 6.3. Lateral loading pattern in static test frames

6.2. Sample Calculations for Nonlinear Hinges

The procedures detailed in Section 3.2 were used to define the nonlinear hinges used in computer model. Section 6.2 shows some sample calculations to obtain force-displacement or stress-strain relationships of structural elements of test frames.

6.2.1. Moment (M) Hinges

The procedure given in Section 3.2.1.1 was used to define the moment hinges. Figure 6.4 shows the moment-curvature analysis of beam B101, conducted using Ersoy's Excel Spreadsheet Program [24].

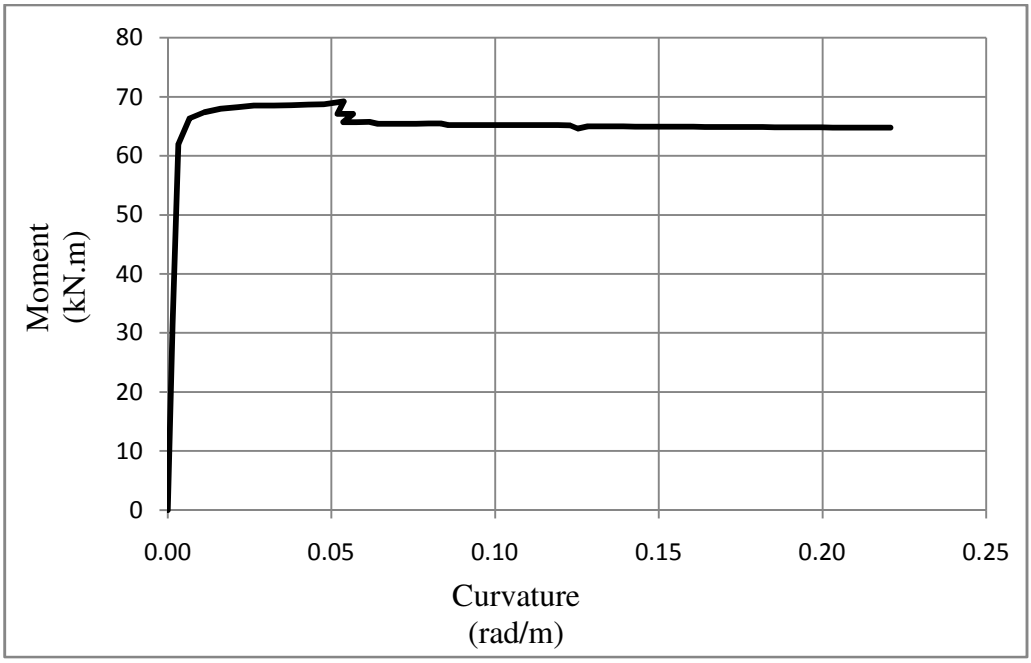

Figure 6.4. Moment-curvature relationship of beam B101

In accordance with the graph in Figure 6.4, yield moment and curvature at yield moment were determined as 65 kN.m and 0.0066 rad/m, respectively. Half the section depth was used for hinge length, which equals to 0.3 m. The computer program SAP2000.v11.0.0 uses the hinge length to calculate the plastic rotation of a hinge. The section moment curvature relationship was entered to the computer program by normalizing it with yield values. Table 6.1 shows the normalized values of moment and curvature, used in the computer program.

Table 6.1. Normalized moment-curvature values of beam B101

Curvature / SF	Moment / SF
0	0
0	1
8	1
20	1
33	1

Figure 6.5 shows the backbone model of plastic moment hinge of beam B101 used in computer model.

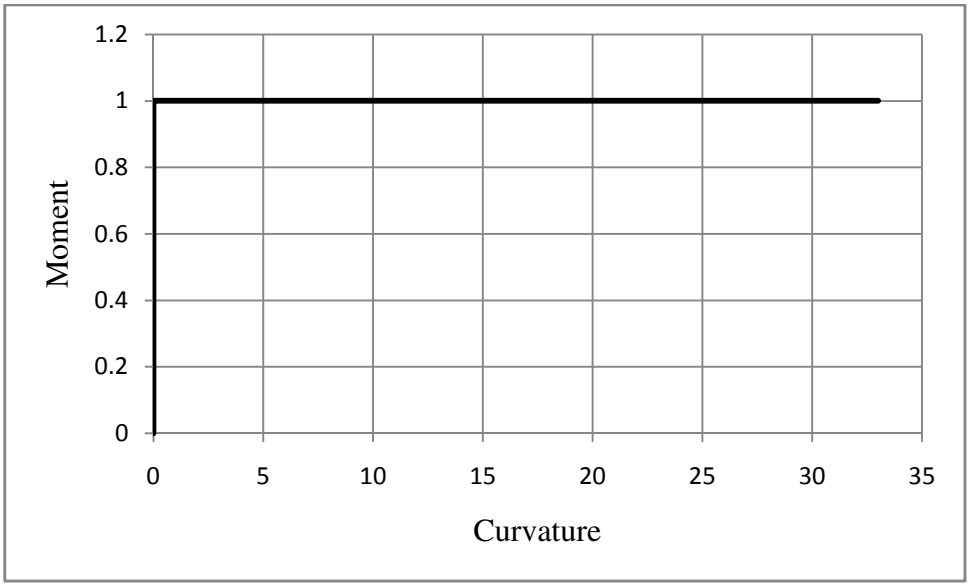

Figure 6.5. Backbone model of plastic moment hinge of beam B101

Up to yield point, the elastic behavior of the frame element is represented by modulus of elasticity and cracked section stiffness multiplier. The plastic behavior is represented by nonlinear plastic hinge backbone model, shown in Figure 6.5.

6.2.2. Normal Force-Moment (P-M) Hinges

The procedure given in Section 3.2.1.2 was used to define the normal force-moment hinges. Figure 6.6 shows the interaction relationship of column C201 obtained using Ersoy's Excel Spreadsheet Program. The section properties of column C201 are given in Table 5.1.

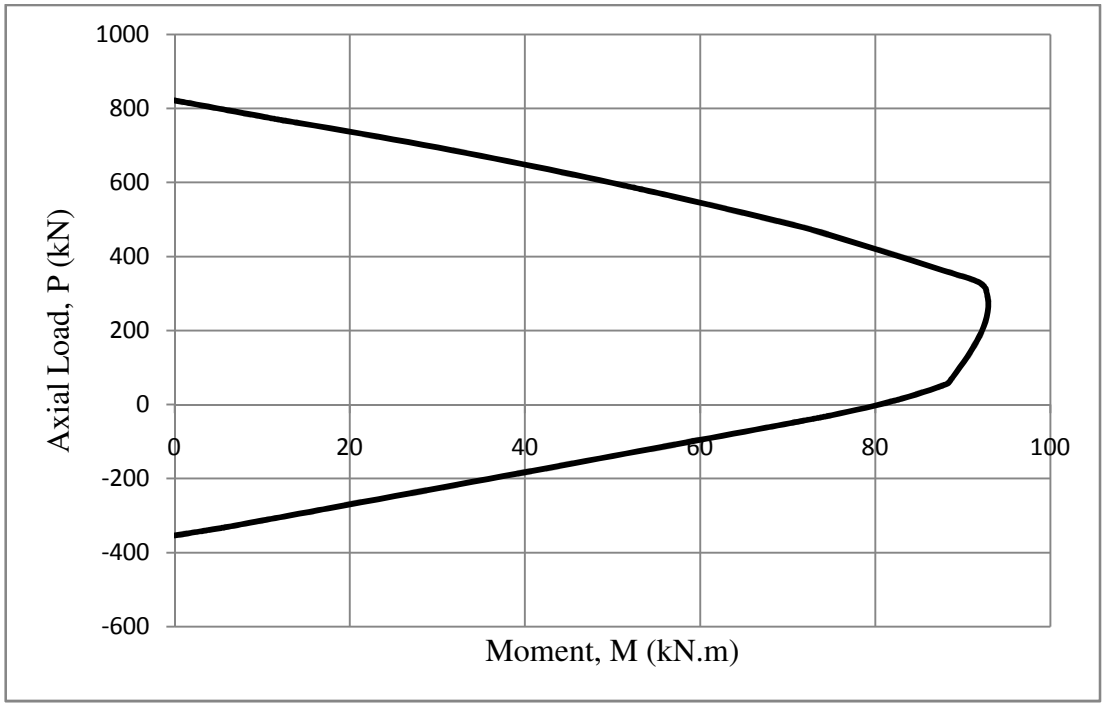

Figure 6.6. P-M interaction curve of column C201

In accordance with the interaction graph in Figure 6.6, moment and normal force values at balance point were determined as 92.89 kN.m and 276.56 kN, respectively. Half the section depth (275 mm) was used for hinge length. It is impossible to enter the curve continuously to the computer software. Due to this, a linearization is required. As the number of defined points on the curve increase, the moment-normal force behavior of a section becomes more accurate. A minimum of four point linearization is preferred. For such a representation, pure compression point, balance point, pure bending point and pure tension point can be used. Table 6.2 shows the normal force-moment values for these points and Figure 6.7 shows the linearized interaction curve of column C201.

Table 6.2 Linearization points of the interaction diagram (C201)

P (kN)	M(kN.m)	Point
821.26 (C)	0	Pure Compression
276.59 (C)	92.89	Balance
0	80.50	Pure Bending
353.76 (T)	0	Pure Tension

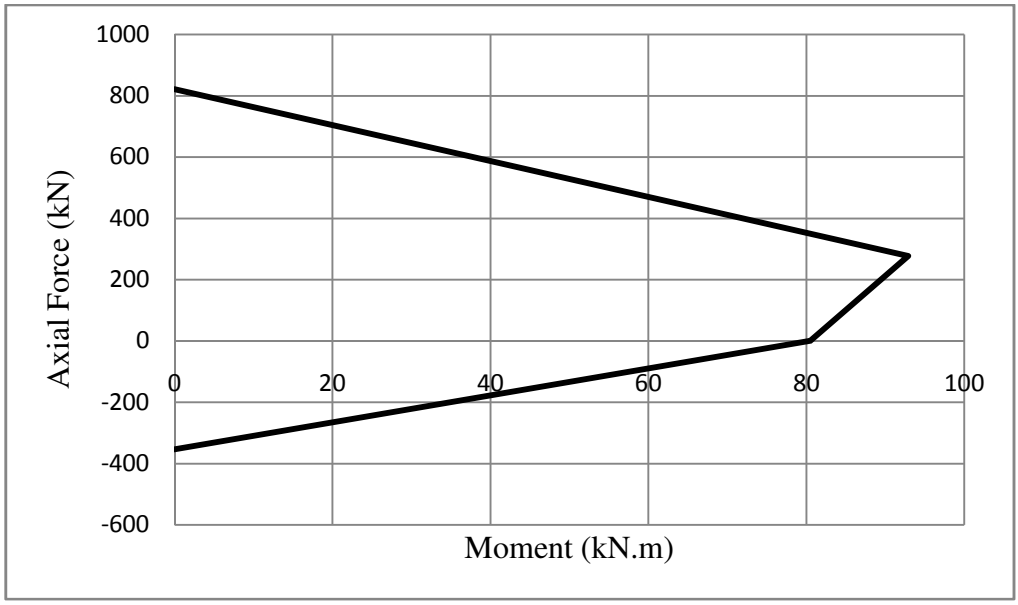

Figure 6.7. Linearized interaction curve of column C201

The moment-curvature analysis of the section is needed under the axial loads used in the linearized interaction curve. The procedure to define a moment hinge with the moment-curvature relationship summarized in Section 6.2.1 is applicable for this case.

6.2.3. Axial Hinges (P)

Force-displacement relationships are used to model axial hinges. Concrete and steel forces are used to determine the compression part of the force-displacement curve. Since the concrete tensile strength is very low, only the steel force is considered to determine the tension part. Hognestad stress-strain relationship given in Figure 3.1 and the steel stress-strain relationship given in Figure 3.4 are used in the analyses. Figure 6.8 shows the axial force-displacement behavior of column C102. The sharpness of the curve at peak compressive force occurred due to 4 MPa concrete strength in Şehit Adem Yavuz Primary School Building. As the concrete strength increases, ε_{co} value in Hognestad curve increases and a smoother transformation from increasing axial load to decreasing one occurs.

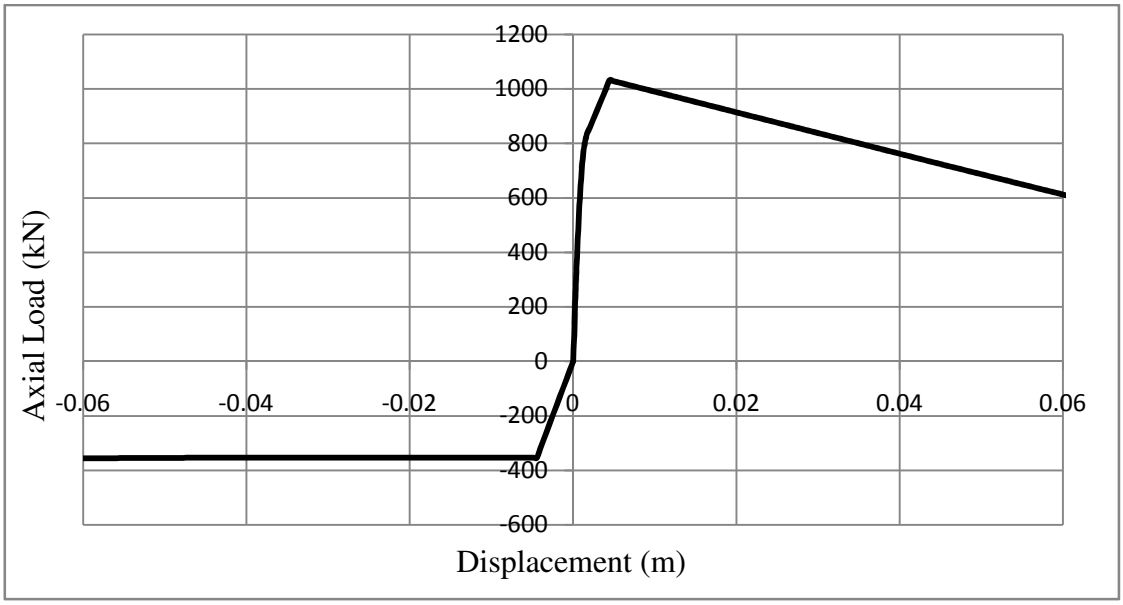

Figure 6.8. Axial force-displacement relationship of column C102

The force-displacement relationship is defined in the computer model by normalizing it and using the yield values as scale factors. Table 6.3 shows the normalized force-displacement relationship of column C102. The scale factors (SF) are 1032 kN for yield compression force, 354 kN for yield tension force, and 0.0045 mm/mm for strains at compression and tension yield points.

Table 6.3. Normalized force-displacement curve of column C102

Displacement / SF	Force / SF
-66.7	-0.378
-66.7	-0.378
-19.8	-0.374
0.0	-1.000
0.0	0.000
0.0	1.000
66.7	1.102
66.7	1.102
66.7	1.102

6.2.4. Shear (V) Hinges

There are two types of shear hinges described in Section 3.2.1.4. One of them is the hinge proposed by Elwood and Moehle [28] in which both the flexural and the shear behaviors of the frame section are represented by a single hinge. In order to use this hinge, the frame would have to be a shear critical member. The second shear hinge defined in Section 3.2.1.4 represents only the shear behavior. The force-displacement or stress-strain behavior of a frame element has to be calculated to define a shear hinge. The shear capacities of sections can be determined in accordance with the equation 3.20. The displacement behavior can be represented by specified plastic rotations according to the study by Wu and Xue [3] or the empirical relationships by Elwood and Moehle [28] in accordance with the hinge type. Table 6.4 and Table 6.5 show the calculation summary of shear capacity calculation of frame members of the proposed test building.

Table 6.4. Summary of shear capacity calculation-contribution of concrete

Column #	h (mm)	b (mm)	L (m)	A_{st} (mm^2)	Area (m^2)	Minimum Compressive axial load (kN)	Nd/Ac (MPa)	Ψ	V_c (kN)
C101	600	250	4.05	1608	0.15	142	0.95	1.07	53.85
C102	700	250	4.05	1608	0.175	208	1.19	1.08	64.56
C201	550	250	3.15	1608	0.1375	111	0.81	1.06	48.55
C202	550	250	3.15	1608	0.1375	159	1.16	1.08	49.67
B101	600	250	5.75	1608	0.15	0	0.00	1.00	50.51
B201	600	250	5.75	1608	0.15	0	0.00	1.00	50.51

Table 6.5. Summary of shear capacity calculation-contribution of steel and total shear capacity

Column #	A_{sw} (mm^2)	s (mm)	d (mm)	V_w (kN)	Vcap. (kN)
C101	150.80	250	555	73.65	128
C102	150.80	250	655	86.92	151
C201	150.80	250	505	67.01	116
C202	150.80	250	505	67.01	117
B101	100.53	250	555	49.10	100
B201	100.53	250	555	49.10	100

For displacement behavior of frame members, specified plastic rotations by Wu and Xue [3] are used. The scales representing the force behavior of force-displacement curve are determined according to FEMA 356 [41]. Table 6.6 shows the normalized force-displacement values of frame members.

Table 6.6. Normalized force-plastic rotation values of frame members

Rotation(%)	Force(kN)
0	0
0	1.0
1.5	1.05
1.5	0.2
3.0	0.2

The shear capacities of frame members and member lengths are used as scale factors. For instance, for column C101, yield shear force is estimated as 128 kN and member length is 4.05 m. By multiplying the forces and the rotations given in Table 6.6 with the scale factors, the actual shear behavior of column C101 can be found. Figure 6.9 and Figure 6.10 shows the normalized force-plastic rotation and force-displacement relationships of column C201.

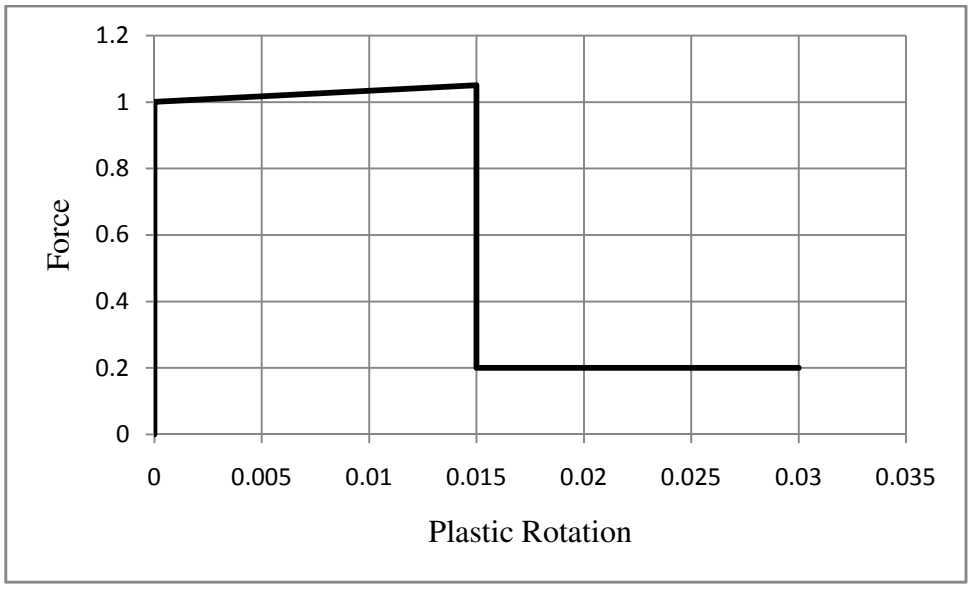

Figure 6.9. Normalized force-plastic rotation relationship of column C201

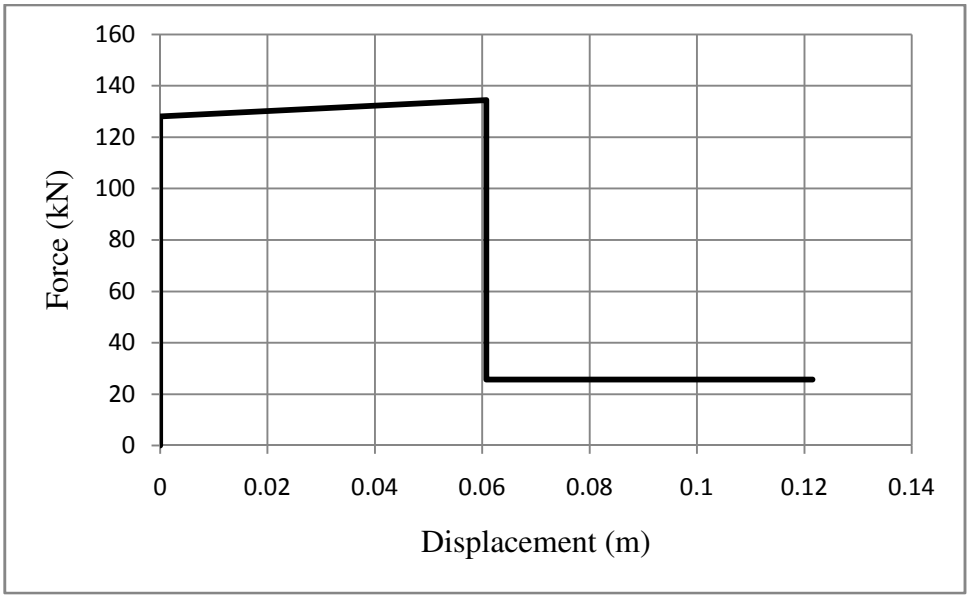

Figure 6.10. Force-displacement relationship of column C201

6.2.5. Axial (P) Hinges for Brick Walls

The formulations given in Section 3.2.2 are used while modeling the infill walls of static test frames. Because the height of an infill wall is an important parameter affecting the length of equivalent truss, two types of equivalent trusses and axial hinges are modeled depending on storey heights. Some assumptions were made while modeling the infill walls. The bricks of the infill wall are assumed standard Turkish bricks. To determine the uniaxial compressive strength of mortar and brick, a prior study by Atmaca [44] is used.

Brick dimensions are taken as $190\times190\times135\text{mm}$. Horizontal and vertical seam widths (g_h and g_v) are taken as 5mm. Uniaxial compressive strength f_{mc} of mortar is taken to be 5MPa, and the uniaxial compressive strength f_{bc} of brick is taken to be 16MPa.

The formulations given in Section 3.2.2 and the strength and size assumptions lead to an equivalent truss length of 6.16 m in first storey and 5.77 m in second storey. Equivalent truss areas come out to be 0.408 m^2 for the first storey and 0.326 m^2 for the second storey. Ultimate strength of brick wall is calculated as 200 kN for the first storey and 175 kN for

the second storey. Ultimate displacement of brick wall is found to be 0.104 m in the first storey and 0.0080 m in the second storey.

The parameters and the graphical representation of the first storey infill wall hinge are shown in Table 6.7 and Figure 6.11, respectively; while those of the second storey hinge are given in Table 6.8 and Figure 6.12.

Table 6.7. Nonlinear axial hinge parameters of first storey infill wall

Points	disp/sf	force/sf
A	0	0
B	0	1.00
C	1.00	0.51
D	8.00	0.51
E	8.00	0.51

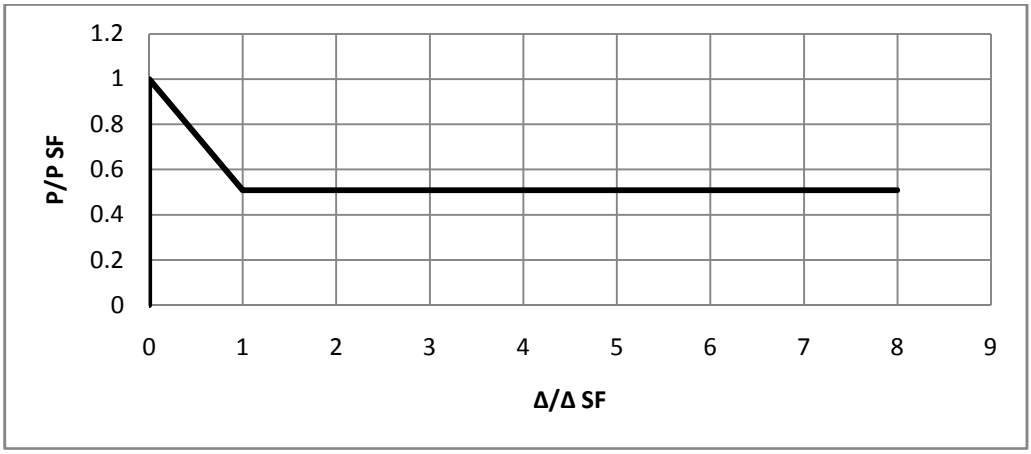

Figure 6.11. Nonlinear axial hinge of first storey infill walls

Table 6.8 Nonlinear axial hinge parameters of second storey infill wall

Points	disp/sf	force/sf
A	0	0
B	0	1.00
C	1.00	0.58
D	7.06	0.58
E	7.06	0.58

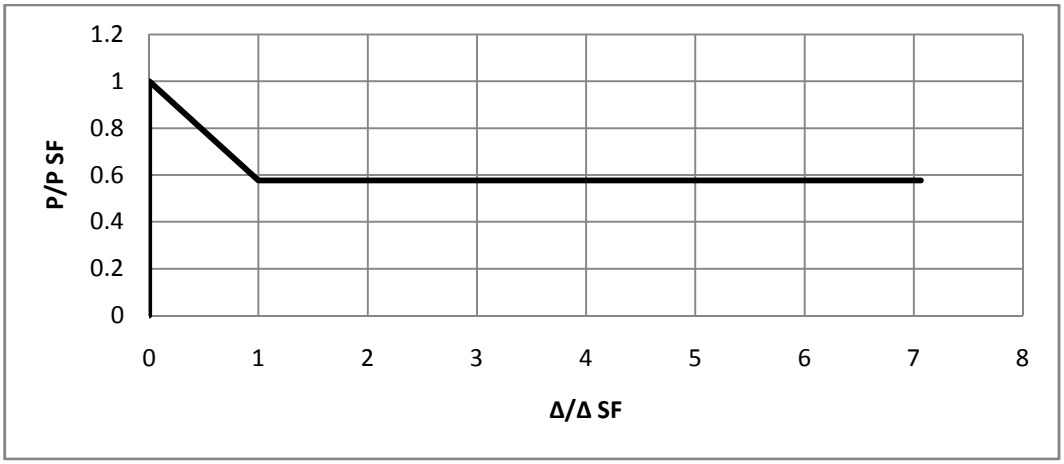

Figure 6.12. Nonlinear axial hinge of second storey infill walls

6.2.6. Axial (P) Hinges for Tension Ties

Binici and Ozcebe's [17] approach is used to model the tension ties as detailed in Section 3.2.4. According to this, a trilinear stress-strain response for truss members to simulate the behavior of the strengthened infill wall is calculated and defined in the computer program. Some assumptions are made in accordance with Binici and Ozcebe's [17] and Atmaca's [44] prior studies: The width w_f of CFRP provided is assumed as 700 mm; thickness t_f of CFRP is assumed as 1.25 mm; thickness of plaster t_p is assumed as 10 mm; and thickness t_{in} of wall is assumed as 200 mm. Nominal compressive strength f_{mc} of mortar is assumed as 5 MPa, and nominal tensile strength f_{pt} of mortar is assumed as 0.5 MPa. Modulus of elasticity of CFRP and mortar are used as 230,000 MPa and 12,421 MPa, respectively. The effective strain $\varepsilon_{f,eff}$ was assumed as 0.002 and the strain at which complete failure of FRP occurs ε_{tu} is assumed as three times the effective strain (0.006). In accordance with the assumptions made and the formulations given in Section 3.2.4, Figure 6.13, which shows the stress-strain behavior of CFRP tie, is obtained.

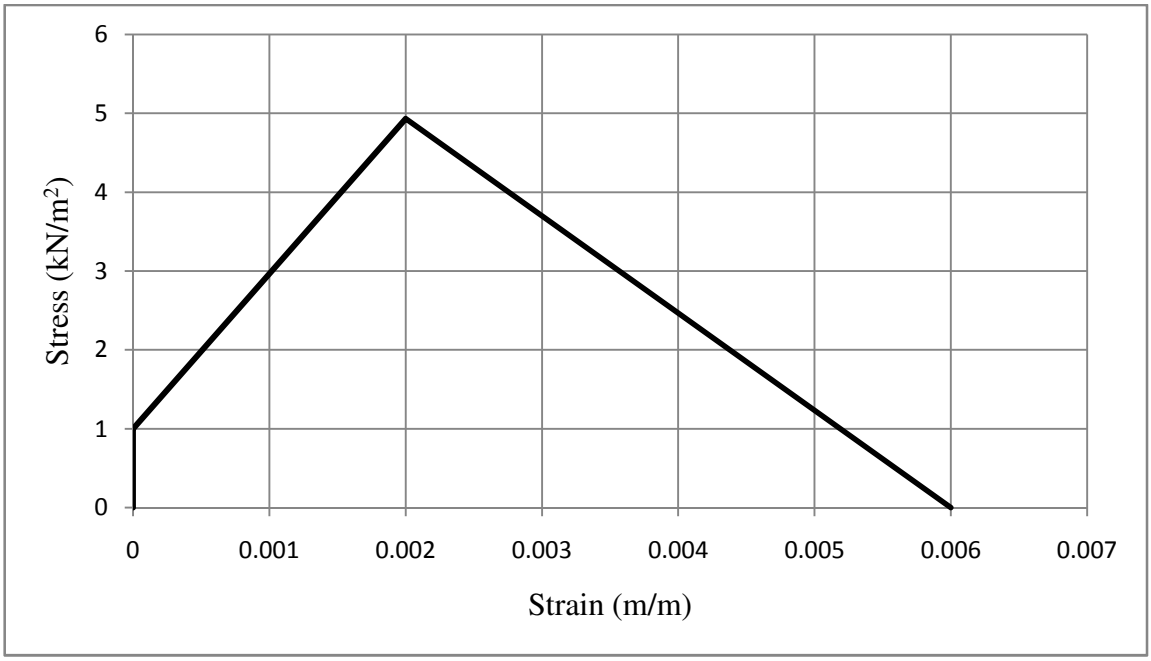

Figure 6.13. Stress-strain relationship of the tension tie

6.2.7. Shear (V) Hinges for RC Walls

An RC wall is designed in accordance with TEC 2007 [16]. The existing columns are assumed as boundary columns of the RC wall. $\phi 10/250$ mm reinforcement bars are used both for horizontal and vertical bars. The concrete compressive strength is determined as 20 MPa. The anchorages of reinforcement bars to existing columns are realized according to TEC 2007. $\phi 12$ anchorage bars with anchorage depth of 10ϕ (120 mm) and spacing of 125 mm are used. Figure 6.14 shows the top and side views of the RC wall designed for seismic rehabilitation.

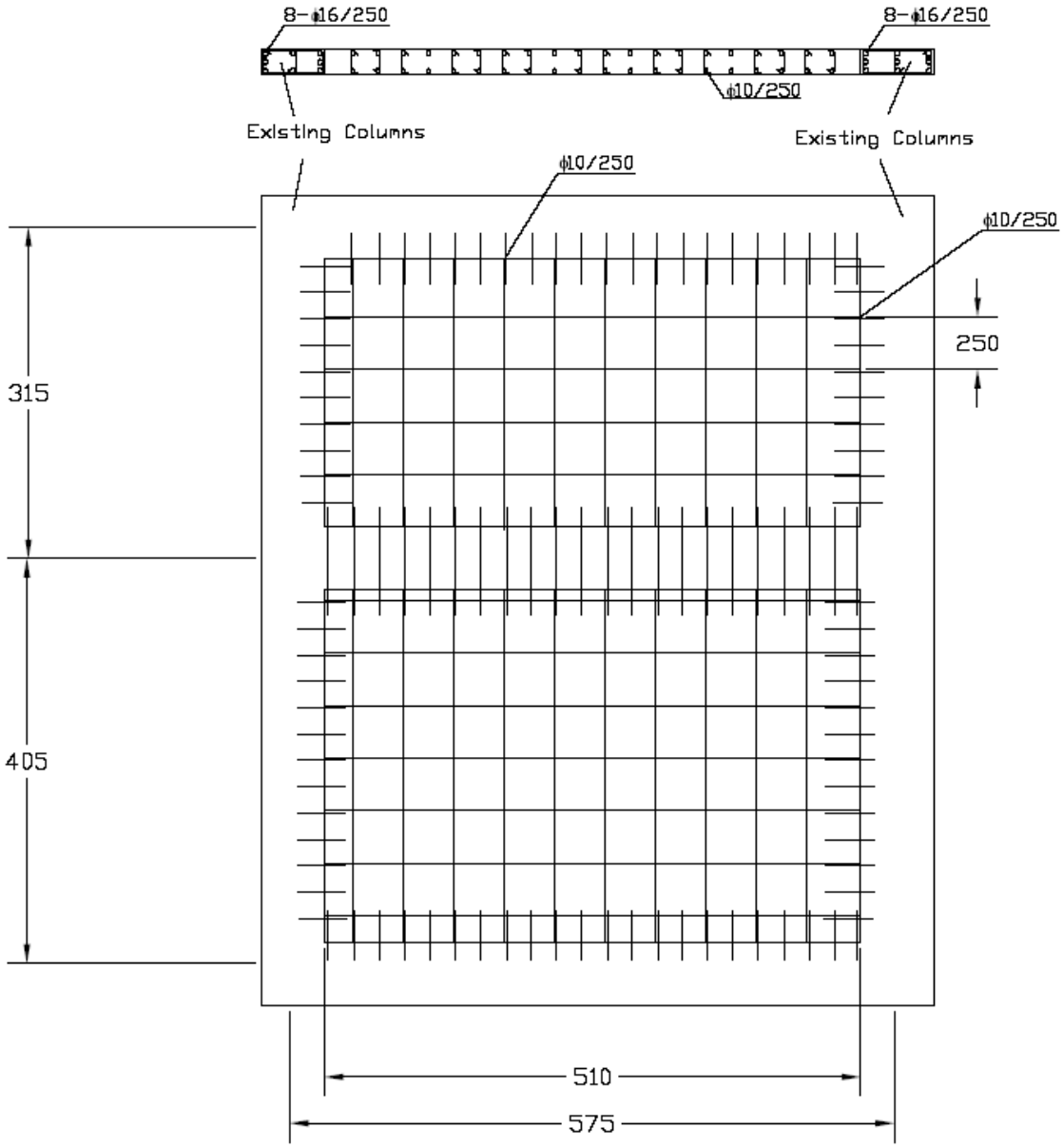

Figure 6.14. Top and side views of RC wall

Equivalent wide column model is used to model the RC walls for numerical analysis as detailed in Section 3.2.3. The bound columns of RC wall are considered as two axial springs and wall in between is considered as a central equivalent wide column with flexural, axial and shear resistance. The sample calculations in Section 6.2 are valid for axial, flexural, and shear behavior. ATC 40 [45] approach is used to model the displacement behavior of shear hinges of the RC wall. According to this, the peak shear capacity is reached at a rotation of 0.0075 rad and shear failure occurs at a rotation of 0.02

rad. Shear capacity of the section is calculated by Equation 3.20 in accordance with TS500-2000 [23]. Figure 6.15 shows the shear force-drift ratio relationship of the RC wall:

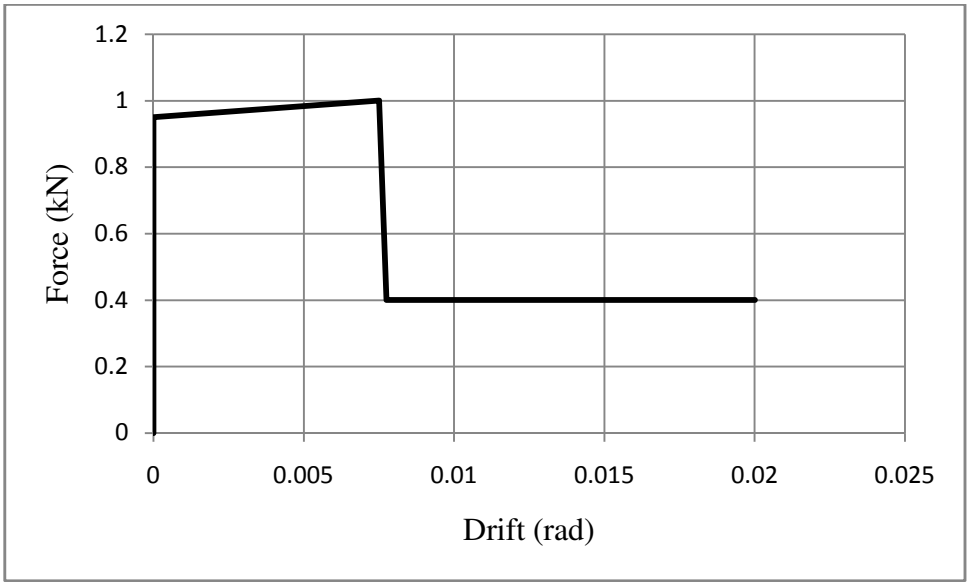

Figure 6.15. Shear force-drift ratio relationship of shear hinge of first storey RC shear wall

6.3. Analyses Results

6.3.1. Analysis Results of Test Frames

Displacement controlled nonlinear pushover analyses are performed on pre-determined two-storey-single-bay planar test frames of Sehit Adem Yavuz Primary School building for (i) bare frame, (ii) infilled frame, (iii) CFRP strengthened infilled frame, and (iv) RC wall strengthened frame. The analyses show that, a collapse mechanism occurrs at 89 kN in the bare frame case, at 237 kN in the infilled frame case, at 500kN in the CFRP strengthened frame case, and at 1100 kN in the RC wall strengthened frame case. The lateral force-displacement relationships and detailed frame deformation behaviors of test frames are investigated in the following sections.

6.3.1.1. Capacity Determination of Bare Frame. Figure 6.16 shows the force-displacement relationship of bare frame obtained. According to this analysis, the yielding of bare frame occurred under 89 kN lateral load at 40 mm lateral displacement. After this point, the lateral load degraded. The initial stiffness of bare frame was calculated as 5,685 kN/m.

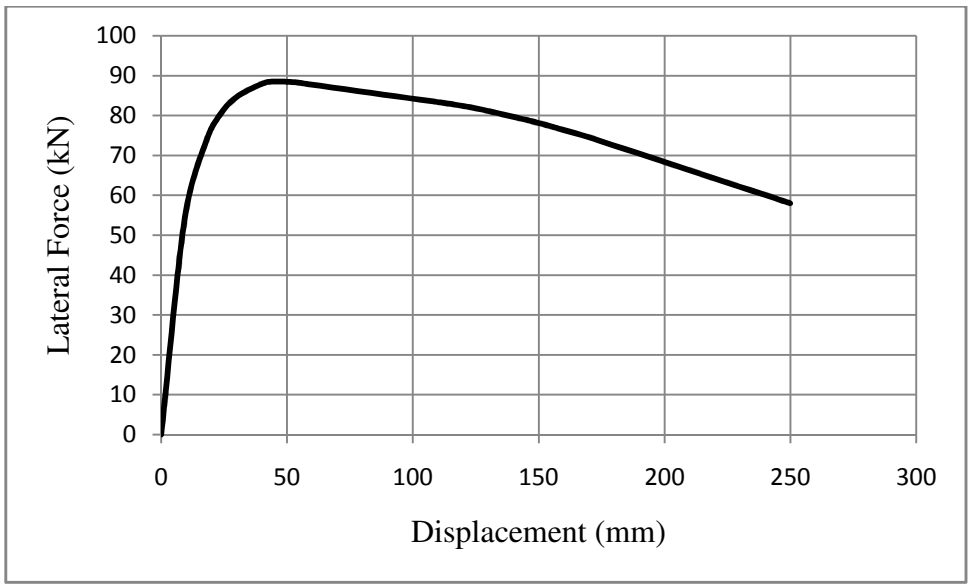

Figure 6.16. Displacement-lateral force relationship of bare frame

6.3.1.2. Hinge Formation Sequence of Bare Frame. The information about hinge formation sequence allows determination of the types and locations of damage mechanisms under loading. A step by step investigation is done to determine the collapse mechanism of test frames. Figure 6.17 shows the step by step investigation of hinge formation sequence for the bare frame.

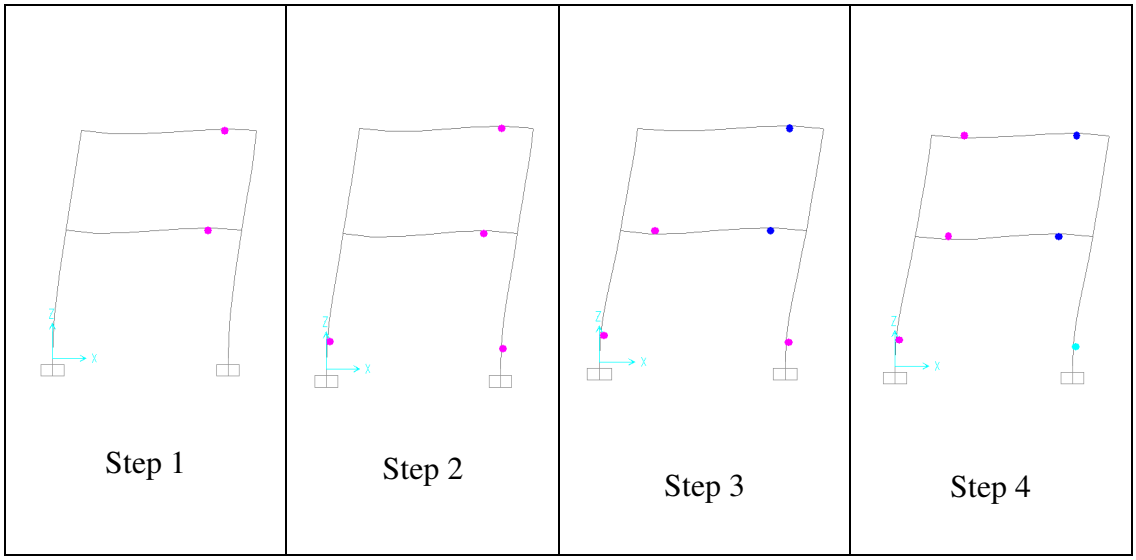

Figure 6.17. Hinge formation sequence for the bare frame

At first step, roof displacement is obtained as 9 mm. Two plastic M-K hinges occurred on first and second floor beams. It is observed that beams are weaker than columns and first yielding occurred on beams. At second step, roof displacement is obtained as 18 mm. Two plastic P-M hinges occurred on first storey columns. The yielding of both first storey columns resulted flexural deformations and fast lateral displacement under lateral loads. At third step, roof displacement reached 30 mm. One new plastic M-K hinge occurred on the first storey beam. Next step showed roof displacement of 40 mm. One new plastic M-K hinge occurred on second storey beam. At this step, the lateral load capacity of 89 kN is reached, after which point the capacity curve started to degrade. Degradation of the lateral load-displacement curve means that the collapse mechanism occurs at this displacement and further load cannot be beared by the frame.

6.3.1.3. Capacity Determination of Infilled Frame. Figure 6.18 shows the force-displacement relationship of infilled frame obtained by using Chen's [34] infill model according to the formulations given in Section 3.2.2.

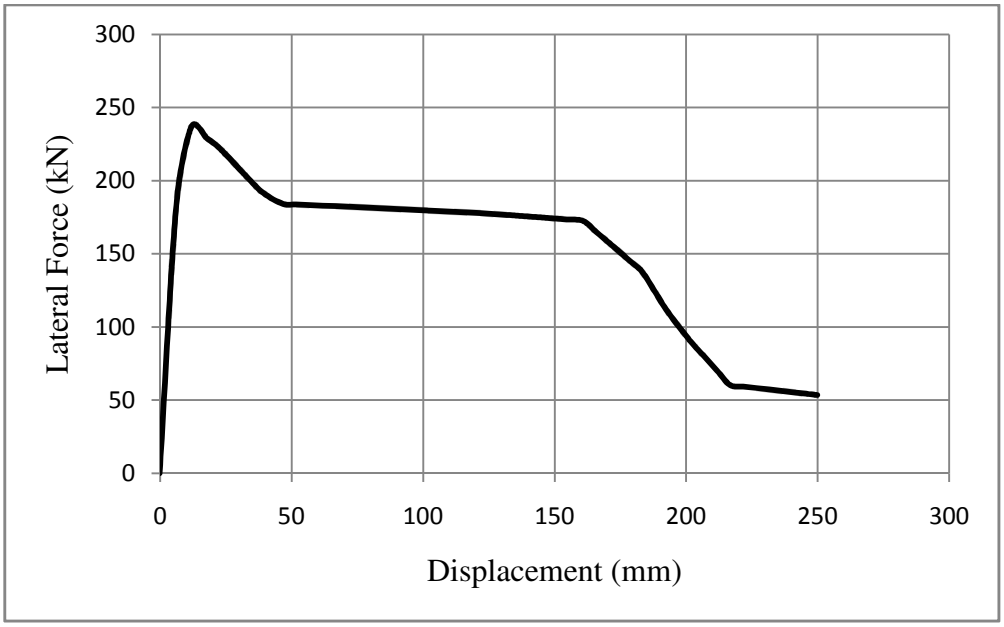

Figure 6.18. Displacement-lateral force relationship of infilled frame model by Chen[34]

According to this analysis, the lateral load capacity of infilled frame is 237 kN at 14 mm lateral displacement. The initial stiffness of infilled frame is calculated as 28,704 kN/m.

By modeling the equivalent truss representing the infill wall in accordance with Binici's trilinear stress-strain relationship for infill walls, Figure 6.19 is obtained.

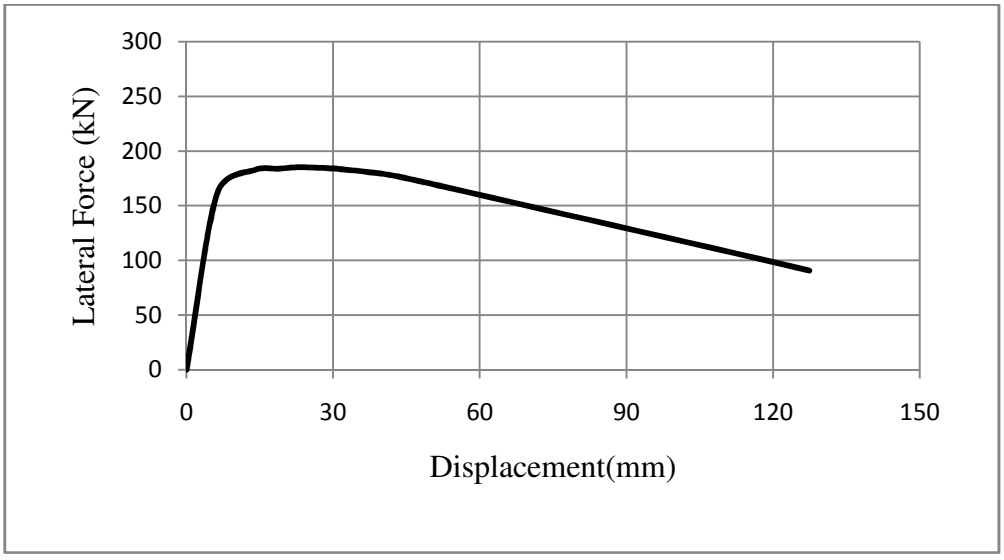

Figure 6.19. Displacement-lateral force relationship of infilled frame by Binici and Ozcebe [17] model

According to this analysis, the lateral load capacity of the infilled frame was 211 kN at 48 mm lateral displacement. The initial modulus of elasticity of this frame was calculated as 25,517 kN/m. The infill wall model presented in TEC 2007 [16] leads to similar results. Although the lateral load capacities of both models are similar, the displacement behaviors are different. The divergence in displacement behaviors, lateral load capacities and initial stiffness are mainly due to the differences between the accepted assumptions for material properties and plastic hinge definitions by models.

6.3.1.4. Hinge Formation Sequence of Infilled Frame (Chen's [34] Model). Figure 6.20 shows the hinge formation sequence of infilled frame.

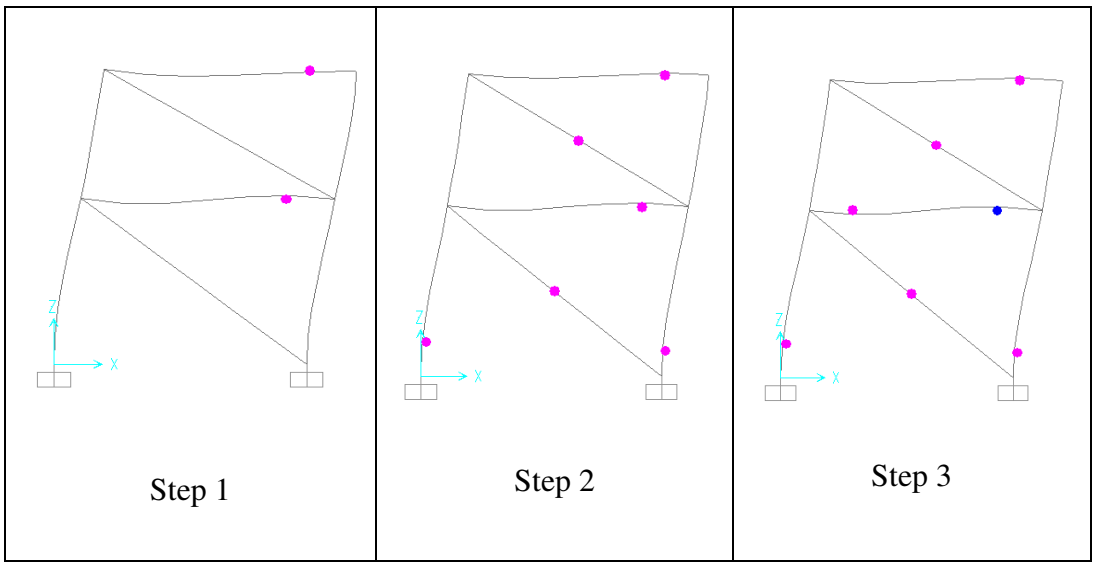

Figure 6.20. Hinge formation sequence of infilled frame

Initially, at 5 mm roof displacement, two plastic M-K hinges occurred on beams of first and second stories due to flexural yielding. Subsequently, at 14 mm roof displacement, first storey columns yielded. The existence of infill walls resulted in smaller displacement to yield for columns, compared to bare frame. The equivalent trusses representing the infill walls reached their axial capacity and peak lateral load capacity of 237 kN was observed. The lateral load capacity was reached at a small displacement compared to bare frame because the trusses representing the infill walls increased rigidity of the frame. Finally, at 30 mm roof displacement, a new M-K hinge occurred at first storey beam. After this step, lateral load started to degrade with increasing displacement.

6.3.1.5. Capacity Determination of Infilled Frame Strengthened with CFRP. Figure 6.21 shows the force-displacement relationship of infilled frame strengthened with CFRP, according to Binici and Ozcebe's [17] model. The procedures detailed in Section 3.2.4 are used in this analysis.

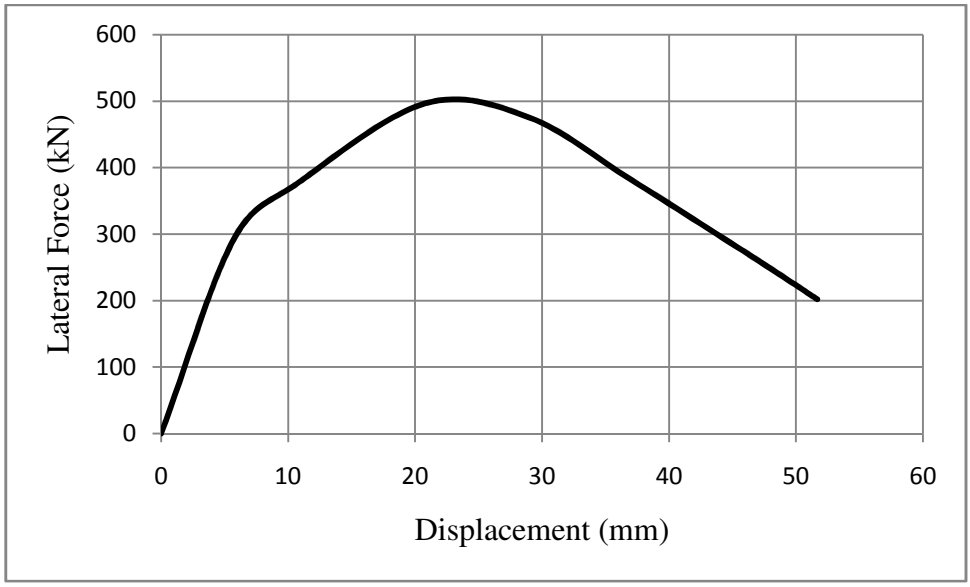

Figure 6.21. Displacement-lateral force relationship of infilled frame strengthened with CFRP

In accordance with Figure 6.21, the lateral load capacity of infilled frame strengthened with CFRP is 496 kN at 21 mm lateral displacement. The initial stiffness of this frame is calculated as 51,138 kN/m. The rapid degradation of the pushover curve is mainly occurred due to anchorage and debonding failures of CFRP. In computer analysis, the analysis ended at 50 mm lateral displacement. While testing, it would be expected that at higher displacement levels, the frame will behave like bare frame.

6.3.1.6. Hinge Formation Sequence of Infilled Frame Strengthened with CFRP. Figure 6.22 shows the hinge formation sequence of infilled frame strengthened with CFRP.

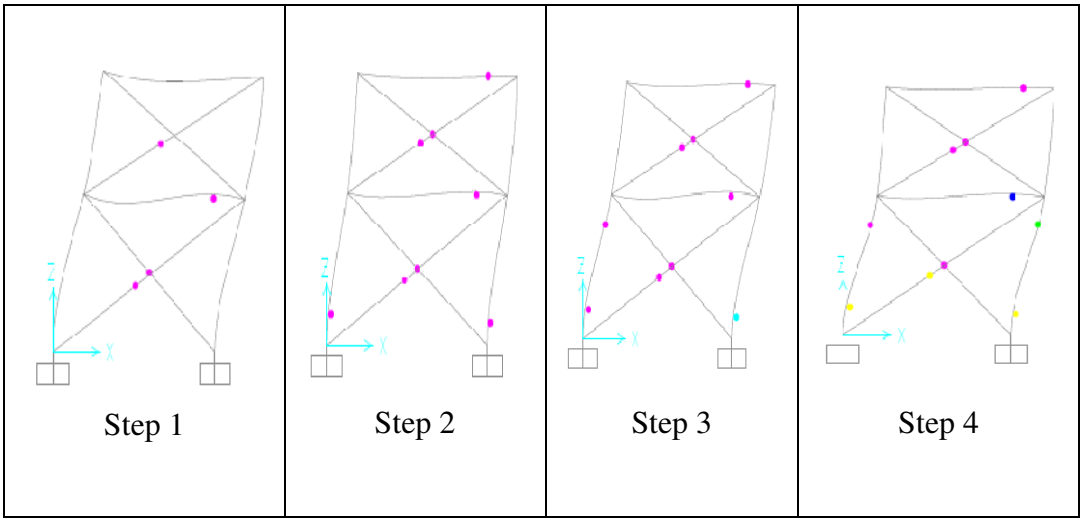

Figure 6.22. Hinge formation sequence of infilled frame strengthened with CFRP

At first step, roof displacement is 6 mm. Compression strut in first storey, tension ties in both storeys and first storey beam yielded at this step. These would be caused by anchorage and debonding failures. When roof displacement become 11 mm, and flexural column capacities are reached. The slope of the pushover curve changed in this step, meaning the stiffness of the system degraded. Also, the infill wall failure in second storey occurred in this step. At the third step, the lateral load capacity of 496 kN was observed at 21 mm lateral displacement. With the flexural failure of the first storey columns at both ends, the lateral load started to degrade with the increasing displacement.

6.3.1.7. Capacity Determination of RC Wall Strengthened Frame. The analyses are conducted on two types of RC Wall strengthened frame models. In first model, RC wall strengthened frame is modeled by two axial springs representing the boundary columns of RC wall and a central equivalent wide column representing the wall panel. Figure 3.15 shows the first model. The second model is represented by single line elements, which included both flexural and shear hinges on it. The section builder of SAP2000.v11.0.0 [26] is used to make the sectional analyses. Figure 6.23 shows the typical shear wall analysis in SAP2000.v11.0.0 and Figure 6.24 shows the displacement-lateral force relationship of first model.

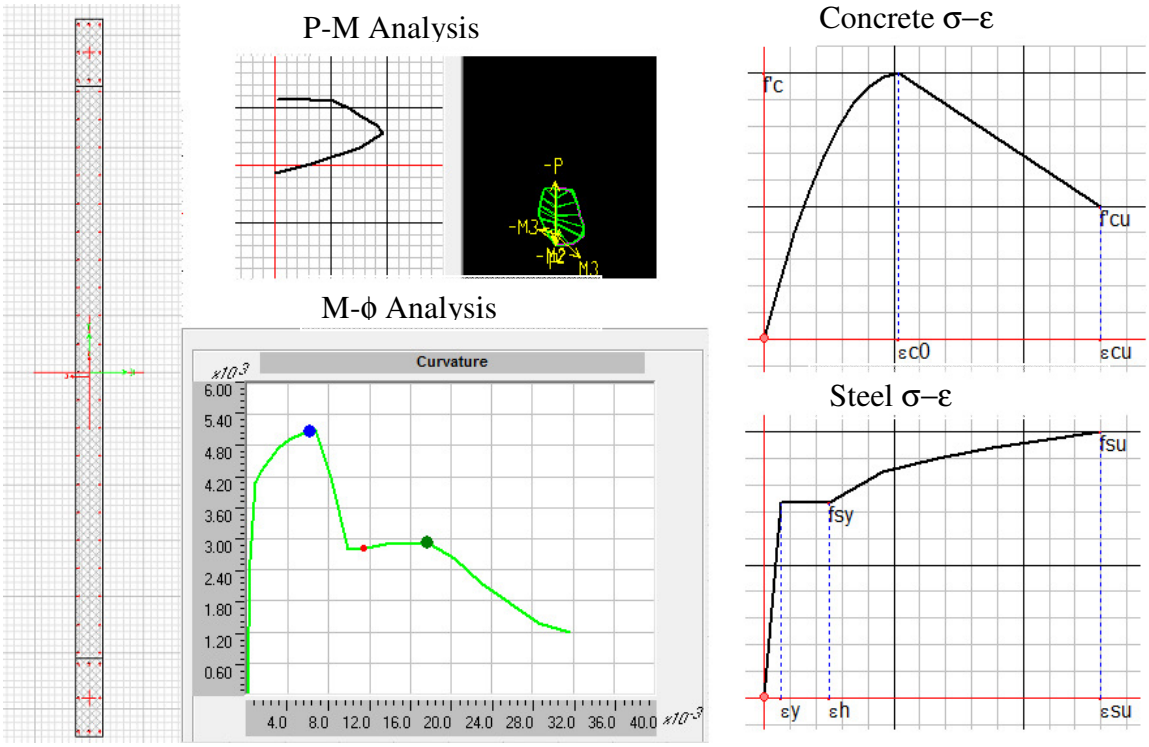

Figure 6.23. Typical shear wall analysis in SAP2000.v11.0.0[26]

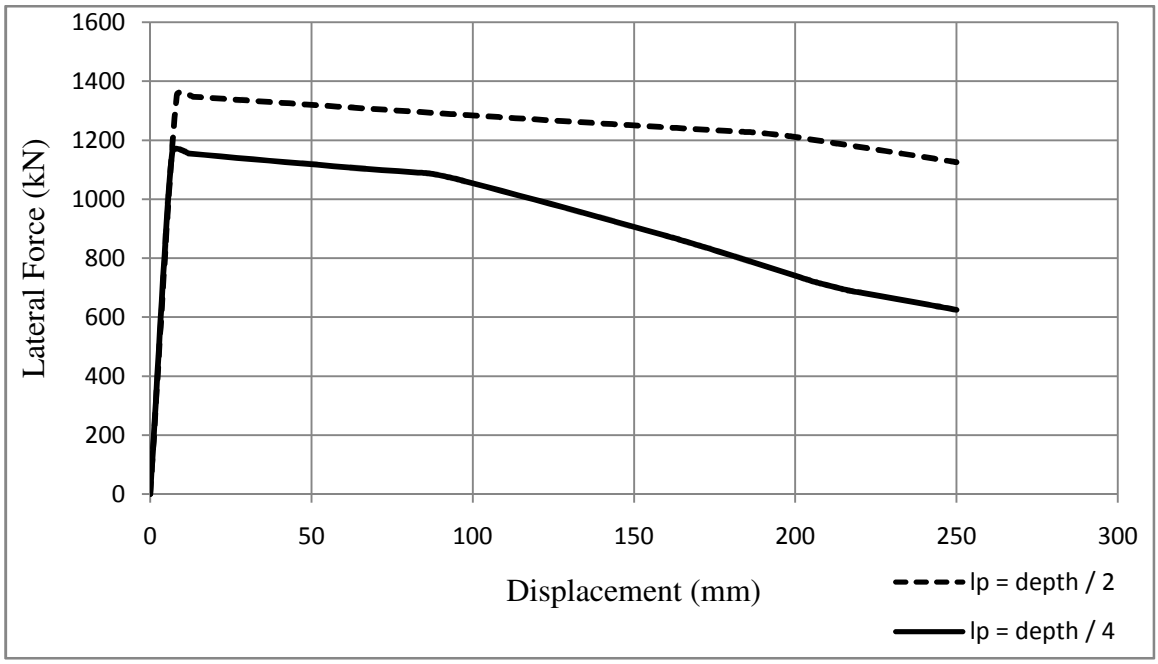

Figure 6.24. Displacement-lateral force relationship of RC wall strengthened frame by first model

The analyses yield a lateral load capacity of 1,351 kN at 8 mm lateral displacement. In the prior frame analyses, the plastic hinge length was assumed as half the section depth in accordance with the codes. A 5.1 m long shear wall results with a plastic hinge length of 2.55 m if half the section depth is considered. By using 1 m long plastic hinges, 1,161 kN peak lateral force is reached at 7 mm lateral displacement. The initial stiffness of the frame is calculated about 165,000 kN / m for both of the two plastic hinge length changing cases.

Using a single line element to represent a shear wall yields close lateral load capacities compared to first model. The displacement behavior of RC wall strengthened frame changed in the analysis of second model. Figure 6.25 shows the displacement-lateral force relationship of the second model.

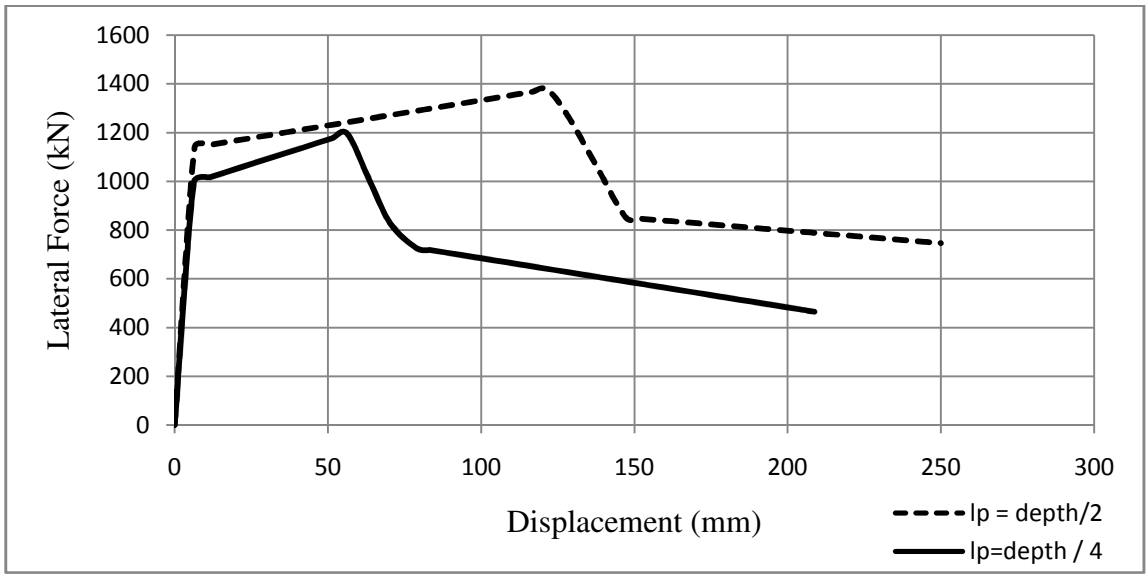

Figure 6.25. Displacement-lateral force relationship of RC wall strengthened model by second model

1377 kN lateral load at 122 mm lateral displacement is observed if half the section depth is used in the analyses. Using plastic hinge length as one fourth of the section depth yields with 1,195 kN lateral force at 56 mm lateral displacement. The initial stiffness of the second analysis is close to first analysis which was about 160,000 kN / m.

6.3.1.8. Hinge Formation Sequence of RC Wall Strengthened Frame. During the analysis, only axial hinges on boundary columns and flexural hinge on bottom region of central wide column occurred on first storey of first model. Figure 6.26 shows the hinges occurred on the RC wall strengthened model. The analysis done by single equivalent frame showed only the flexural hinge at the bottom region.

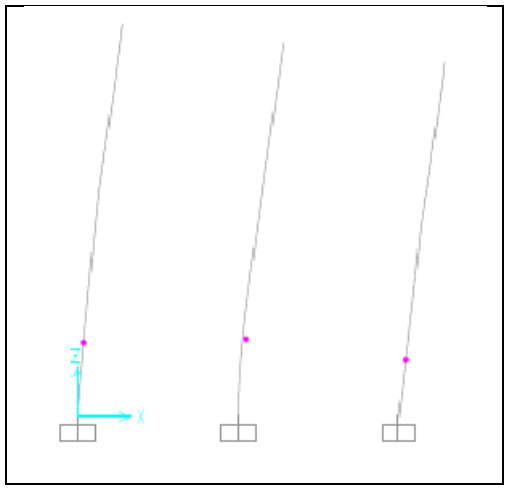

Figure 6.26. Hinge formation of RC wall strengthened frame

According to Figure 6.26, it would be expected that, the flexural deformations will occur on the RC wall. The capacity of this frame will be decisive while determining the capacities of the hydraulic actuators due to the fact that greatest lateral load capacities were obtained in this case.

6.3.1.9. Comparison of Analyses Results. Including infill walls to the structural system increased lateral load capacity of bare frame 2.68 times and it increased initial stiffness 5.05 times. In the CFRP strengthened infilled frame case, it is observed that the lateral load capacity increased 5.61 times relative to the bare frame value and the initial stiffness increased 9 times. Strengthening with RC walls increased lateral load capacity 13.11 times relative to bare frame. It also increased the initial stiffness 28.15 times. According to this, the upper bound of the lateral load capacity for test frames is determined as 1377 kN. This capacity is used for determining the load capacity of the hydraulic actuators. Table 6.9 and Figure 6.27 show the tabular and graphical representation of the effects of different strengthening methods.

Table 6.9. Summary table for the effects of different strengthening methods

	Increase in Lateral Load Capacity (times)	Increase in Initial Stiffness (times)
Bare Frame	1.00	1.00
Infilled Frame	2.68	5.05
CFRP Frame	5.61	9.00
RC Wall Frame	13.11	28.15

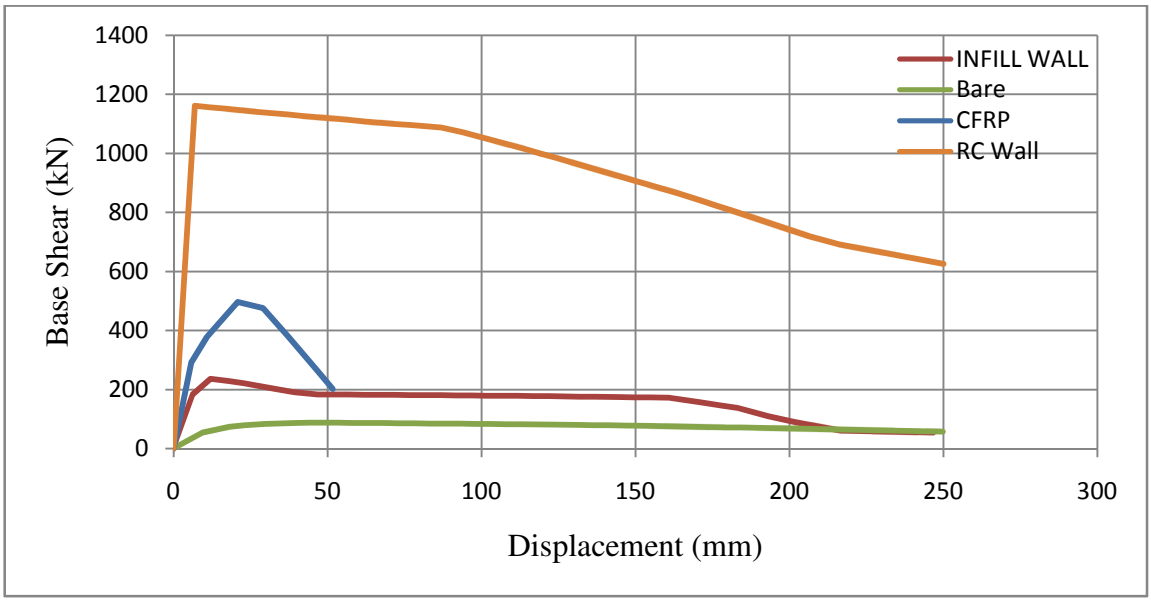

Figure 6.27. Comparison of displacement-lateral force curves of different strengthening methods

6.3.1.10. Comparison of Analyses Results to Literature. Table 2.1 shows the summary of different lateral strengthening techniques by researchers worldwide. The computer analyses of two-storey-single-bay frames resulted with similar results compared to literature. Table 6.10 shows the comparisons of the increase in lateral load capacities of analytical study results to literature results.

Table 6.10. Comparison of analytical study results to literature

Increase in Lateral Load Capacity (times)	Analytical Study	Literature (Bounds)	Literature (2 storey-single bay)
Bare Frame	1.0	1.0	1.0
Infilled Frame	2.7	1.3-5.5	5.5
CFRP Frame	5.6	1.9-10.7	10.7
RC Wall Frame	13.1	1.9-13	8.0-13.0

The comparison of the results of the analytical study to literature for infilled frames presents differences for two-storey-single-bay frames. This is mainly occurred due to the assumptions made on material strengths while modeling the equivalent truss representing the infill walls. The comparison of CFRP strengthened infilled frames also have differences compared to bare frame, but this divergence resulted due to the difference between the results for the infilled frames. The comparison of CFRP strengthened infilled frames relative to infilled frames result with smaller divergence. The literature shows that CFRP strengthened infilled frame has lateral load capacity of 1.94 times compared to infilled frame. In the analytical study, it is observed that CFRP strengthened infilled frame has lateral load capacity of 2.09 times compared to infilled frame.

6.3.1.11. The Effects of Column Splice Lengths to Analysis Results. Splice length of the reinforcement bars in columns is a crucial parameter that affects the lateral load capacity of a structure since, if the development length of reinforcement bars are poorly developed, slippage problems occur. Due to the lack of information about the splice lengths of columns of Şehit Adem Yavuz Primary School, splice lengths are assumed as well developed and the analyses are performed accordingly.

According to TS500-2000 [23], splice lengths have to be bigger than 300 mm or 20 times the diameter of longitudinal reinforcement bars (for deformed bars), or 40 times the diameter of straight reinforcement bars. If all the longitudinal bars are under compression at all loading cases, splice length can be decreased by a quarter of the code specified value. According to TEC 2007 [16], if the splice region is at the bottom side of the columns (which is the most probable approach for Şehit Adem Yavuz Primary School building) the splice length calculated from TS 500-2000 [23] has to be increased to 1.5 times of it.

The earthquake resistant design codes of TEC 1968 [46] and TEC 1975 [47] and the general idea of the engineers worked in construction between 1960-1980 indicate that the splice lengths used for columns was 25-30 times the diameter of the longitudinal bars.

For Şehit Adem Yavuz Primary School Building, by considering the above given information for buildings constructed between 1960-1980, it is assumed that splice lengths of longitudinal bars are half (1/2) the current code determined value. Due to this, bond slippage is expected during the in-situ tests. Accordingly, the expected lateral load capacities of the structure would be less than the determined ones by the analytical study.

6.3.2. Analysis Results for Block-B

Four nonlinear, three-dimensional pushover analyses are performed on Block-B of Sehit Adem Yavuz Primary School building. The corresponding loading behaviors which occur due to analyses of the static test frames are used in analyses of Block-B. Therefore, four analyses are performed on Block-B with same lateral loading conditions, on same axis with static test frames.

Initially, the analyses are performed on the existing structure and lateral load capacity of Block-B is determined for different loading configurations. The results of the analyses show that, lateral load capacity of Block-B is 2,400 kN while loading along axis 4 and axis 5, lateral load capacity is 2,000 kN while loading along axis 6, and lateral load capacity is 2,600 kN while loading along axis 7 of Figure 5.15. Test frame analyses in Section 6.3.1 showed that, 2-D nonlinear analysis of bare frame resulted with 89 kN lateral load capacity. Seismic rehabilitation of frames on Block-A with infill walls resulted with 237 kN lateral load capacity. Using CFRP on infill walls resulted with 496 kN lateral load capacity. Seismic rehabilitation by means of an RC wall resulted in 13.11 times the lateral load capacity of the bare frame, which equals to 1,161 kN. According to these results, the bare frame test is determined to be done on axis 4. Because axis 5 includes an infill wall on the second storey, by constructing an infill wall on the first storey, the infilled frame test can be accomplished here. Axis 7 includes infill walls in both storeys, and it has higher lateral load capacity then the others. Due to this, CFRP strengthened infilled frame test can be done here. It is determined that, in order to accomplish the RC wall strengthened frame

test, it is better to increase the lateral load capacity of Block-B, to be on the safe side while testing. Due to this, diagonal braces are determined to be used to increase the lateral load capacity of Block-B. Two diagonal braces can be placed between C – E' axis in first and second stories and a diagonal brace can be placed between A-C axis in first storey, in axis 6 of Figure 6.31. In accordance with this, axis 6 is determined to be used for RC wall strengthened frame test. Figure 6.28 shows the location of the brace elements along axis 6.

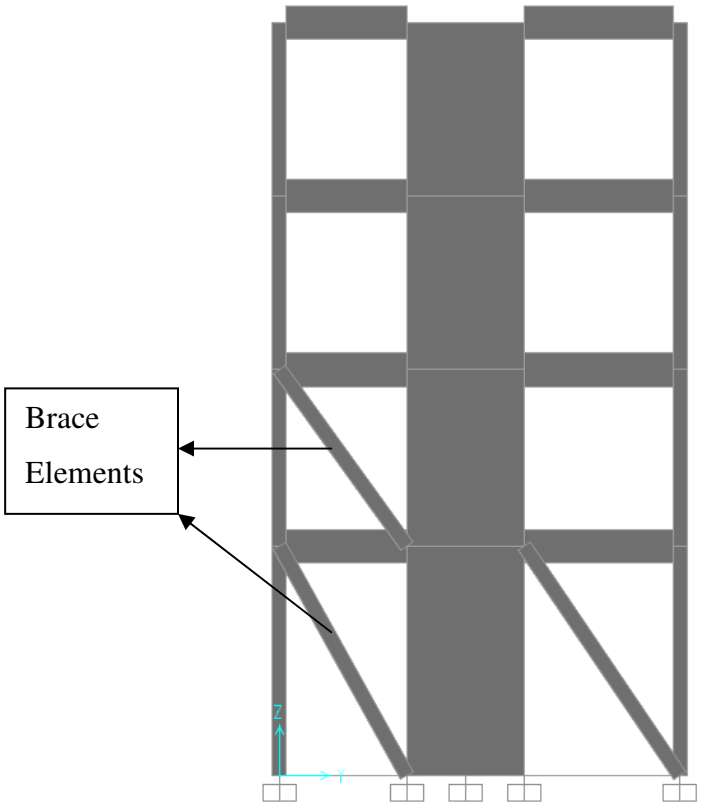

Figure 6.28. Location of brace elements at axis 6

In accordance with AISC (American Institute of Steel Construction) steel profile chart, W14×54 steel brace elements with cross sectional area of 10,200 mm^2 are chosen to be used in strengthening of reaction block. Figure 6.29 shows the cross sectional view of the brace elements.

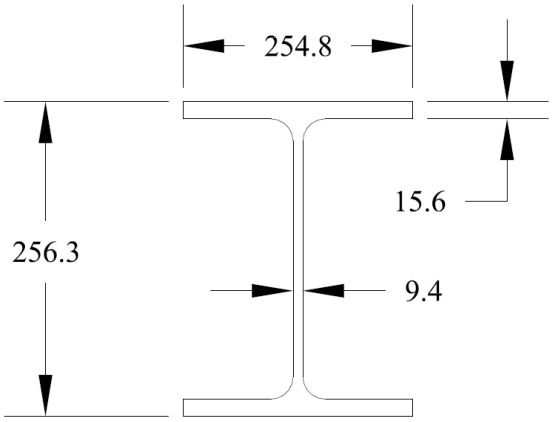

Figure 6.29. Cross sectional view of brace elements (in mm's)

The stress-strain relationship given in Figure 6.30 is used for the material model of the brace element.

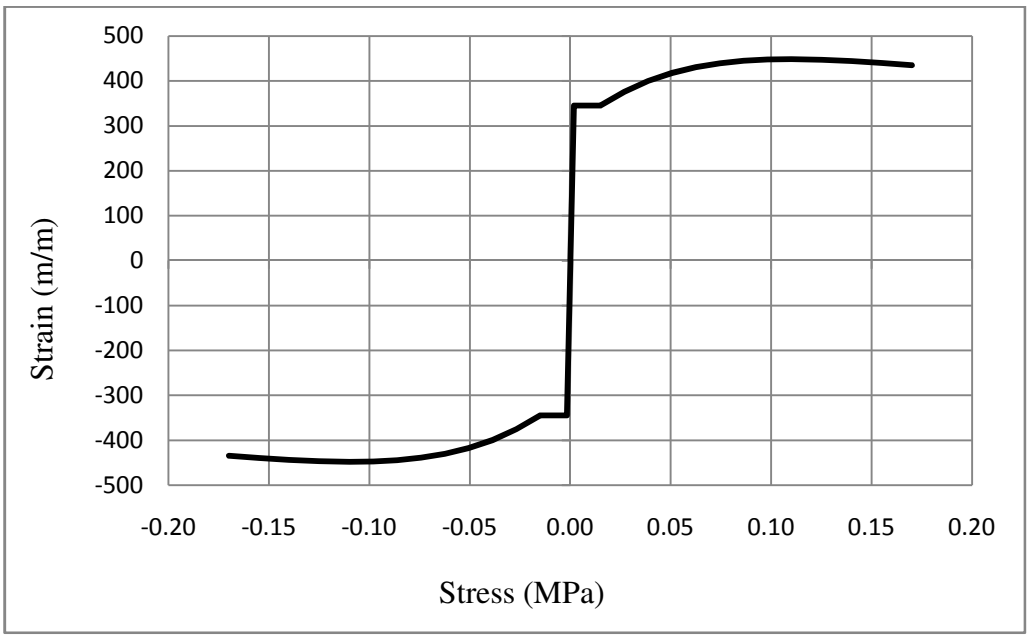

Figure 6.30. Stress-strain relationship of steel

Figure 6.31 shows the plan view of the building with test frame locations.

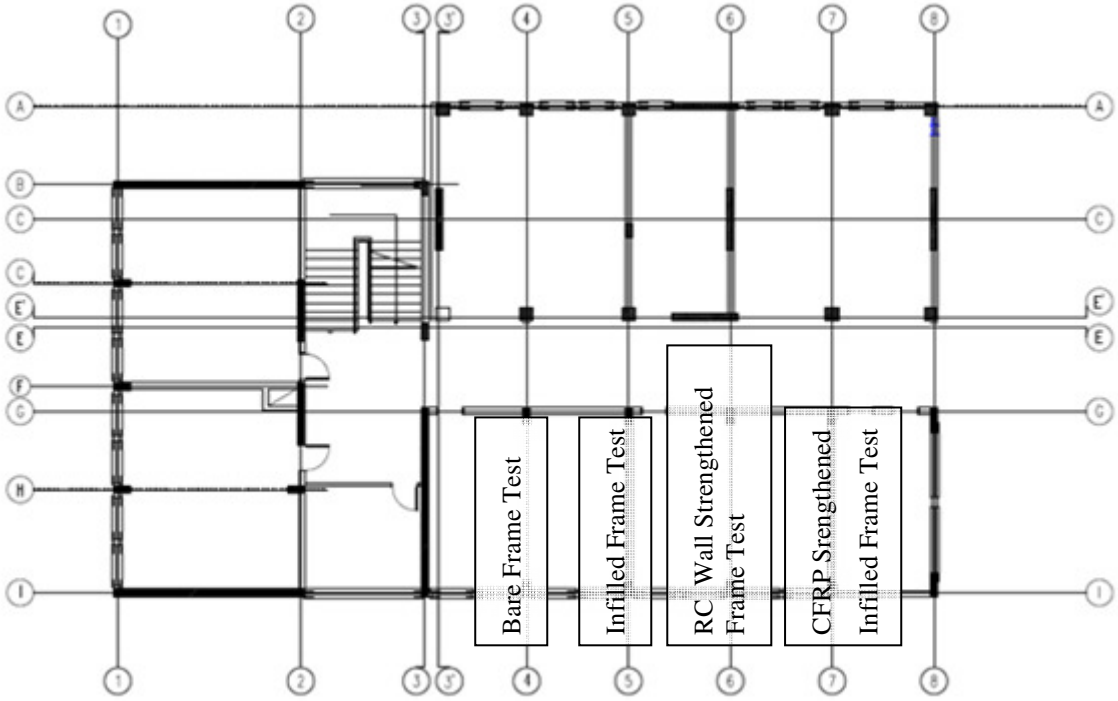

Figure 6.31. Plan view of the building with locations of test frames

The frames on axes 4, 5, 6 and 7 of Block-B are named as Frame 1, Frame 2, Frame 3, and Frame 4, respectively. Figure 6.32 shows the general view and frame labeling of Block-B according to loading conditions.

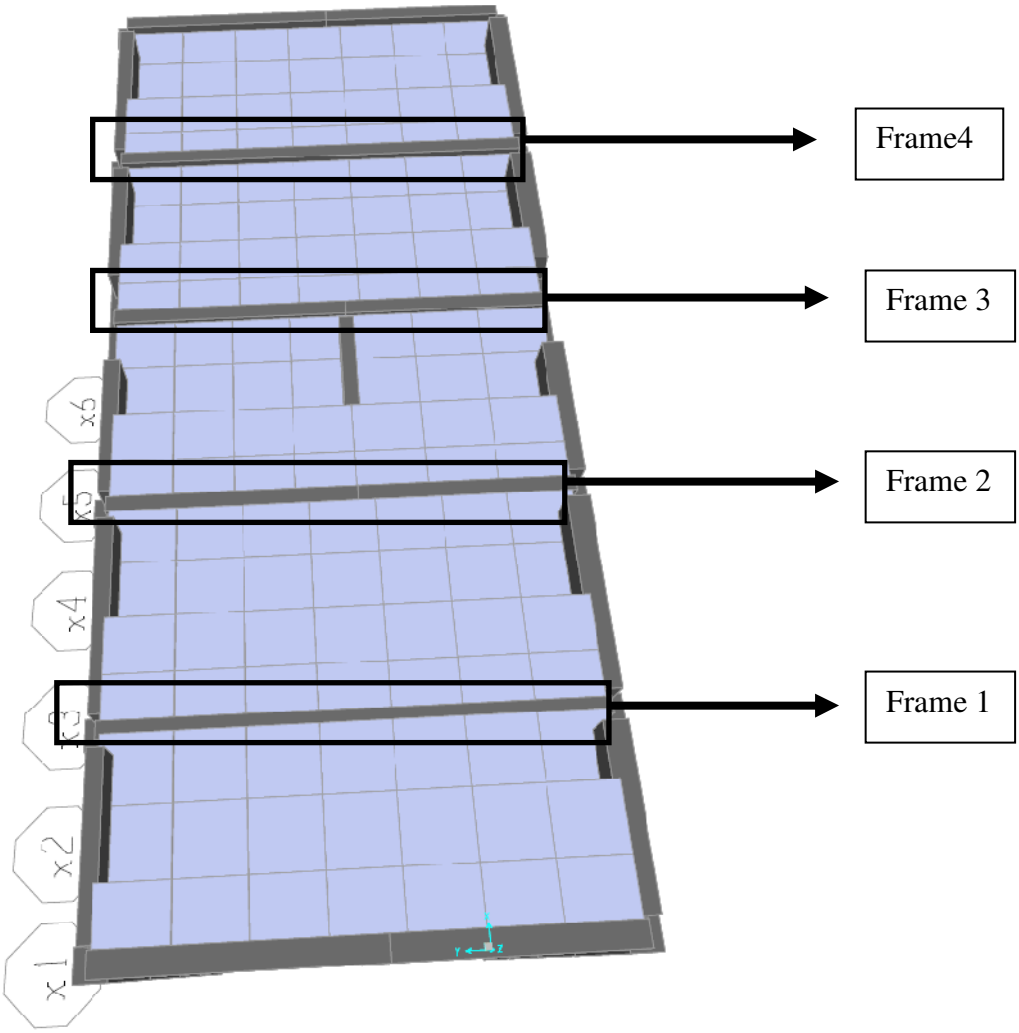

Figure 6.32. Frame labeling of Block-B

6.3.2.1. Capacity Determination for Block-B. The analyses of Block-B are used to determine whether it could be used as a reaction block or not. Figure 6.33 shows the lateral force-displacement relationship of Block-B at loading of Frame 1 for existing and strengthened cases.

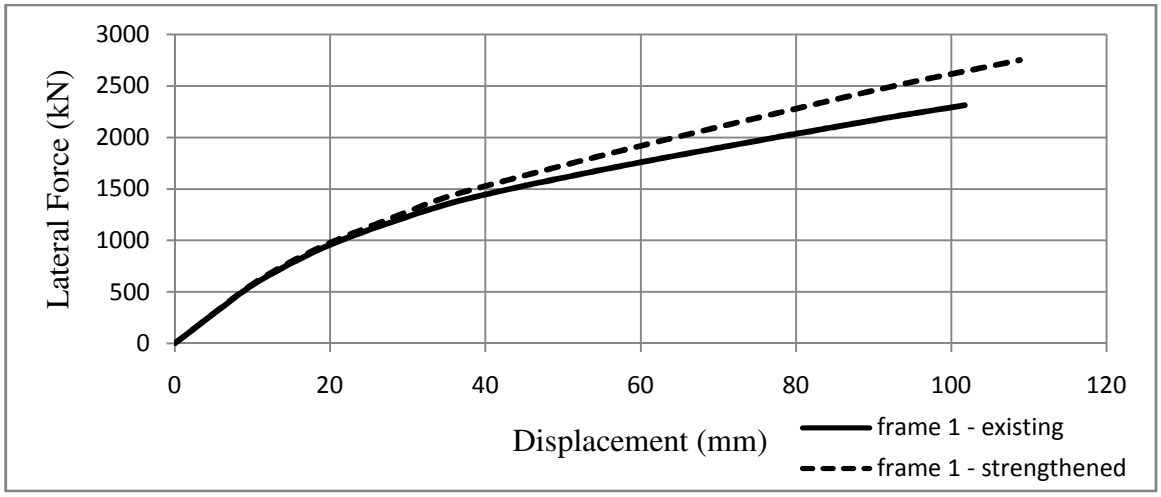

Figure 6.33. Lateral force-displacement relationship of Block-B when loading along frame 1

According to Figure 6.33, the lateral load capacity of Block-B is 2,750 kN after steel brace strengthening. Using Block-B as a reaction block also depends on whether lateral displacements can be restrained. Due to this, the initial stiffness becomes more important. Under the loading of Frame 1 for strengthened case, at 17 mm lateral displacement, the lateral force was 860 kN. The initial stiffness of the building is calculated as 50,588 kN/m.

Figure 6.34 shows the lateral force-displacement relationship of Block-B when loading is along Frame 2.

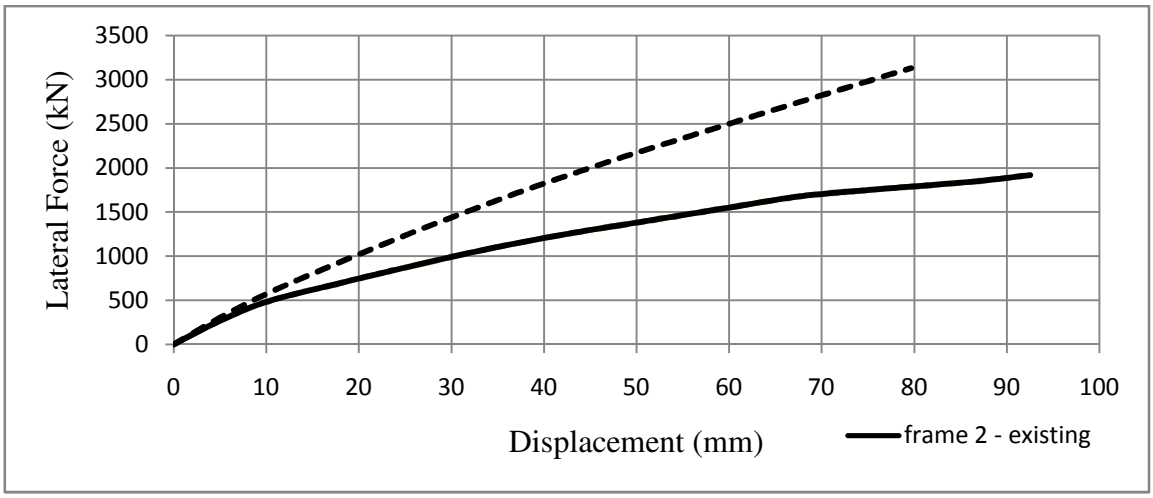

Figure 6.34. Lateral force-displacement relationship of Block-B when loading along frame 2

Loading along Frame 2 results with lateral load capacity of 3,129 kN after strengthening of Block-B and the initial stiffness of strengthened case is calculated as 55,000 kN/m.

Figure 6.35 shows the lateral force-displacement relationship of Block-B when loading along Frame 3.

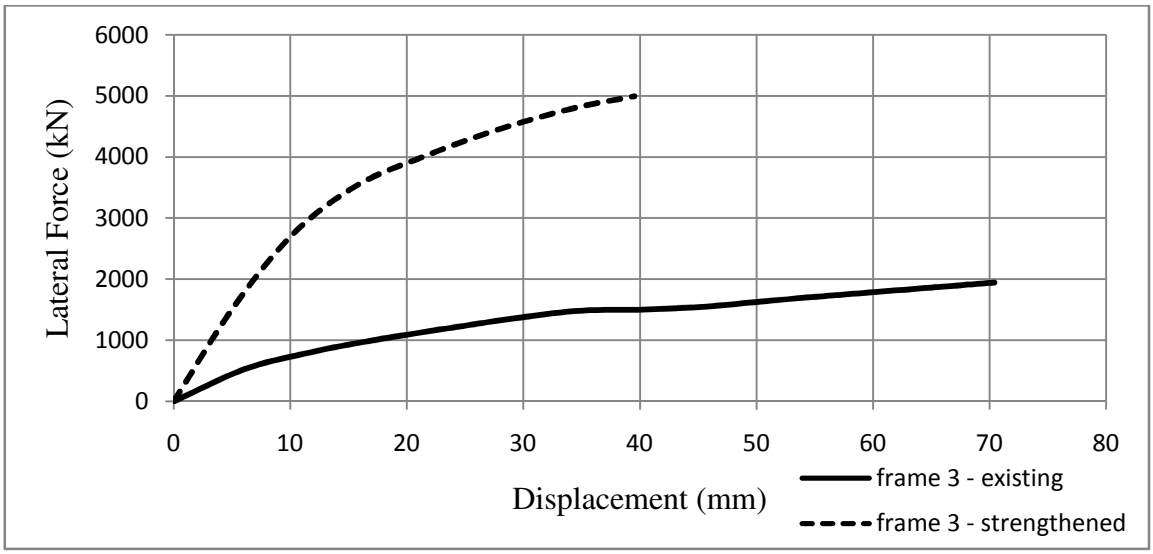

Figure 6.35. Lateral force-displacement relationship of Block-B when loading along frame 3

The main goal of installing steel braces along axis 6 is to increase the lateral load capacity of Block-B for RC wall strengthened case of test frames. The comparison of lateral load capacities of existing and strengthened cases of Block-B results with an increase of lateral load capacity of 2.75 times. The lateral load capacity of strengthened case is 5,335 kN whereas it is 1,918 kN in the existing case. The initial stiffness of Block-B is 266,366 kN/m in strengthened case whereas it is 86,556 kN/m in the existing case.

Figure 6.36 shows the lateral force-displacement relationship of Block-B when loading along Frame 4.

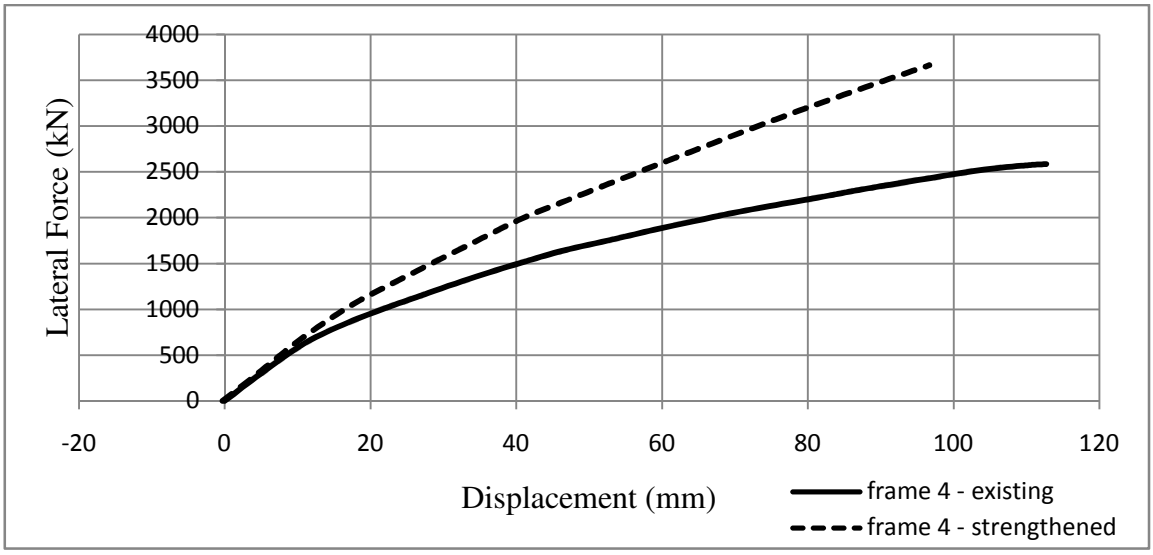

Figure 6.36. Lateral force-displacement relationship of Block-B when loading along frame 4

Lateral load capacity of Block-B is 3,661 kN in the strengthened case. It is observed that steel braces located along axis 6 make no difference at small lateral displacements whereas they make Block-B more rigid at higher levels of displacements. The initial stiffness of Block-B, while loading along Frame 4, was 57,285 kN/m in both of existing and strengthened cases. This value degrades very fast for the existing case compared to strengthened case.

6.3.2.2. Comparison of the Results for Different Loading Cases. Figure 6.37 compares the pushover curves of the four loading conditions; loads on Frame 1, loads on Frame 2, loads on Frame 3, and loads on Frame 4, respectively.

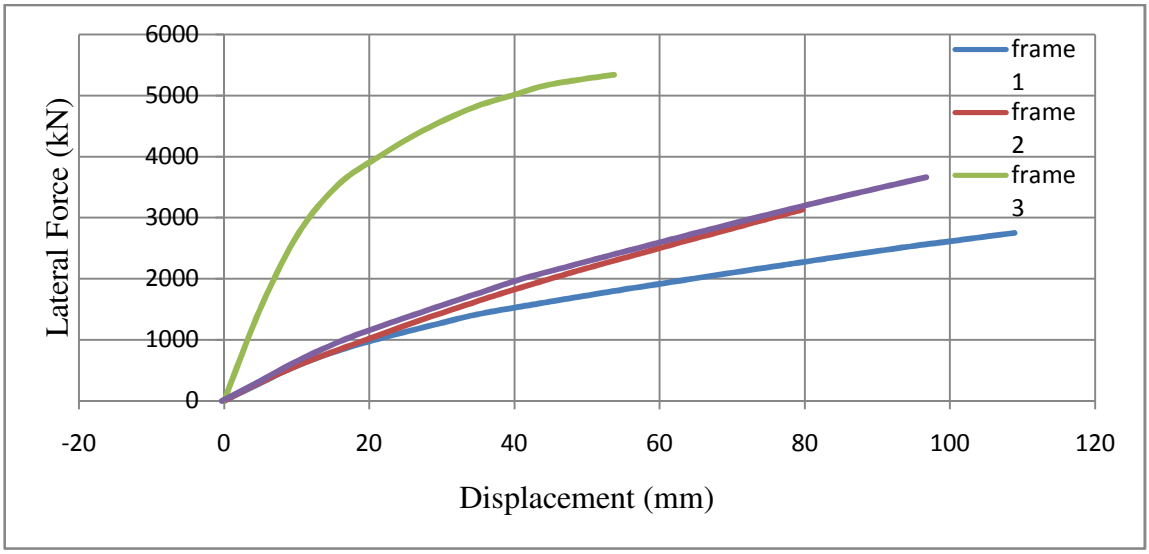

Figure 6.37. Comparison of four loading conditions

It is observed that initial stiffness of Frame 3 case is higher compared to other three loading cases. This behavior occurs because the steel braces are placed only on axis 6.

The safety factors for lateral resistance of Block-B for different types of tests ((i) bare frame, (ii) infilled frame, (iii) infilled frame strengthened with CFRP, and (iv) RC wall strengthened frame) are also determined. Table 6.11 shows the tabular form of factor of safety values calculated for the different test types. A minimum factor of safety of 3.95 is reached in the analyses.

Table 6.11. Factor of safety values for tests

Block Type	A Block			
Test	Bare Frame	Infilled Frame	Infilled Frame Strengthened with CFRP	RC Wall Strengthened Frame
Capacity (kN)	89	237	496	1,351
Block Type	B Block			
Test	Frame 1	Frame 2	Frame 4	Frame 3
Capacity (kN)	2,750	3,130	3,661	5,335
Factor of Safety	30.90	13.21	7.38	3.95

In accordance with the calculated safety factors, it is determined that using Block-B as reaction block in static, two-dimensional frame tests is suitable. It is determined to place

displacement gauges both on the test frames and reaction block during the in-situ tests in order to find the net displacements because it is expected that the reaction block will experience some lateral displacement during tests.

6.3.3. Analysis Results of Steel Resisting Frames

6.3.3.1. First Proposal. A three-dimensional, rectangular steel frame system is the first proposed system for resisting out-of-plane actions that can occur during in-situ tests. Figure 6.38 shows the computer model of this frame.

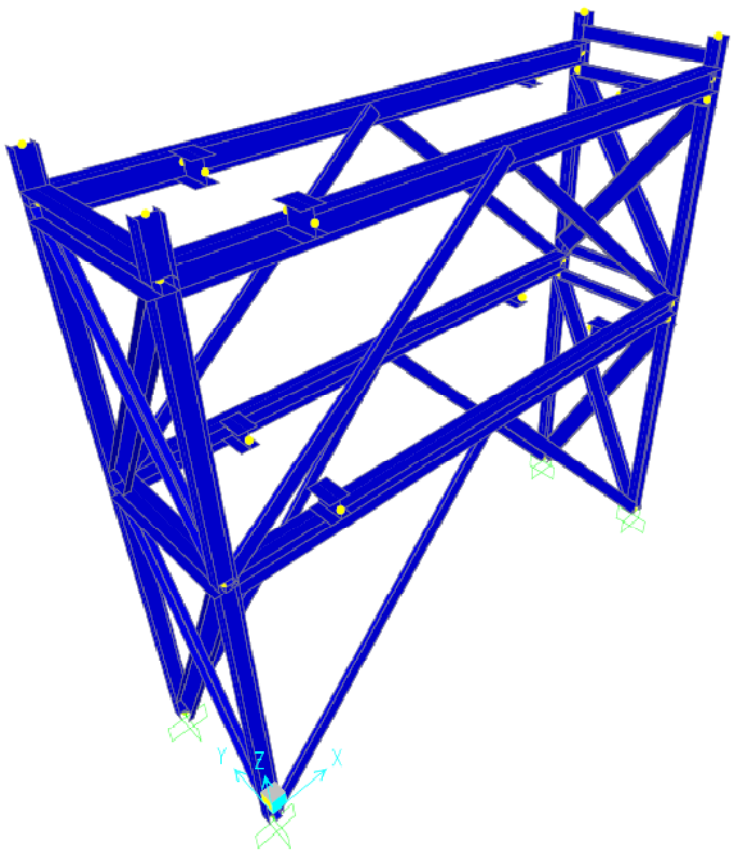

Figure 6.38. Computer model of three dimensional, rectangular steel frame system

12.5 per cent of maximum lateral load expected during static tests (100 kN for second storey and 50 kN for first storey) is applied to two opposite corners in Y axis of resisting frame, to represent twisting of test frame. Under these loads, the safe cross-sections are determined. For columns and beams, W10X68 I-sections are used whereas for diagonal members, C12.5X25 sections are used. Figure 6.39 shows general views of cross

sections of frame/brace elements and Table 6.12 shows sectional properties of frame/brace elements.

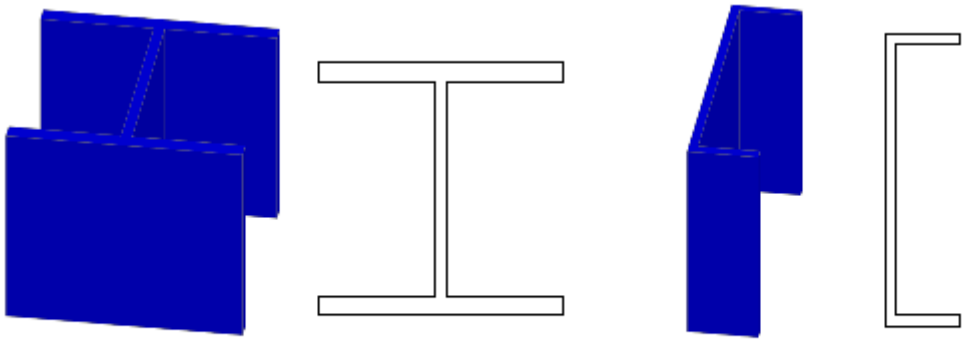

Cross sections for columns and beams Cross sections for braces

Figure 6.39. General views of cross sections of frame/brace elements

Table 6.12. Sectional properties of frame / brace elements

C12X25	(mm)	W10X68	(mm)
Outside Depth	304.8	Outside Height	264.2
Outside FlangeWidth	77.5	Top / Bottom Flange Width	256.5
Flange Thickness	12.7	Top/Bottom Flange Thickness	19.6
Web Thichness	9.83	Web Thickness	11.9

Although the determined sections were safe under assumed loading, the deformations turn out to be higher than expected values. 24 mm lateral displacement in positive Y axis and 15 mm lateral displacement in negative Y axis occurs at top floor under the applied loading. In order to decrease the lateral deformations, either steel braces on XY plane or increasing sectional dimensions is needed. It is impossible to use steel braces on horizontal XY plane of resisting frame due to physical constraints of the test setup. Increasing the section dimensions for decreasing displacement can be a solution for such a case but it is unfeasible.

6.3.3.2. Second Proposal. Second proposed system consists of 4 columns supported by diagonal braces, composing a triangular truss system. Two of the triangular truss systems would be located on one side of the test frame with 5 m spacing whereas the other two

would be located on other side. Figure 6.40 shows the general view of computer model of one of the triangular truss systems.

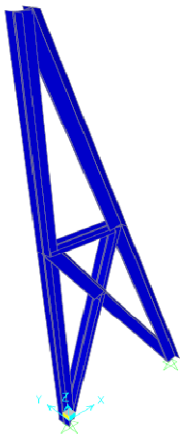

Figure 6.40. Computer model of triangular truss system

12.5 per cent of maximum lateral load, expected during static tests, (100 kN for second storey and 50 kN for first storey) is applied on storey levels of truss system. Under these loads, double angles with cross sections of 2L7X4X5/8X3/4XLLBB are determined safe for every element of truss system. St 37 steel with yield strength capacity of 240 MPa and ultimate strength capacity of 370 MPa is used for the double angles. Figure 6.41 shows the general view of cross sections of double angles determined and Table 6.13 shows sectional properties of double angle sections.

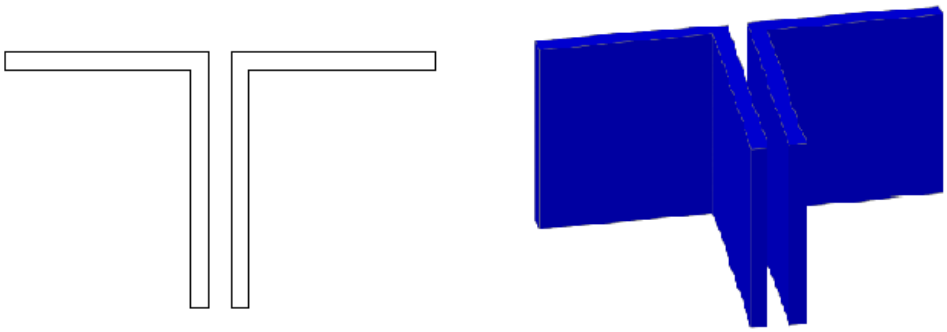

Figure 6.41. Cross sections of double angles for truss members

Table 6.13. Sectional properties of double angle sections

2L7X4X5/8X3/4LLBB	(mm)
Outside Depth	177.8
Outside Width	222.3
Horizontal Leg Thickness	15.9
Vertical Leg Thickness	15.9
Back to Back Distance	40

The analyses show that 2 mm lateral displacement occurs at first storey and 10.6 mm lateral displacement occurs on second storey. The displacements for this case are more acceptable compared to the first frame system. Also, the constructability is easier due to using same cross sections for every element.

Perfect greasing of extension I-sections at resisting frames and C-plates on test frames, to obtain a frictionless surface, becomes more important for the triangular truss system case. If a frictional force occurs in testing direction during loading, truss systems may fail because they are very weak under loads along the testing direction. In the analyses, it is assumed that a frictionless surface will be obtained during in-situ tests.

In accordance with the analyses results, it is determined that using the triangular truss system is the better solution for out-of-plane actions. In accordance with this, only detailing of triangular system is done. According to the calculations, the thickness of the gusset plates will be 32 mm. Two M40 bolts for every connection are sufficient to safely transmit the forces. The base plates will be 32 mm thick. Four M40 bolts are sufficient to safely anchor the base plates to foundations at ground. Figure 6.42 show the general views of final test setup and triangular truss system.

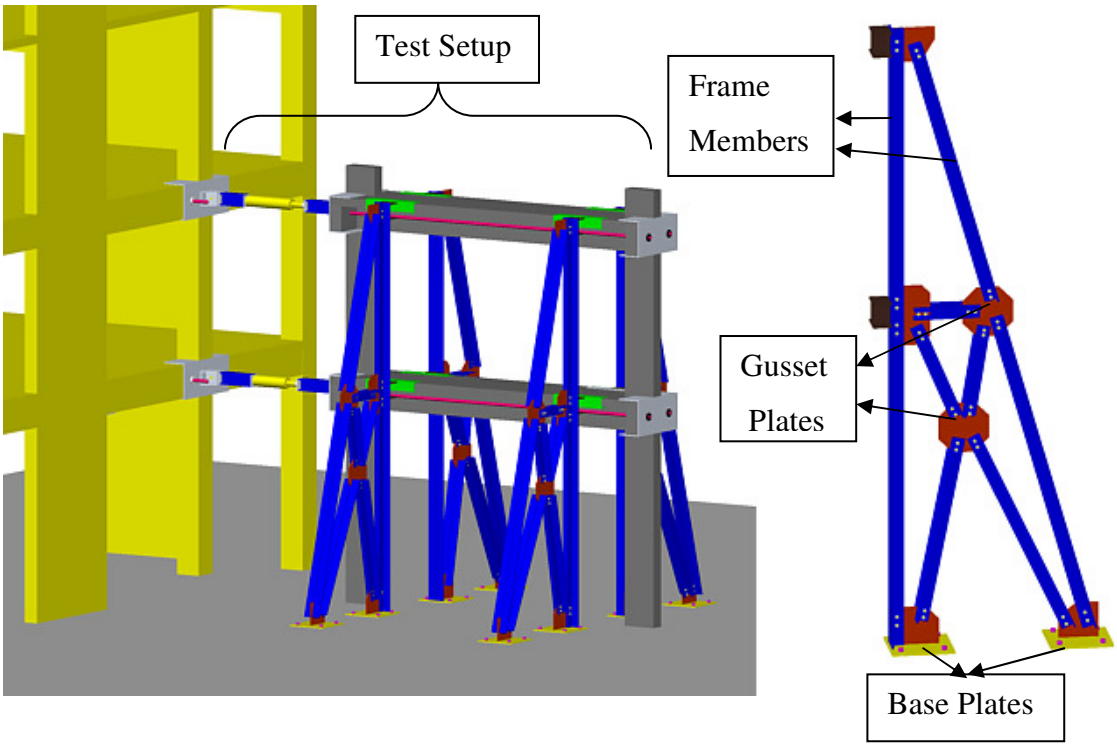

Figure 6.42. General views of final test setup and triangular truss system

7. DETERMINATION OF TEST EQUIPMENTS AND SPECIFICATIONS OF EQUIPMENTS FOR IN-SITU TESTS

The required in-situ testing equipments and their specifications in accordance with the proposed test setup in Chapter 5.5 and the analyses results in Chapter 6 are determined in Chapter 7. The required equipments are listed as follows:

- Two sets of “Hydraulic Loading Equipment”
- Two “Load Cells”
- Two “Loading Equipment”
- Two “ Assemblage System of Test Frames”
- Two “Assemblage System of Frames of Block-B”
- Two “Assemblage System of Shear Wall of Block-B”
- Four “Triangular Steel Resisting Truss System”
- Three ”Steel Braces”
- Three “Reference Columns of Test Frames”
- Four “Reference Columns of Block-B”
- “Displacement gauges (LVDT’s)”
- “Data Acquisition System”

7.1. Hydraulic Loading Equipment

Two sets of hydraulic loading equipment are required to apply static lateral loads to test frames during in-situ tests. The specifications of the hydraulic loading equipments are determined as follows:

First set: Double acting hydraulic cylinder with 2,000 kN loading capacity for compression and 1,000 kN loading capacity for tension, with a minimum of 600 mm stroke capacity is required. In order to drive the hydraulic cylinder, an electrical air pump with a pressure capacity of 700 bars, reservoir capacity of 20 liters, and constant flow capacity of 0.8 liters/sec is required. The electrical air pump has to include a needle valve which is

needed to regulate the flow of hydraulic fluid to or from the cylinders, a gauge adapter and a gauge to monitor pressure of the hydraulic circuit, hoses to transport the hydraulic fluid, and a cooling system. The first set hydraulic loading equipment will be used to load the top storey of the test frame.

Second set: Double acting hydraulic cylinder with 1,000 kN loading capacity for compression and 500 kN loading capacity for tension, with a minimum of 450 mm stroke capacity is required. In order to drive the hydraulic cylinder, an electrical air pump with a pressure capacity of 700 bars, reservoir capacity of 10 liters, and constant flow capacity of 0.5 liters/sec is required. The electrical air pump has to include a needle valve which is needed to regulate the flow of hydraulic fluid to or from the cylinders, a gauge adapter and a gauge to monitor pressure of the hydraulic circuit, hoses to transport the hydraulic fluid, and a cooling system. The second set hydraulic loading equipment will be used to load the bottom storey of the test frame. Figure 7.1 shows the schematic view of hydraulic loading equipment.

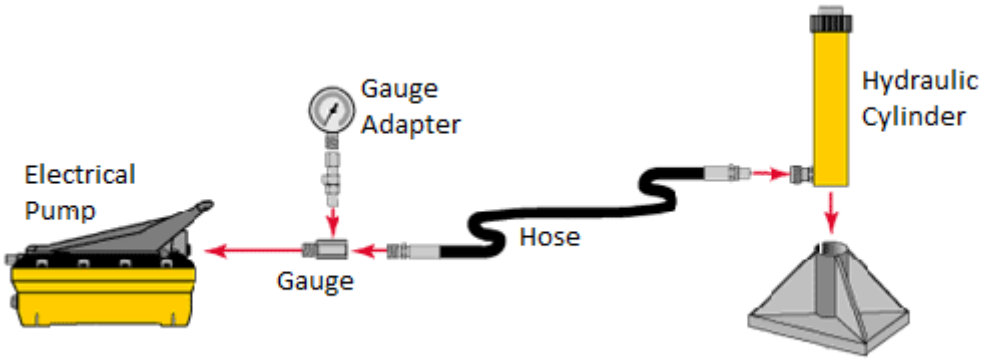

Figure 7.1. Schematic view of hydraulic loading equipment [48]

7.2. Load Cells

In order to measure the loads during in-situ tests, two load cells which have tensile load capacities of 1,000 kN are required. It is determined that load cells will be both compression and tension resistive, flat shaped, and slim. Figure 7.2 shows a typical view for a slim load cell.



Figure 7.2. Typical view for slim load cell [49]

7.3. Loading Equipments

Two loading equipments to install the hydraulic cylinders and load cells on it are required for static in-situ tests. Both edges of the loading equipments have to include spherical hinges. Each of the loading equipments are composed of two spherical hinges and two I-profiles which have welded steel plates on their edges. Figure 7.3 shows the general view of loading equipments.

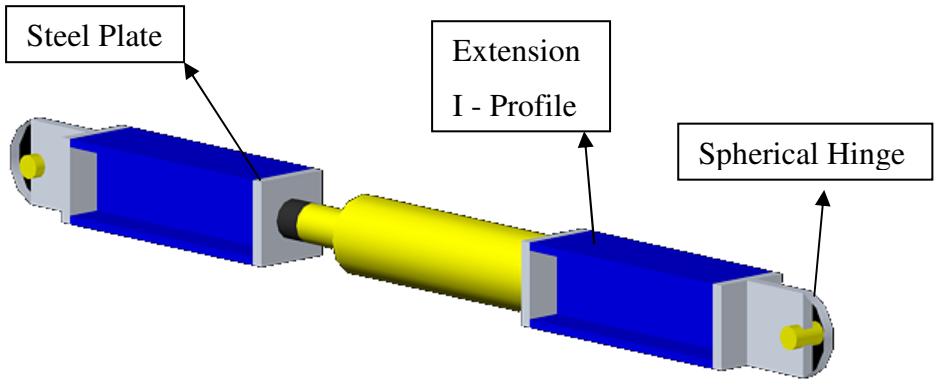

Figure 7.3. General view of loading equipments

7.4. Assemblage System of Test Frames

For installation of loading equipments on test frames, two assemblage systems for test frames are required. Every assemblage system consists of two steel U-plates (one of them includes a connection hinge for loading equipments whereas the other doesn't),

connected to each other with two steel wires. U-shaped plates will be located to beam-column junctions along the G and I axis at each storey of test frames. Steel wires will penetrate 500 mm long beam extensions along G and I axis and they will be used to connect U-shaped plates at beam-column junctions with bolts. General views of assemblage systems for test frames are shown in Figure 7.4.

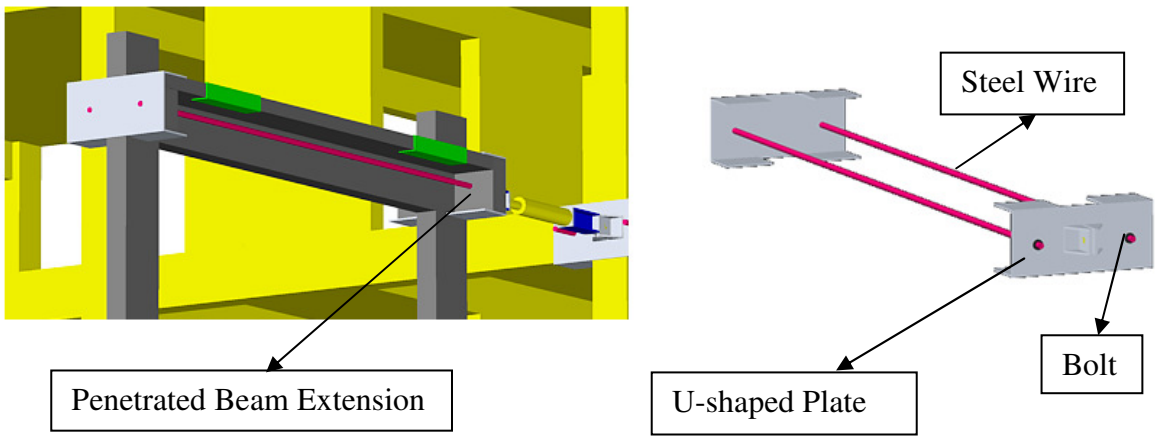

Figure 7.4. General views of Assemblage Systems of test frames

7.5. Assemblage System of Frames of Block-B

For installation of loading equipments on frames at Block-B along axis 4, 5, and 7, two assemblage systems of frames of Block-B are required. Every assemblage system consists of two steel U-plates (one of them includes a connection hinge for loading equipments whereas the other doesn't), connected to each other with two steel wires. U-shaped plates will be located to beam-column junctions at E' and A axis of frames along axis 4, 5, and 7 at basement and ground floors of Block-B. Steel wires will penetrate 500 mm long beam extensions at E' and A axis and they will be used to connect U-shaped steel plates at beam-column junctions, with bolts. General views of assemblage systems for frames of Block-B are represented in Figure 7.5.

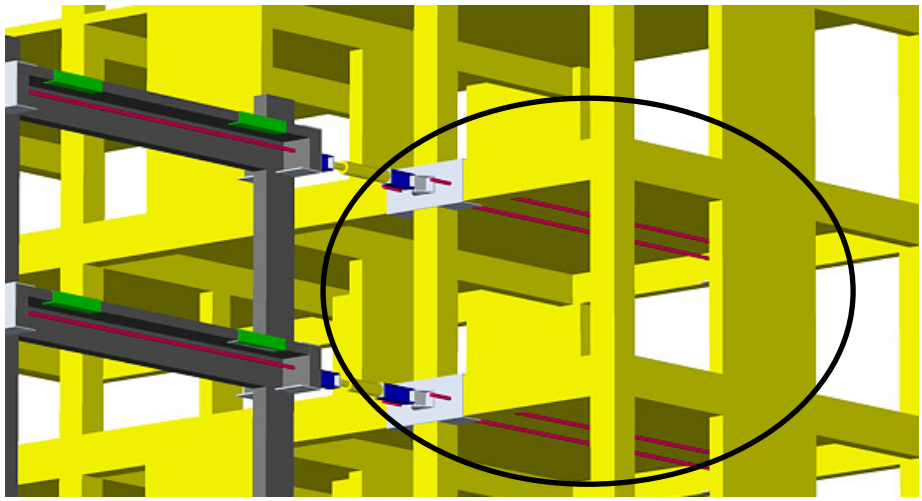

Figure 7.5. General view of installed assemblage system for frames of Block-B

7.6. Assemblage System of Shear Wall at Block-B

For installation of loading equipments on frames at Block-B along axis 6, two assemblage systems of shear walls of Block-B are required. Every assemblage system consists of two steel plates (one of them includes connection hinge for loading equipments whereas the other doesn't), connected to each other with two steel wires. One side of the steel plates will be U-shaped whereas the other side will be linear. The plates will be located to beam-shear wall junctions along E' and A axis of frames on axis 6 at basement and ground floors of Block-B. Steel wires will penetrate 500 mm long beam extensions along E' and A axis and they will be used to connect steel plates with bolts. General view of assemblage system for shear wall of Block-B is shown in Figure 7.6.

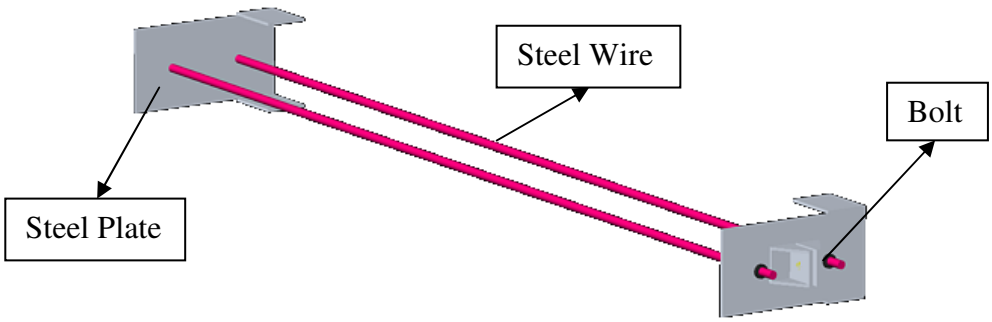

Figure 7.6. General view of assemblage system for shear wall at Block-B

7.7. Triangular Steel Resisting Truss System

In order to prevent total collapse and out-of-plane twisting of test frames while loading, four steel resisting truss systems are needed. Figure 5.12 shows the general view of steel resisting truss system in accordance with the analyses results.

Steel resisting frame consist of truss members of double angle sections, extension I profiles, gusset plates for connections of truss members, steel base plates, and bolts. It is determined that double angle sections will be 2L7X4X5/8X3/4XLLBB and extension I-sections will be W14X54. The thickness of the gusset plates will be 32 mm. Two M40 bolts will be used in all connections of double angle profiles to gusset plates. Figure 7.7 shows the dimensions of the steel resisting truss system.

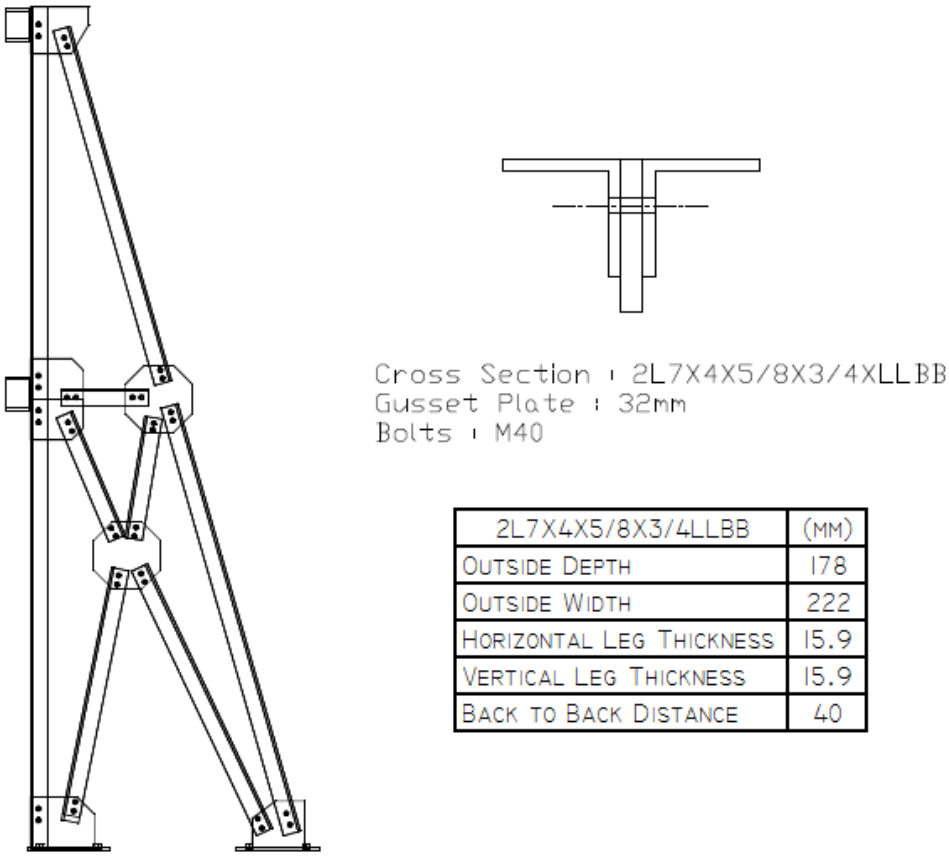

2L7X4X5/8X3/4LLBB	(MM)
OUTSIDE DEPTH	178
OUTSIDE WIDTH	222
HORIZONTAL LEG THICKNESS	15.9
VERTICAL LEG THICKNESS	15.9
BACK TO BACK DISTANCE	40

Figure 7.7. Dimensions of steel resisting truss system (mm)

Chemical anchors will be used to anchor base plates to existing reinforced concrete foundations. In accordance with the analyses results, it is determined that four M40 rods (40 mm diameter rods) will be used to anchor each base plate to the existing concrete foundations. In calculations, the rods are assumed to meet the requirements of ISO 898-Class 5.8 (400 MPa for yield strength of steel and 500 MPa for ultimate strength of steel is assumed).

7.8. Steel Braces

Two diagonal braces will be located between $C-E'$ axes on first and second stories and a diagonal brace will be located between A-C axes on first story along axis 6 of Block-B in order to increase the lateral load capacity and stiffness. $W14\times54$, St 37 steel frame sections will be used as braces. The braces will be pin connected to beam-column junctions. Figure 6.29 shows the cross-section of the brace elements.

7.9. Reference Columns of Test Frames

Three reference columns to place displacement gauges, which will be used to measure lateral displacements at storey levels of test frames, are required. Each reference column consists of a base plate and 7,500 mm long steel box profiles. Welded steel connections will be used to connect base plates and the box profiles. Base plates will be anchored to the existing reinforced concrete foundation, with four 20 mm diameter chemical anchor bolts.

7.10. Reference Columns of Block-B

Four reference columns to place displacement gauges, which will be used to measure lateral displacements at storey levels of Block-B, are required. Each reference column consists of a base plate and 14,000 mm long steel box profiles. Welded steel connection will be used to connect the base plates and the box profiles. Base plates will be anchored to the existing reinforced concrete foundations with four 20 mm diameter chemical anchor bolts.

7.11. Linear Variable Displacement Transformers (LVDT)

LVDTs will be used to measure relative and absolute storey displacements of test frames and Block-B. Each of them will be approximately 1 kg and they will be placed on reference columns of test frames and Block-B. Arrays of LVDTs will be used to measure flexural and shear deformations at column ends, beams ends, and beam-column joints. Figure 7.8 shows general views of LVDTs.

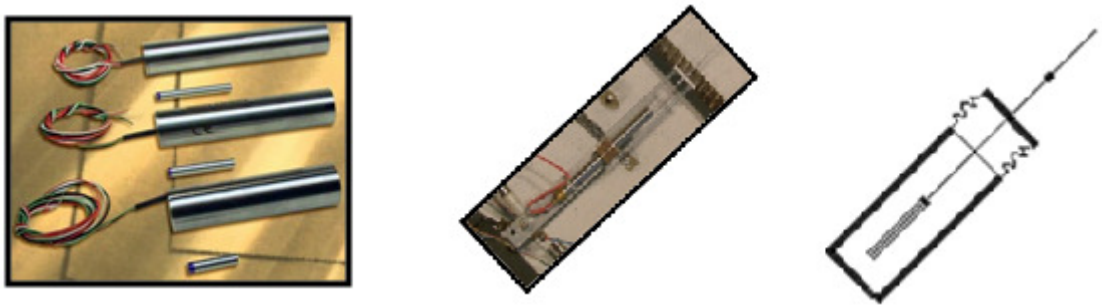

Figure 7.8. General views of LVDTs [50]

7.12. Data Acquisition System

A data acquisition system with suitable number of channels for LVDTs is required. Data acquisition system must be able to acquire continuous data during tests.

7.13. Summary of Required Equipments for In-Situ Static Tests

Table 7.1 shows the summary table for required equipments for in-situ static tests in accordance with Section 7.1 - Section 7.12.

Table 7.1. Summary of required equipments for in-situ static tests

Items	No's
Hydraulic Loading Equipment	2
Load Cells	2
Loading Equipment	2
Assemblage System of Test Frames	2
Assemblage System of Frames of Block-B	2
Assemblage System of Shear Walls of Block-B	2
Triangular Steel Resisting Truss System	4
Steel Braces	3
Reference Columns for Test Frames	3
Reference Columns for Block-B	4
LVDT	---
Data Acquisition System	In accordance with no’s of LVDTs

8. SUMMARY, CONCLUSIONS AND RECOMMENDATIONS FOR FUTURE WORK

8.1. Summary

Results of Taiwan school building tests replicated successfully using an analytical model that incorporates: combined shear-flexure model to simulate short column failure, rigid zones representing windowsills, and flexural hinges and shear hinges for frame members.

Blind prediction studies performed for a typical non-ductile RC building in Turkey using detailed analytical models which consider: diagonal strut and tie members for brick infill walls with or without CFRP overlays, alternative modeling methodologies for RC infill walls to be used in seismic rehabilitation, and flexural hinges and shear hinges on frame members.

A static pushover testing scheme is proposed and designed including: construction works, loading mechanisms, strengthening techniques, and stability issues.

8.2. Conclusions

A configuration for conducting in-situ pushover tests on a real existing building is supplied in this thesis. In the first part of the thesis (Chapter 2 and Chapter 3), a brief study on seismic rehabilitation techniques and nonlinear modeling strategies are investigated. In the next chapter (Chapter 4), the accuracy of nonlinear modeling techniques investigated are tested on a Taiwanese school building, namely the Hsin-Tseng Junior High School building. The unknowns affecting the analysis results are determined by comparing the analytical study results to the test results presented in the literature. In the last chapters (Chapter 5, Chapter 6, and Chapter 7), a sample Turkish School, namely Sehit Adem Yavuz Primary School in Istanbul is chosen as a sample test building for in-situ pushover tests and a test configuration is proposed in accordance with the geometrical properties of

the building and analytical predictions of the determined tests. The conclusions obtained from this study can be summarized as follows:

- An analytical study to predict the results of a retrofitting technique has to be accomplished before application. The modeling technique chosen for the structure affects the analysis results. Due to this, firstly, the expected behavior of the building has to be predicted in accordance with previous research and then the analytical study has to be conducted. For example, in Chapter 4, the analyzed structure was determined as a shear building due to short columns occurred by presence of windowsills and geometrical properties of the structural elements. Elwood and Moehle's [28] model for shear critical columns is used to model the shear critical columns in this structure.
- The analyses at Chapter 4 showed that, effective stiffness values of structural members is one of the most important factors affecting the initial and pre-yield stiffnesses of the force-displacement curves. Using the code determined values gives a general idea about the behavior of structure under lateral loads but using moment-curvature relationships is better to define the effective stiffness values to predict the behavior of the structure more accurately. Also, the code determined effective stiffnesses diverge from each other in accordance with the assumptions considered by codes. For instance, the difference of the effective stiffnesses of FEMA 356 [41] and TEC 2007 [16] is shown in Figure 4.5.
- The analyses at Chapter 4 and Chapter 6 and previous research by other researchers showed that infill walls have to be accepted as structural elements. Although there are codes such as the Eurocode-8 [30] that include rather detailed procedures for designing infilled RC frames, presence of infill walls have been ignored in most of the seismic codes (except for their weight). It is observed that including infill walls to structural system increases the lateral load capacities up to two-three times the infill wall neglected cases under small lateral displacements. Under high lateral displacements, the infill walls crush and the frames behave like bare frames.
- There are different techniques presented in the literature for modeling the infill walls. Most of them are based on the equivalent truss concept. Although they are based on the same concept, each of them has different assumptions for unknowns. Due to this, while modeling the infill walls, a detailed study on properties of infill walls has to be

done on field to minimize the number of unknowns. The dimensions of bricks and their type and thicknesses of mortar have to be correctly determined. If possible, modulus of elasticity of the materials has to be determined experimentally rather than empirically.

- The code-recommended modulus of elasticity values differ from each other significantly. For instance, the concrete modulus of elasticity can be calculated as $E_c = 3250\sqrt{f_{ck}} + 14000$ via TS500-2000 [23] and $E_c = 4750\sqrt{f_{ck}}$ via ACI, and they have very significant differences. If possible, it is proposed that modulus of elasticity values have to be found experimentally rather than empirically.
- Two different modeling techniques were used in the analyses of shear wall strengthened frames in Chapter 6. It was observed that both of the curves resulted similarly in terms of initial stiffnesses and lateral load capacities although the deformation behaviors were different due to definition of hinges. It is said in FEMA 356 [41] and ATC-40 [45] that half the section depth can be used for plastic hinge lengths. But for long shear walls, half the section depth assumption for plastic hinge length is unrealistic. Due to this, it is proposed that using a plastic hinge length of quarter the section depth for similar shear walls used in this study is more reliable in accordance with the prior shear wall strengthened frame studies.
- While proposing an in-situ test model for a structure, it is proposed that first, a detailed study on structural plans and a comprehensive field investigation are required. The required tests have to be done to determine the material properties of the structure. In accordance with geometrical properties and material properties of the structure, a testing scheme has to be determined. While determining the testing schemes, the following factors have to be investigated: (i) the number and types of tests going to be proposed, (ii) the properties of test frames considered, (iii) the need for constructing a reaction block or including an available structure/part of a structure to be used as a reaction block, (iv) the required construction works to be done before tests, (v) the need for constructing an out of plane preventing structure or availability of it, and (vi) the availability of the field for such tests.
- If a cyclic pushover test is going to be conducted, one of the important factors to be considered is the behavior of the test frame and reaction block under tensile forces. While pulling the test frame, high tensile forces occur on the loading equipment

connected regions of the test frame and reaction block which may result local failures. In order to prevent this, the assemblage systems shown in Figure 7.4 and Figure 7.6 can be used. While pulling the test frame, the frame will behave like pushed on the other side via the assemblage system.

- In accordance with the proposed test setup for Sehit Adem Yavuz Primary School building, a time period of 16 weeks is enough for such an in-situ pushover test. For another structure, the time period can diverge depending on the geometry of the structure and the proposed test types but the flow chart given in Figure 5.16 and the schedule given in Figure 5.17 can be used as reference while proposing an in-situ testing scheme for a real existing building.
- The analytical study of proposed tests showed that including infill walls to the structural system, strengthening via CFRP, and strengthening via RC shear walls increase the lateral load capacities significantly in accordance with previous studies in the literature. Table 6.9 and Figure 6.27 show the comparison table and graph of different lateral strengthening techniques, respectively.
- Hydraulic loading equipments, load cells, loading equipments, assemblage system for test frames and reaction blocks, steel resisting frames, reference columns for measurements, LVDTs, and data acquisition system are determined as main equipments to run in-situ pushover tests.

8.3. Recommendations for Future Work

In accordance with the geometrical properties of test building supplied, a limited number of reinforced concrete frames were considered in this study. Only three types of seismic rehabilitation techniques can be investigated with such a building. In order to accomplish an extensive study, more frames with similar dimensions are needed, meaning that a larger test building is required. By using a larger building, it would be possible to investigate more seismic rehabilitation techniques.

Also, by using a larger building as a test specimen, it would be possible to test three-dimensional frames rather than two dimensional ones. Considering three-dimensional test frames for in-situ pushover tests make possible to investigate the affects of out of plane infill walls to lateral resistance and deformation behavior. By such tests, it would be

possible to find a new methodology to model the out of plane walls with nonlinear frame elements.

Rather than analyzing the out of plane resisting frames under the assumed point loads that can be exerted from test frames, a more realistic methodology considering both the test frame and the resisting frame at the same time have to be done. Out of plane forces have to be exerted on resisting frame by touching of structures due to twisting of test frame.

Finally, this study contains only the analytical studies, predictions, and proposed configurations of in-situ pushover tests for a sample building. It would be possible to check the accuracy of nonlinear modeling techniques by actually conducting such field tests.

APPENDIX A: DRAWINGS OF SEHIT ADEM YAVUZ PRIMARY SCHOOL

The drawings of Sehit Adem Yavuz Primary School are given in Appendix A. The usage and dimensions of the rooms and corridors are detailed in the drawings. Figure A.1 shows floor plan of basement floor, Figure A.2 shows floor plan of ground floor, Figure A.3 shows floor plan of first storey, and Figure A.4 shows floor plan of second storey.

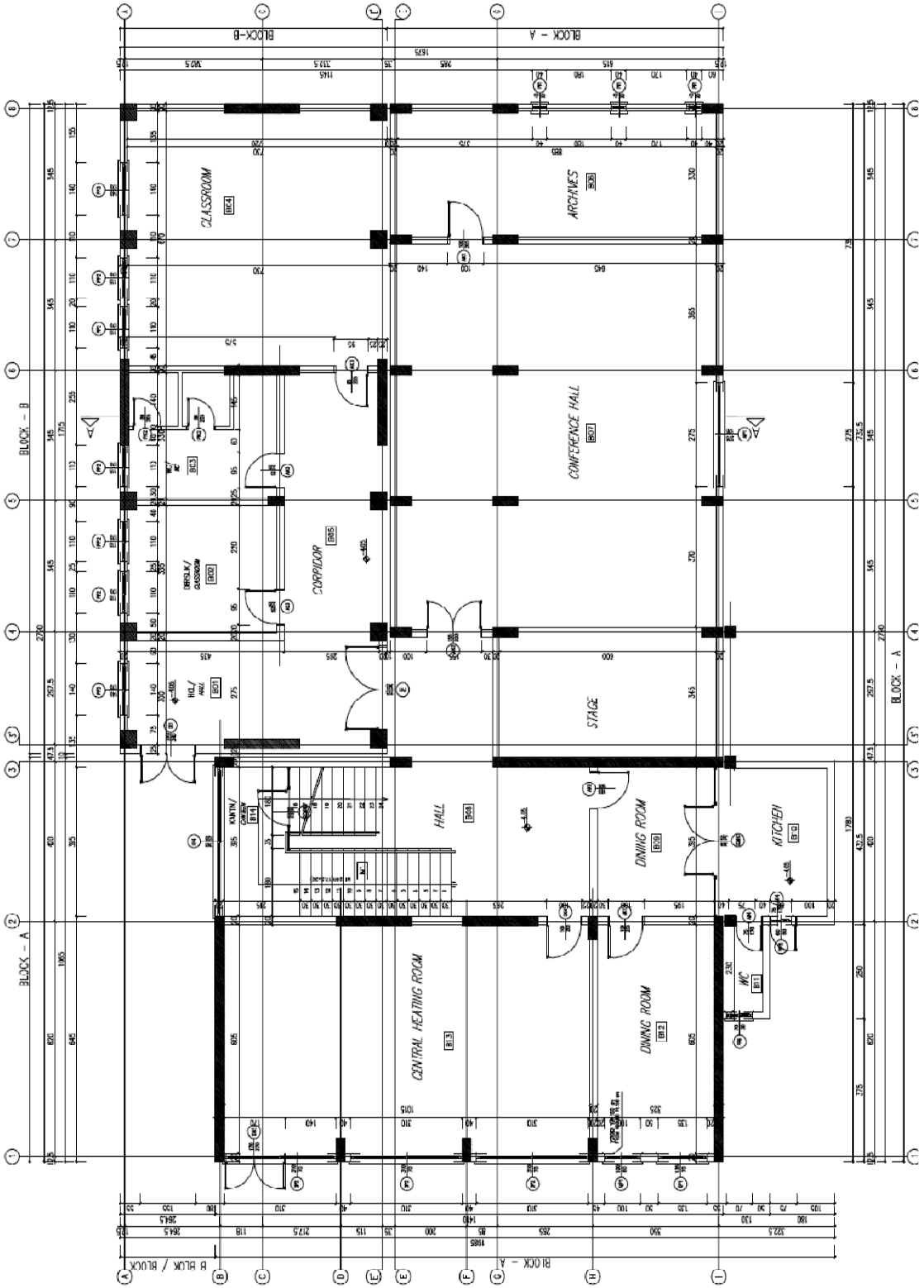

Figure A.1. Plan view of basement floor of Sehit Adem Yavuz Primary School

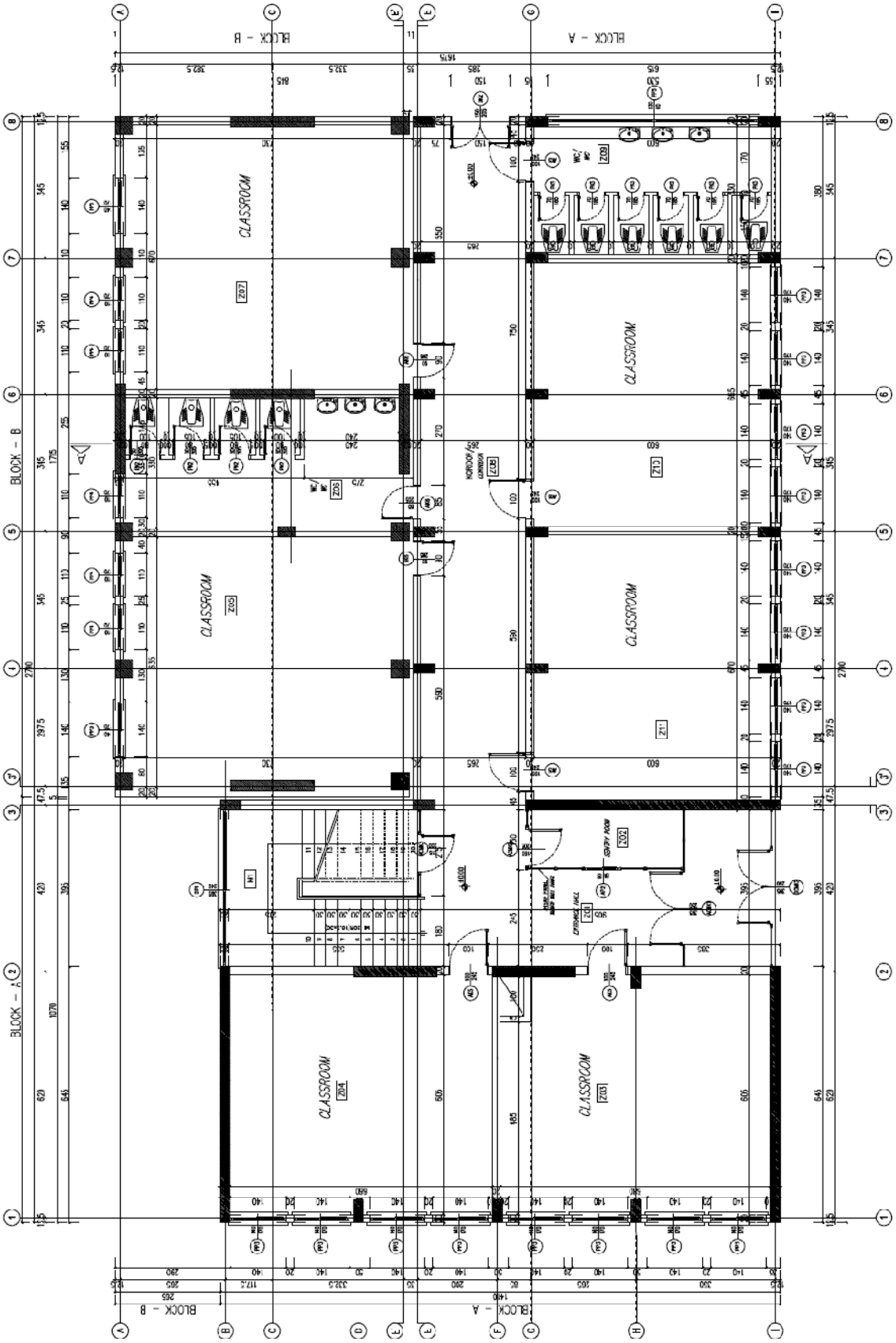

Figure A.2. Plan view of ground floor of Sehit Adem Yavuz Primary School

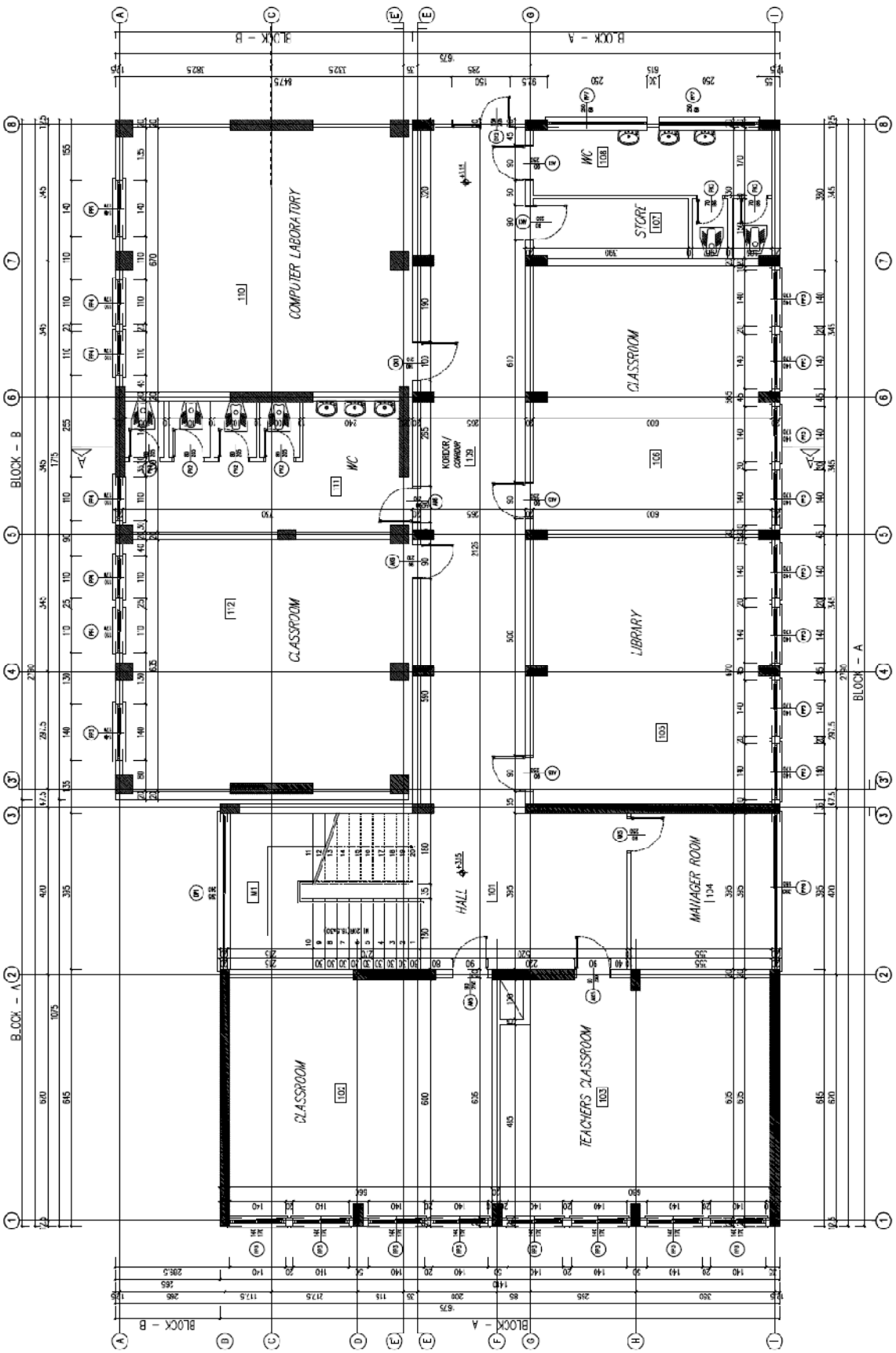

Figure A.3. Plan view of first storey of Sehit Adem Yavuz Primary School

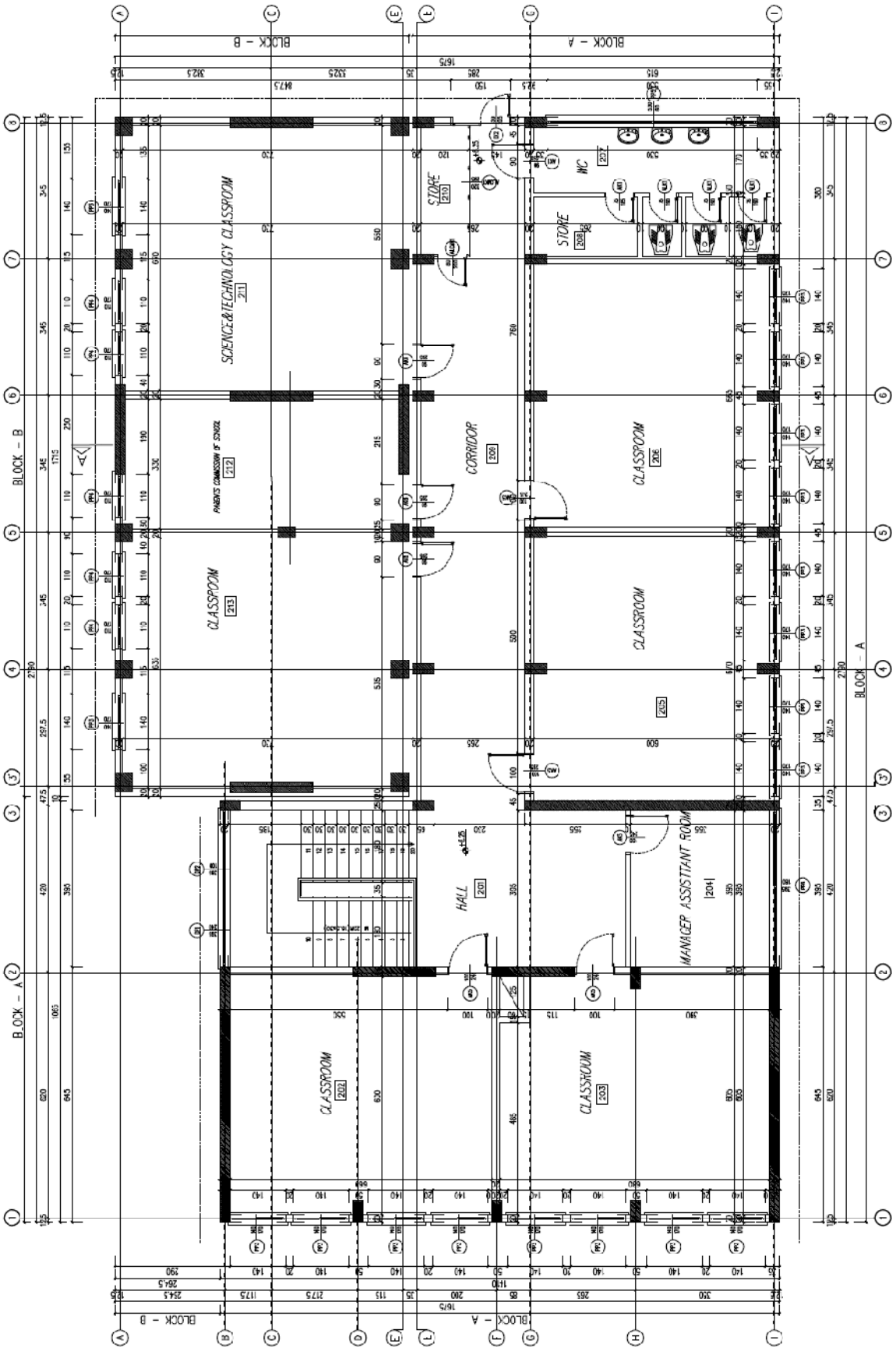

Figure A.4. Plan view of second storey of Sehit Adem Yavuz Primary School

APPENDIX B: GENERAL VIEWS OF THE PROPOSED TEST CONFIGURATION

The general views of the proposed test configuration are given in Figure B.1 and Figure B.2. Figure B.3 shows the general view of the gusset plates and M40 bolts. Figure B.4 shows the three dimensional general view of the loading system.

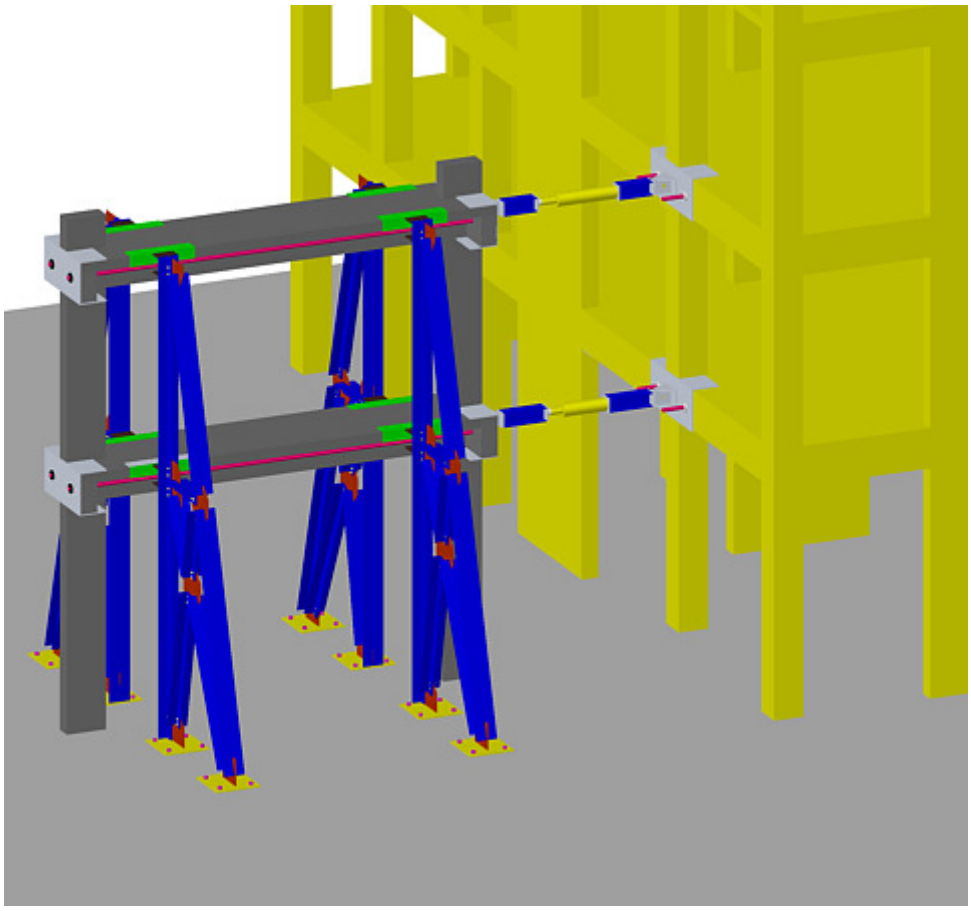

Figure B.1. Three dimensional general view of the test setup-1

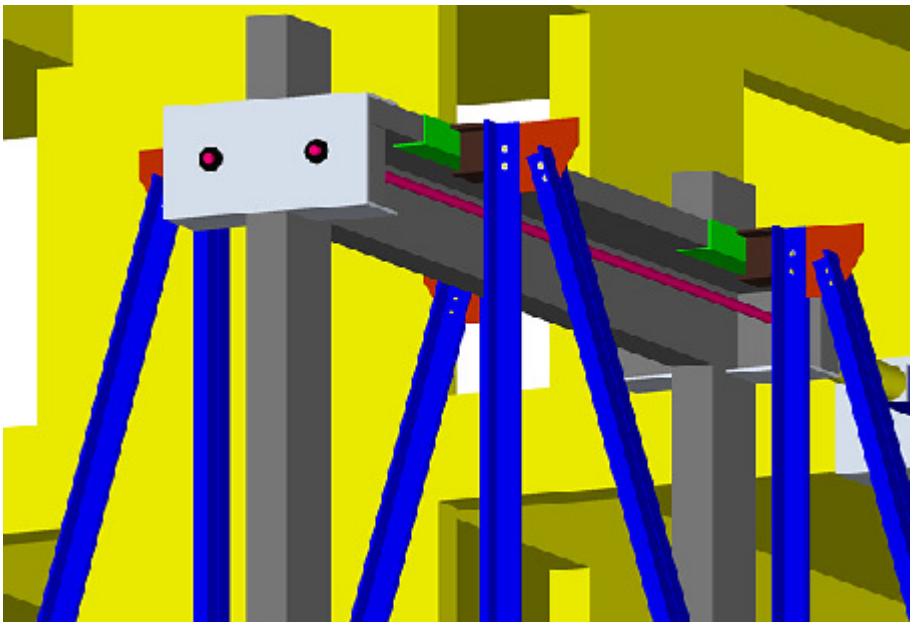

Figure B.2. Three dimensional general view of the test setup-2

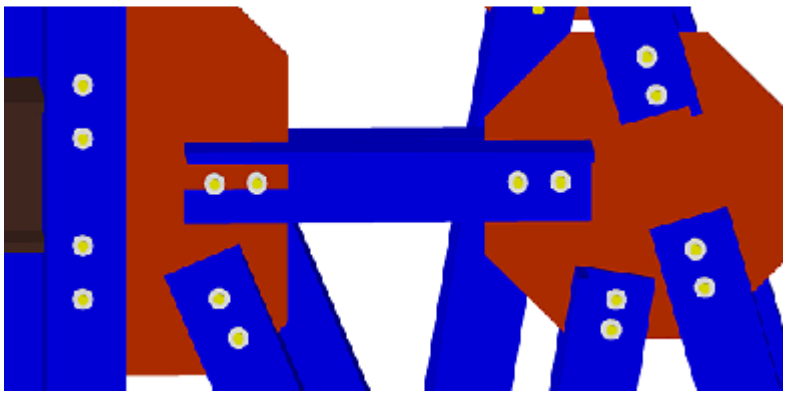

Figure B.3. General view of the gusset plates and M40 bolts

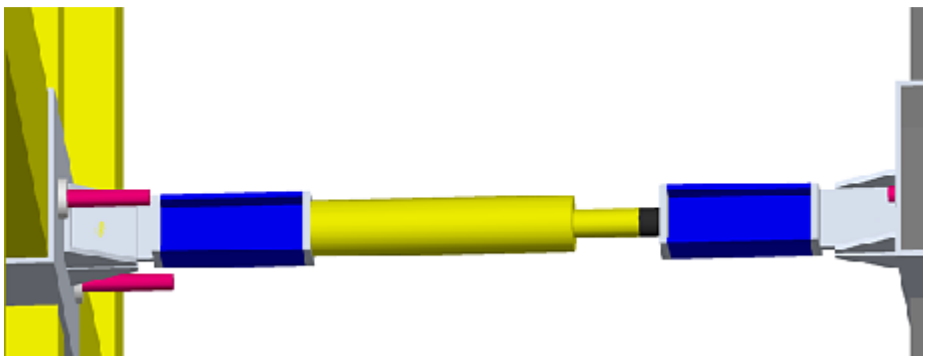

Figure B.4. General view of the loading system

APPENDIX C: DETAILED DRAWINGS OF ASSEMBLAGE SYSTEMS OF TEST FRAMES AND BLOCK-B

The general views and detailed drawings of assemblage systems of test frames and Block-B are given in Appendix C. Plates at front include the hinges that will be used for connections of loading equipment. The dimensions are determined by approximations. Figure C.1 shows the assemblage system of test frame, Figure C.2 shows the assemblage system of frames of Block-B, and Figure C.3 shows the assemblage system of shear wall of Block-B.

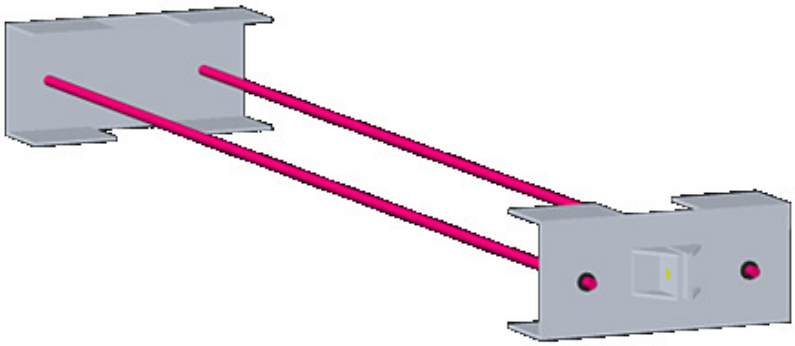

Plate at front:

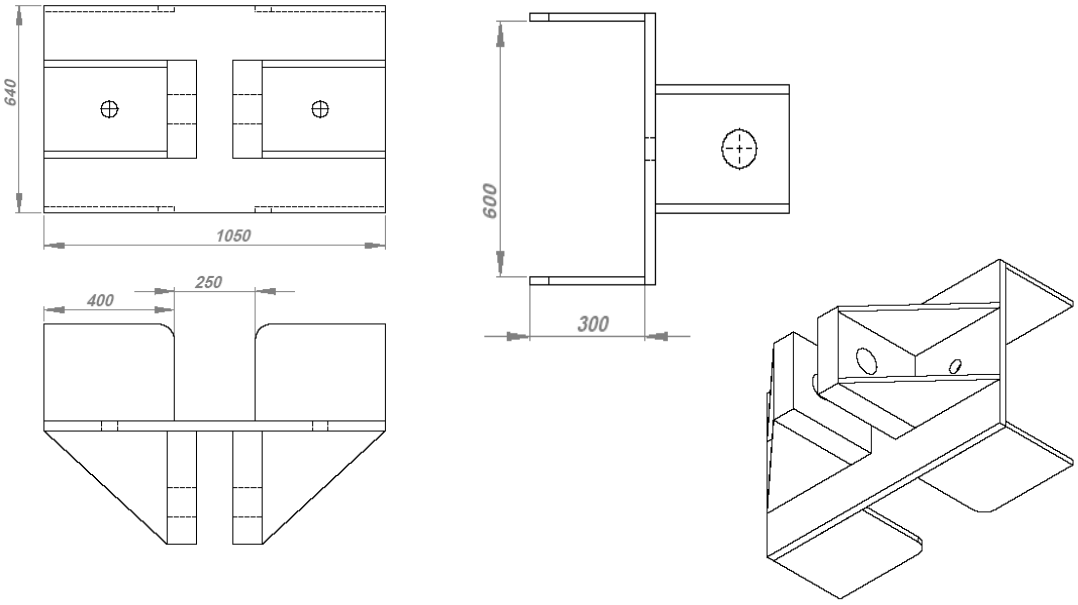

Plate at back:

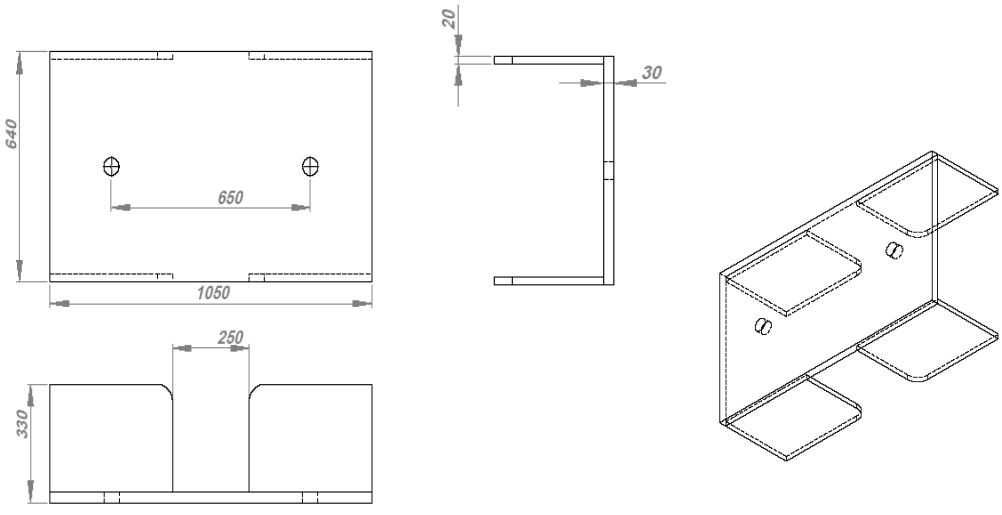

Figure C.1. General view and dimensioning of assemblage system of test frames

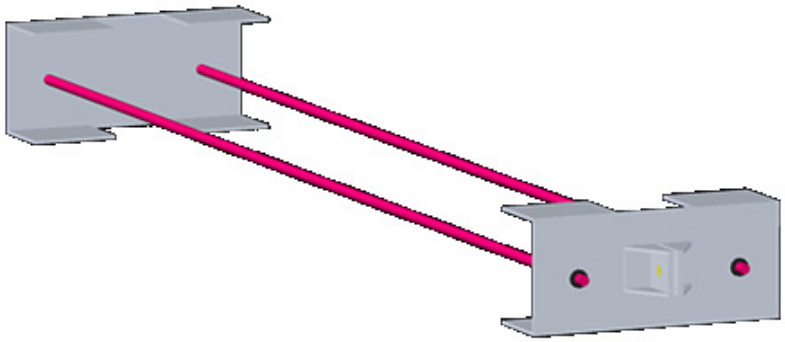

Plate at front:

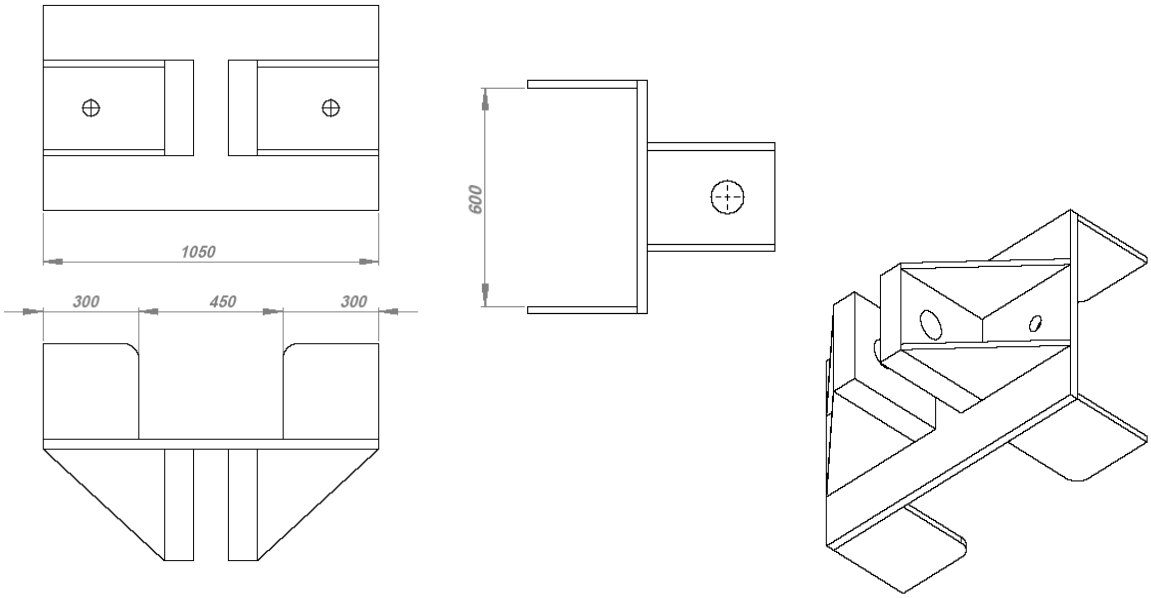

Plate at back:

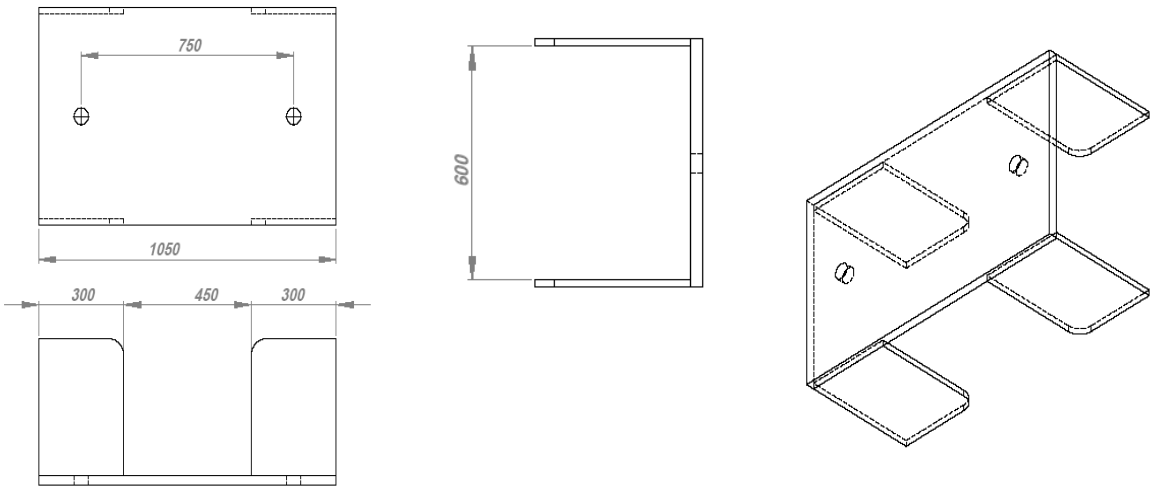

Figure C.2. General view and dimensioning of assemblage system of frames of Block-B

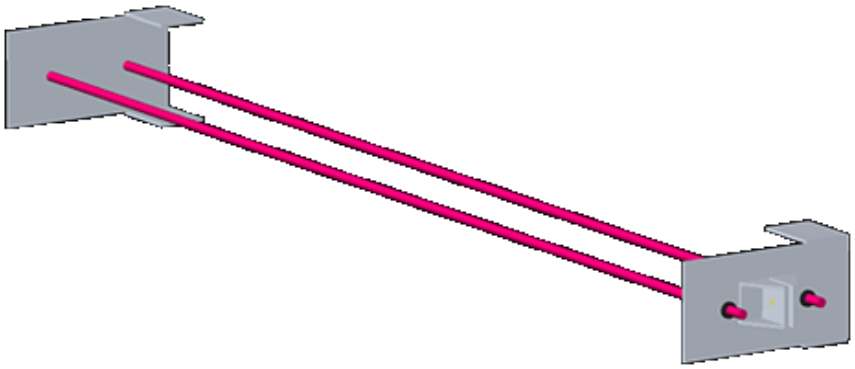

Plate at front:

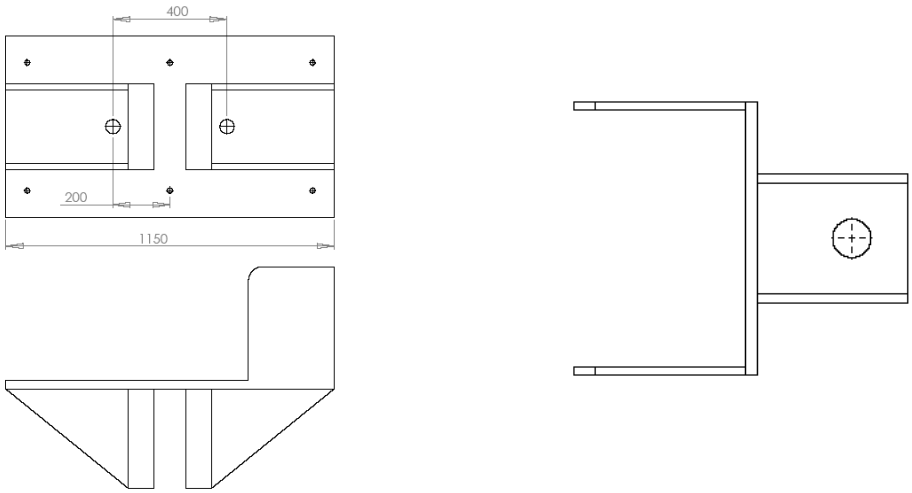

Plate at back:

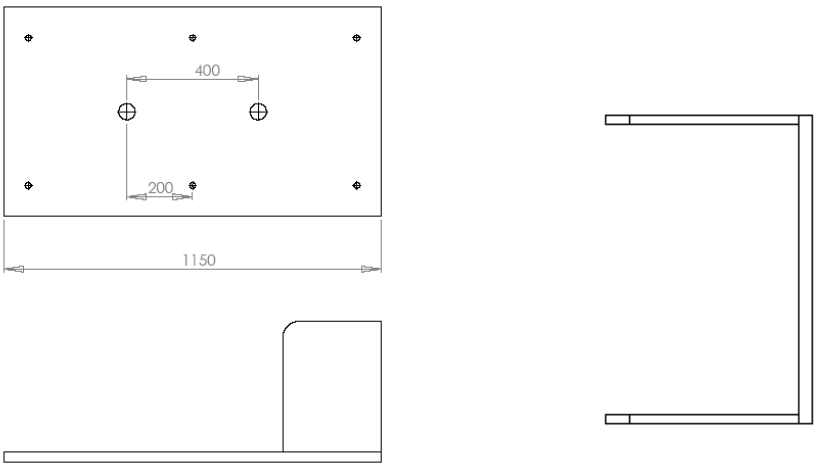

Figure C.3. General view and dimensioning of assemblage system of shear wall of Block-B

REFERENCES

1. Tu, Y.-H., W.-W. Kuo and S.-J. Hwang, *In-situ Test of School Building Structure in Taiwan*, http://exp.ncree.org/rpes/a03-e.pdf, 2006.

2. Hsiao, F.-P., Y.-K. Yeh, W.-C. Shen, L.-L. Chung and S.-J. Hwang, "Seismic Evaluation of Existing School Buildings", *7th International Training Program for Seismic Design of Structures and Hazard Mitigation,* ITP2008, NCREE, Taipei, Taiwan, October 20-24, 2008.

3. Wu, C.-W. and Q. Xue, "Seismic Capacity Evaluation of Kouhu Elementary School Buildings", *4th International Conference on Earthquake Engineering*, October 12,13 2006, Paper No. 124, Taipei, Taiwan, 2006.

4. Weng, Y.-T., K.-C. Lin and S.J. Hwang, "Experimental and Analytical Performance Assessment of In-Situ Pushover Tests of School Buildings in Taiwan", *4th International Conference on Earthquake Engineering*, October 12,13 2006, Paper No. 154, Taipei, Taiwan, 2006.

5. Erdem I., U. Akyuz, U. Ersoy and G. Ozcebe, "An Experimental Study on Two Different Strengthening Techniques for RC Frames", *Engineering Structures*, Vol. 28, pp. 1843-1851, 2006.

6. Canbay E., U. Ersoy and G. Ozcebe, "Contribution of Reinforced Concrete Infills to Seismic Behavior of Structural Systems", *ACI Structural Journal*, Vol. 100, No. 5, pp. 637-643, September-October 2003.

7. Yazgan, A. U. and M. Nishiyama, *Seismic Performance Evaluation of Existing RC Structures According to the Japanese Standard and Retrofitting with Precast CFT and FRC Braces*, http://iisee.kenken.go.jp/syndb/?action=down&p=200805076858300f.pdf&t=application/pdf&n=MEE06003_Ahmet_Utku_YAZGAN_2007.pdf, 2007.

8. Saatcioglu M., F. Serrato and S. Foo, “Seismic Retrofit of Masonry Infill Walls using CFRP Sheets”, *The Proceedings of the Natural Hazard Mitigation Workshop*, PWGSC, Ottawa, July, 2002.

9. Ozden, S. and U. Akguzel, “CFRP Overlays in Strengthening of Frames with Column-Rebar Lap Splice Problem”, *NATO International Closing Workshop Under Subproject of 4 of NATO Project*, Sfp 977231, May 2005, Istanbul, Turkey, 2005.

10. Tankut, T., U. Ersoy, G. Ozcebe, M. Baran and D. Okuyucu, “In Service Seismic Strengthening of RC Framed Buildings”, *NATO Sfp Workshop on Seismic Assessment and Rehabilitation of Existing Buildings,* NATO Science Series, Vol. 29, Kluwer Academic Publishers, Oct. 2003.

11. Turk, A.M., *Rehabilitation of Reinforced Concrete Frames by Reinforced Concrete Infills*, Ph.D. Thesis, Department of Civil Engineering, Bogazici University, 1998.

12. Pinto, A.V. and F. Taucer, “Assessment and Retrofit of Full Scale Models of Existing RC Frames”, *Proceedings of Advances in Earthquake Engineering for Urban Risk Reduction,* pp. 1-16, Netherlands, 2005

13. Brokken, S.T. and V.V. Bertero, *Studies on Effects of Infills in Seismic Resistant R/C Construction*, EERC Report No. 81-12, University of California, Berkeley, October 1981.

14. Aboutaha, R.S., O.J. Jirsa, M.D. Engelhardt and M.E. Kreger, *Seismic Strengthening of Reinforced Concrete Columns with Inadequate Lap Splices*, Extending the Lifespan of Structures: IABSE Symposium Report, San Francisco, 1995.

15. Girgin, K. and K. Darilmaz, “Seismic Response of Infilled Framed Buildings Using Pushover Analysis”, *ARI The Bulletin of the Istanbul Technical University*, Vol. 54, No. 5, July 2007.

16. Turkish Earthquake Resistant Design Code 2007, *Specifications of Buildings to be Built in Disaster Areas,* The Ministry of Public Works and Settlement, Ankara, Turkey, 2007.

17. Binici, B. and G. Ozcebe, "Seismic Evaluation of Infilled Reinforced Concrete Frames Strengthened with FRPS", *Proceedings of the 8th U.S. National Conference on Earthquake Engineering*, Paper No: 1717, April 18 - 22, San Francisco, California, USA, 2006.

18. Richart, F.E., A. Brandtzaeg and R.L. Brown, *The Failure of Plain and Spirally Reinforced Concrete in Compression*, Engineering Experimental Station, University of Illinois, Bulletin No. 190, 1929.

19. Sheikh, S.A. and S.M. Uzumeri, "Analytical Model for Concrete Confinement in Tied Columns", *Journal of the Structural Division*, ASCE 108, pp. 2073 - 2722, 1980.

20. Mander, J.B., M.J.N. Priestley and R. Park, "Theoretical stress-strain model for confined concrete," *Journal of Structural Engineering, ASCE*, Vol. 114, No. 8, pp. 1804-1826, 1998b.

21. Hognestad E., *A Study of Combined Bending and Axial Load in Reinforced Concrete Members*, Engineering Experimental Station, University of Illinois, Bulletin No. 399, 1951.

22. Kent D.C. and R. Park, "Flexural members with confined concrete" *Journal of the Structural Division,* ST7, 97, pp 1969-1990, 1971.

23. TS 500, *Requirements for Design and Construct of Reinforced Concrete Structures,* Turkish Standards Institute, Ankara, Turkey, 2000.

24. Ersoy, U., Personal Communication, 2008.

25. TRC/Imbsen Software Systems, XTRACT v. 3.0.1, *Cross Sectional Structural Analysis of Components*, California, USA, 2004.

26. CSI, SAP2000 v.11.0.0, *Linear and Nonlinear Static and Dynamic Analysis and Design of Three-Dimensional Structures*, Computers and Structures Inc., USA, 2007.

27. Elwood, K.J. and J.P. Moehle, *Shake Table Tests and Analytical Studies on the Gravity Load Collapse of Reinforced Concrete Frames*, PEER Report Series, November 2003/01.

28. Elwood, K.J. and J.P. Moehle, "Drift Capacity of Reinforced Concrete Columns with Light Transverse Reinforcement", *Earthquake Spectra*, Vol. 21 (1), pp. 71-89, 2005.

29. Elwood, K.J. and J.P. Moehle, "Axial Capacity Model for Shear-Damaged Columns" *ACI Structural Journal*, Vol. 102 (4), pp. 578-587, 2005.

30. BSI, BS EN 1998-1-4: Eurocode-8, *Design Provisions for Earthquake Resistance of Structures - Structural Analysis Methods and Models*, British Standards Institution, 2006.

31. Madan, A., A.M. Reinhorn, J.B. Mander and R.E. Valles, "Modelling of Masonry Infill Panels for Structural Analysis", *Journal of Structural Engineering*, Vol.123, pp. 1295, 1997.

32. Holmes, M., "Steel Frames with Brickwork and Concrete Infilling", *Proceedings of the Institute of Civil Engineers*, London, England, Vol. 73, Part 2, pp. 473-478, 1961.

33. Mainstone, R.J., "On the Stiffness and Strength of Infilled Frames", *Proceedings of the Institute of Civil Engineers*, Supplement IV, pp. 57-90, London, England, 1971.

34. Chen, Y.-H., *Seismic Evaluation of RC Buildings Infilled with Brick Walls*, Doctoral Dissertation, National Chang Kung University, Taiwan, 2003.

35. Wu, C.-L., T.-C. Chiou, F.-P. Hsiao, L.-L. Chung and S.-J. Hwang, "Seismic Retrofit of Typical Low-rise RC School Buildings" *7th International Training Program for Seismic Design of Structures and Hazard Mitigation,* ITP2008, NCREE, Taipei, Taiwan, October 20-24, 2008.

36. El-Dakhakhni, W., M. Elgaaly and A. Hamid, "Three-strut Model for Concrete Masonry Infilled Steel Frames", *ASCE, Journal of Structural Engineering*, Vol. 129, No.2, pp. 177-185, 2003.

37. Saneinejad, A. and B. Hobbs, "Inelastic Design of Infilled Frames" *ASCE, Journal of Structural Engineering*, Vol. 121, No. 4, pp 634-650, 1995.

38. Flanagan, R.D. and R.M. Bennett, "In-plane Behavior of Structural Clay Tile Infilled Frames", *ASCE, Journal of Structural Engineering,* Vol. 125, No. 6, pp. 590-599, June 1999.

39. Golden Software Inc., Didger v.3.02, *Digitizing Software*, Colorado, USA, 2001.

40. BSI, BS EN 1992-1-1, Eurocode 2, *Design of Concrete Structures*, British Standards Institution, 2004.

41. Building Seismic Safety Council, FEMA 356, *Prestandard and Commentry for The Seismic Rehabilitation of Buildings*, prepared by ASCE, published by the Federal Emergency Management Agency, Washington DC. USA, 2000.

42. Hanoğlu, K.B., *Fiber Reinforced Plastic Overlay Retrofit of Hollow Clay Tile Masonry Infilled Reinforced Concrete Frames*, Ph.D. Thesis, Department of Civil Engineering, Bogazici University, Istanbul, 2002.

43. Autodesk Inc., Autocad 2007, *2D and 3D Design and Engineering Software for Architecture, Manufacturing and Digital Entartainment*, California, USA, 2006.

44. Atmaca, S., *Strengthening of Brick Infilled RC Frames with Different Aspect Ratios by Means of CFRP Overlays*, Ph.D. Thesis, Department of Civil Engineering, Bogazici University, Istanbul, 2002.

45. ATC-40, Applied Technology Council, *Seismic Evaluation and Retrofit of Concrete Buildings*, Vol. 1, Washington DC., USA, 1996.

46. Turkish Earthquake Resistant Design Code 1968, *Specifications of Buildings to be Built in Disaster Areas,* The Ministry of Public Works and Settlement, Ankara, Turkey, 1968.

47. Turkish Earthquake Resistant Design Code 1975, *Specifications of Buildings to be Built in Disaster Areas,* The Ministry of Public Works and Settlement, Ankara, Turkey, 1975.

48. Enerpac Inc., *Visual Representation of Hydraulic Loading Equipment,* http://www.enerpac.com/en/basic-system-set-ups, 2009.

49. Clevaland Motion Controls Inc., *Visual Representation of Slim Load Cell,* http://www.cmccontrols.com/images/web_tension_control/load_cell_slim_cell.jpg, 2009.

50. Bestech Sensors & Instrumentation, *Visual Representation of Linear Variable Displacement Sensors,* http://www.ferret.com.au/odin/images/223026/DC-LVDT-position-sensors-available-from-Bestech-Australia.jpg, 2009.